REPORT DOCUMENTATION PAGE

Form Approved
OMB No. 0704-0188

1. AGENCY USE ONLY (Leave blank)	2. REPORT DATE	3. REPORT TYPE AND DATES COVERED
	1996-January-30	Final Technical 2/1/93-6/30/95

4. TITLE AND SUBTITLE

(U) Detailed Studies of Soot Formation in Laminar Diffusion Flames for Application to Modeling Studies

5. FUNDING NUMBERS

PC - 61102F
PR - 2308
SA - BS
G - F49620-92-J-0161

6. AUTHOR(S)

Robert J. Santoro

7. PERFORMING ORGANIZATION NAME(S) AND ADDRESS(ES)

The Pennsylvania State University
Department of Mechanical Engineering
University Park, PA 16802

AFOSR-TR-96
0277

9. SPONSORING/MONITORING AGENCY NAME(S) AND ADDRESS(ES)

AFOSR/NA
110 Duncan Avenue, Suite B115
Bolling AFB, DC 20332-0001

NA

10. SPONSORING/MONITORING AGENCY REPORT NUMBER

92-J-0161

11. SUPPLEMENTARY NOTES

12a. DISTRIBUTION/AVAILABILITY STATEMENT

Approved for public release; distribution is unlimited.

12b. DISTRIBUTION CODE

19960618 019

13. ABSTRACT *(Maximum 200 words)*

An investigation of soot formation in laminar diffusion flames showed that soot particle surface growth under laminar diffusion flame conditions ceases because of the depletion of hydrocarbon species and not soot particle reactivity loss due to thermal aging of the particles. This result was obtained through direct species concentration measurements under well-controlled conditions, while the particle reactivity effects were calculated based on premixed flame results along with particle temperature/time information available from earlier laminar diffusion flame studies. Comparisons with a soot formation model which incorporated detailed chemistry effects showed good agreement in terms of predicted and measured species concentration and soot particle field evolution. In addition, a novel technique for measuring soot volume fraction was developed based on laser-induced incandescence and was successfully applied to similar laminar diffusion flame studies. This technique was extended to droplet and turbulent diffusion flame conditions where a two-dimensional imaging approach was employed to measure soot volume fraction. Finally, the complete data set from these studies was assembled in a form suitable for dissemination on computer diskettes throughout the research community for comparison with modeling efforts.

14. SUBJECT TERMS	15. NUMBER OF PAGES
Soot Formation, Soot Particles, Diffusion Flames	102
	16. PRICE CODE

17. SECURITY CLASSIFICATION OF REPORT	18. SECURITY CLASSIFICATION OF THIS PAGE	19. SECURITY CLASSIFICATION OF ABSTRACT	20. LIMITATION OF ABSTRACT
UNCLASSIFIED	UNCLASSIFIED	UNCLASSIFIED	UL

DISCLAIMER NOTICE

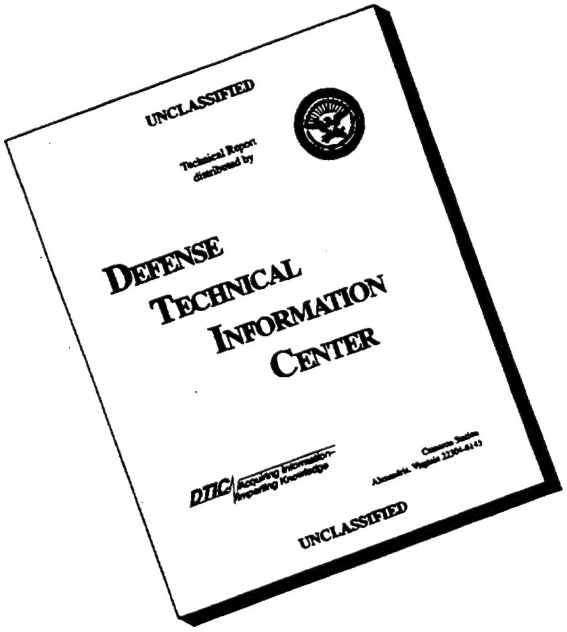

THIS DOCUMENT IS BEST QUALITY AVAILABLE. THE COPY FURNISHED TO DTIC CONTAINED A SIGNIFICANT NUMBER OF PAGES WHICH DO NOT REPRODUCE LEGIBLY.

Final Report

on

Detailed Studies of Soot Formation in Laminar Diffusion Flames for Application to Modeling Studies

AFOSR Grant F49620-92-J-0161

Prepared by

Robert J. Santoro
Department of Mechanical Engineering
The Pennsylvania State University
University Park, PA 16802

Submitted to

Air Force Office of Scientific Research
Bolling Air Force Base
Washington, DC

January 1996

Table of Contents

Summary

An investigation of soot formation in laminar diffusion flames showed that soot particle surface growth under laminar diffusion flame conditions ceases because of the depletion of hydrocarbon species and not soot particle reactivity loss due to thermal aging of the particles. This result was obtained through direct species concentration measurements under well-controlled conditions, while the particle reactivity effects were calculated based on premixed flame results along with particle temperature/time information available from earlier laminar diffusion flame studies. Comparisons with a soot formation model which incorporated detailed chemistry effects showed good agreement in terms of predicted and measured species concentration and soot particle field evolution. In addition, a novel technique for measuring soot volume fraction was developed based on laser-induced incandescence and was successfully applied to similar laminar diffusion flame studies. This technique was extended to droplet and turbulent diffusion flame conditions where a two-dimensional imaging approach was employed to measure soot volume fraction. The development of laser-induced incandescence as a diagnostic for soot represents a major development in terms of present capability to make soot volume fraction measurements in unsteady inhomogeneous combusting flows. Finally, the complete data set from these studies was assembled in a form suitable for dissemination on computer diskettes throughout the research community for comparison with modeling efforts.

1.0 Research Objectives

The objective of this research effort was to investigate the fundamental phenomena controlling soot particle formation and destruction in combustion systems. The emphasis and approach chosen for the present studies was based on previous results developed under AFOSR support which have proven the soundness of the methodology being utilized [1-10]. The present studies were conducted in a series of well-characterized laminar diffusion flames in which fuel constituents, temperature, concentration and transport processes are systematically varied and/or measured. A laminar diffusion flame environment was selected because it provides a relatively simple environment in which mixing processes are important while allowing for a wide range of measurement techniques to be employed. The importance of mixing in practical combustor situations is well recognized and, thus, it is critical to study soot formation processes under conditions where mixing has a significant role.

Specifically, the effort emphasized detailed measurements of the preparticle chemistry, particle inception and surface growth phenomena important in soot particle formation. These studies yielded quantitative measurements of the precursor and surface growth species which contribute to soot particle formation and growth. Data, which is temporally and spatially resolved, are of great value to modeling studies as past studies have demonstrated [11-14]. In fact, the availability of such results has allowed significant progress to be achieved over the past decade in soot modeling capabilities.

Efforts emphasized measurements of species concentration, especially acetylene and benzene concentrations, throughout the flame using both mass spectrometry and gas chromatography. Analysis has concentrated on explaining the soot surface growth process with respect to particle aging, as well as collaborating in a soot modeling effort with Prof. Ian Kennedy of the University of California. Additionally, a new approach for obtaining quantitative soot volume fraction measurements using laser-induced incandescence was developed and demonstrated. In the following sections, the techniques used and results obtained are summarized. More detailed discussions are included in the appendices for most of the results. For this reason, the main body of the report will strive for concise presentations of the most important results.

2.0 Research Approach

For the present studies, a coannular laminar diffusion flame was selected for study. This flame configuration has been widely studied and has been the focus of extensive fuel molecular structure and pressure sensitivity studies in our laboratory [1-10]. Since practical combustors typically involve the separate injection of fuel and oxidizer, laminar diffusion flames provide a simple, tractable environment in which to study soot formation while maintaining conditions where mixing effects are important. Soot formation can be viewed as a series of sequential processes which occur to some degree in all combustion

environments where soot is observed. It is the relative importance of these processes and their coupling which determines the amount of soot formed, its distribution throughout the combustion zone and its eventual emission from a specific combustor. Essential to the study of these processes is the selection of an experimental configuration which can provide the range of conditions typical of fuel-rich combustion zones. Laminar coannular diffusion flame studies have clearly demonstrated that such conditions can be achieved and studied [5]. Furthermore, such studies are proving to be increasingly valuable for the validation of modeling studies. With these points in mind, the coannular laminar diffusion flame represented a highly attractive experimental configuration.

The soot formation studies have been conducted in an atmospheric diffusion flame facility consisting of a coannular diffusion flame burner, burner chimney, positioning system and gas metering system. The burner has a configuration consisting of a 1.1 cm fuel tube surrounded by a 10 cm air annulus. The air passage is partially filled with glass beads followed by a series of fine screens to provide flow conditioning. A ceramic honeycomb 2.54 cm in thickness is used at the exit to provide a uniform flow field. The fuel tube which extends 4.8 mm above the ceramic honeycomb also is partly filled with glass beads to condition the flow. The fuel flow can consist of up to three gases, each metered with a separate rotameter. This allows for mixtures of fuels as well as nitrogen dilution of the fuel for temperature and concentration variation. The air flow is metered using a mass flow meter or rotameter which can monitor flows up to 5 SCFM of air. To protect the flame from room disturbances, a metal chimney has been incorporated into the burner facility. The chimney translates horizontally with the burner while the burner slides vertically within the chimney. Slots machined in the chimney provide access for the optical and intrusive probing of the flame.

A variety of diagnostic techniques were applied in these studies to measure the soot particle, temperature, species concentration and velocity fields. Both non-intrusive laser-based techniques, such as laser light scattering, laser velocimetry, laser-induced incandescence and laser-induced fluorescence, and intrusive probing followed by mass spectrometric and gas chromatographic analysis were utilized. A brief description of the apparatus used for these measurements follows for the reader's information.

2.1 Pulse Laser Systems

An Nd-YAG pulsed-dye laser system was utilized for fluorescence detection of OH radicals as well as for PAH species measurements while the Nd-YAG laser alone provides the light source for the laser-induced incandescence measurements. The major components of the system involve the dye laser, which consists of an Nd-YAG pulsed laser operating at 532 nm, a dye laser module and a doubling crystal. The present system has the capability to tune over a wavelength range extending from 220 to 600 nm. This wavelength range is quite suitable for OH fluorescence as well as PAH measurements. Detection is

achieved using a photomultiplier or an intensified CCD array camera. In the case of the photomultiplier (PMT), the PMT signal is input to a box car integrator to provide for signal averaging and background noise rejection. For the intensified CCD array camera, direct storage of the images on a personal computer is used to record the data. This unit has a 50 ns gate capability and can be used for signal averaging of multiple laser shots. Using this camera, planar laser imaging is also possible, which allows spatially extensive measurements to be obtained.

2.2 Intrusive Probe Sampling for Species Concentration Measurements

In order to provide more quantitative information on the species important in the formation and growth of soot particles, a mass spectrometer system was assembled for these studies. Gas samples from the flames under study were obtained using a quartz microprobe technique similar to the approach taken by Smyth *et al.* [15]. Measurements of gas phase species in the soot precursor and particle inception regions can be obtained using standard sampling probe configurations. Measurements in the present studies were also extended into the surface growth region in order to ascertain the important species responsible for mass addition through surface growth. As part of this research program, approaches allowing sampling of fuel-rich particle laden regions had to be developed to allow measurements in the post-particle inception region of the flame. Sampling probe techniques usually are limited by orifice clogging problems which can only be overcome by increasing the orifice dimensions and sacrificing the spatial resolution of the measurements. To overcome the aforementioned orifice clogging problem, a novel sonic sampling probe has been developed and applied to a series of laminar diffusion flames containing various amounts of soot. Since the details of the design and operation of this probe were previously presented [16], only a brief description is provided below.

The approach, employed to prevent clogging of the probe orifice, involves mechanically oscillating a wire through the orifice region using a spring-loaded solenoid plunger whose driving circuit is electronically interrupted periodically (see Figures 1 and 2). The constant motion of the wire relative to the quartz tube is responsible for keeping the orifice open. For the present probe, the effective orifice is the annulus formed by an oscillating 130 μm diameter Sapphire fiber of uniform cross section and the 160 μm diameter orifice in the quartz tube. Therefore, the effective orifice is equivalent to approximately a 100 μm circular hole. The Sapphire fiber is attached to a 1.59 mm tube which is connected to a spring-loaded soft iron solenoid plunger which oscillates in the orifice. This probe is referred to as the electromechanical sonic probe (EMS) since it employs a sonic sampling orifice with an electromagnetic mechanism to maintain the integrity of the orifice opening.

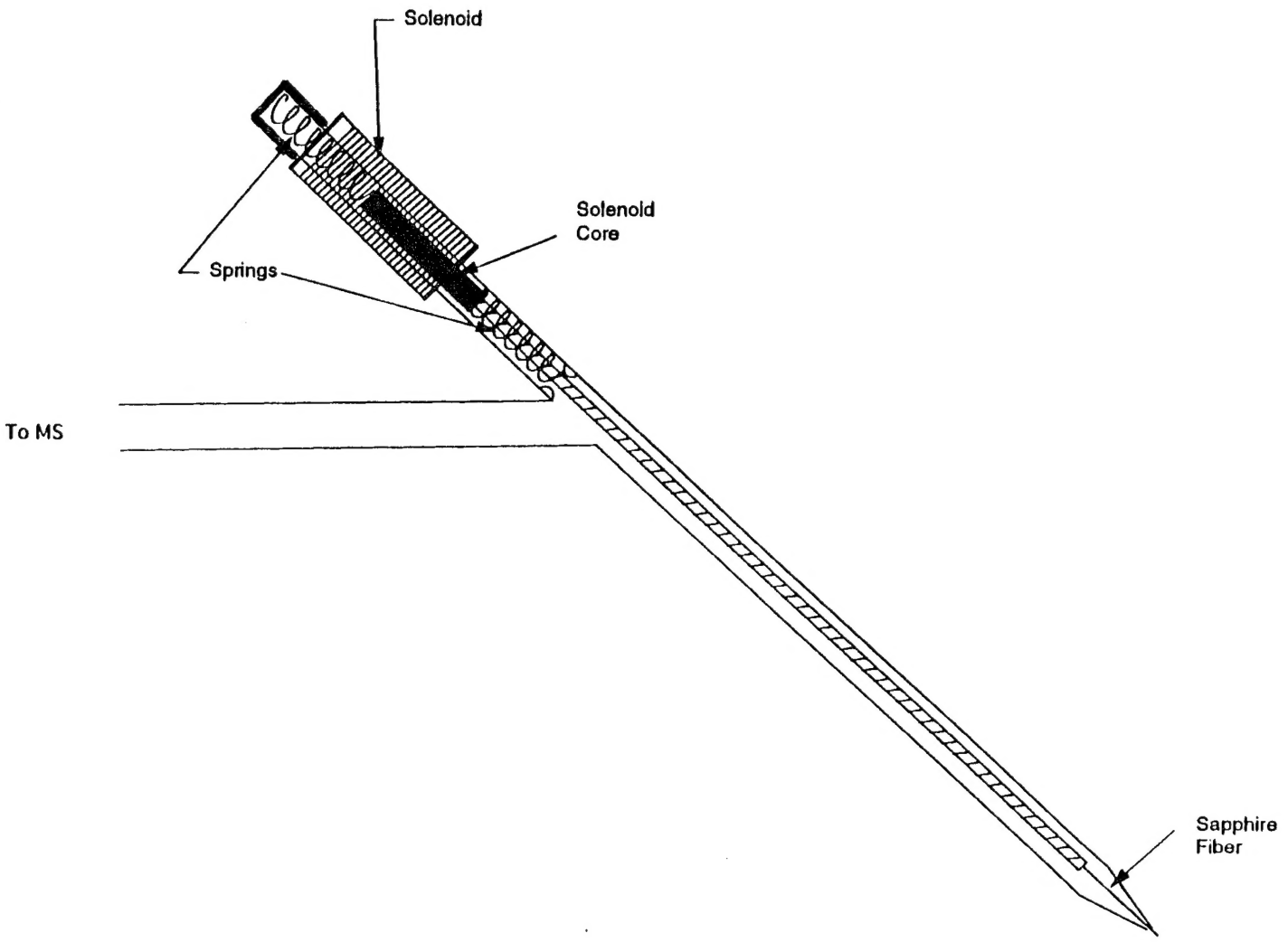

Figure 1. Schematic representation of the electromagnetic sonic probe.

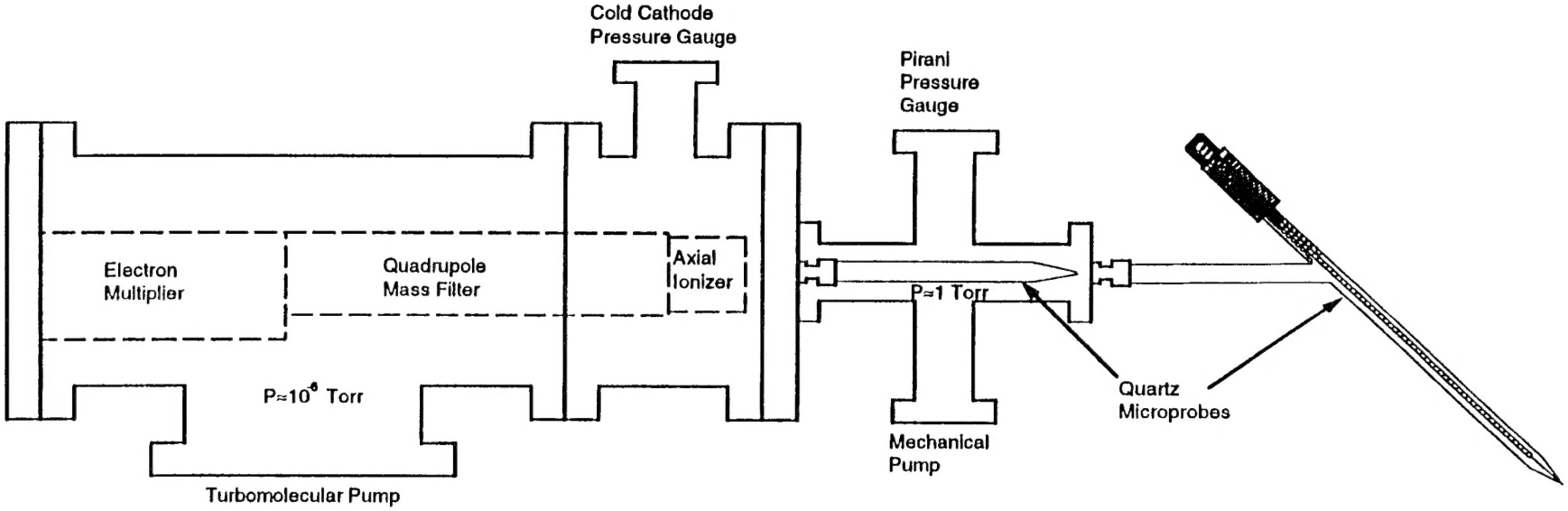

Figure 2. Schematic representation of the quadrapole mass spectrometer and probe assembly.

The mass spectrometer used for these studies utilizes a quadrupole mass filter with a mass range of 1 to 500 amu. This unit (an Extrel Model C-50) has excellent mass resolution (0.1 amu) and high sensitivity. A gas chromatograph (Hewlett-Packard 5860) is also used for gas analysis to complement the mass spectrometer measurements. This system utilizes a specially designed sampling and pressurization approach to allow the EMS probe to be used. Radial profiles of the species concentration as a function of axial position are obtained by traversing the flame in the radial direction. When these measurements are combined with the soot particle and velocity measurements, the temporal evolution of the species concentration and its relationship to soot formation can be investigated.

3.0 Research Accomplishments

The research accomplishments of the grant are summarized in the following sections. Specifically, three areas of activities are described:
(1) soot particle surface growth mechanisms, (2) soot modeling studies and (3) laser-induced incandescence measurements of soot volume fraction. Detailed discussions of these accomplishments are also provided in the appendices, as noted. In addition, an extensive review of the current understanding of soot formation is presented in Appendix A for the interested reader.

3.1 Soot Particle Surface Growth Mechanisms

Extensive spatially resolved measurements of the species concentration field have been obtained with both mass spectrometry and gas chromatography analysis approaches for a well-studied ethene/air laminar diffusion flame. The complete set of mass spectrometry measurements obtained previously has been repeated to allow for an estimation of the accuracy and precision of the measured data. This information is critical for modeling comparisons in order to accurately assess when real differences exist between measurement and prediction. Additionally, similar spatially resolved concentration measurements were obtained with a gas chromatography approach to provide an independent measurement of the concentrations for comparison with the mass spectrometer data. The gas chromatograph also allowed determinations of the concentrations of some key species not easily measured with the mass spectrometer, in particular carbon monoxide.

The major conclusions of these studies were:

1. Soot particle surface growth terminates because of the depletion of the hydrocarbon species responsible for surface reactions which add mass to the particle. In particular, the measurements of acetylene and benzene clearly show these species decrease to trace concentration levels at the peak of the soot volume fraction location.

2. Comparisons with results describing the aging process, which soot particles have been observed to experience under premixed flame conditions, show that this mechanism has only a small contribution to the reduction in the surface growth rate for these laminar flame conditions.

These conclusions are consistent with recent work by Honnery and Kent [17,18], who have shown that in long laminar diffusion flames, soot growth can be extended to very long residence times. A more detailed discussion of these results is contained in Appendix B, where the data and analysis to support the above conclusions are presented.

3.2 Soot Modeling Studies

A collaborative effort was initiated with Prof. Ian Kennedy of the University of California at Davis to compare the measured soot and species concentrations fields with that predicted by a model developed by Prof. Kennedy and his co-workers. A system of elementary reactions were used to describe the gas phase C_1 and C_2 chemistry. The model incorporates a simple description of the growth of soot particles which performs a good job of reproducing the amount of soot in the flame and the transition from non-sooting to sooting conditions. Stable gas phase species measured in the flame along with OH concentrations previously obtained [10] were compared with model predictions. The model reproduced most of the specified concentration profiles quite well. It was found that the assumption of equilibrium concentrations for the minor radical species was grossly in error, particularly near the end of the flame where temperatures were low. Calculated radical species were found in concentrations that were orders of magnitude greater than equilibrium. Comparisons with measured OH concentrations supported this observation. A more detailed discussion of these results is contained in Appendix C, which has recently been submitted to *Combustion and Flame* for publication.

3.3 Laser-Induced Incandescence Measurements of Soot Volume Fraction

Laser-induced incandescence has been used to obtain spatially-resolved measurements of soot volume fraction in a laminar diffusion flame, in which comparisons with laser scattering/extinction data yield excellent agreement. In addition, the laser-induced incandescence signal is observed to involve a rapid rise in intensity followed by a relatively long (ca. 600 ns) decay period subsequent to the laser pulse, while the effect of laser fluence is manifest in non-linear and near-saturated response of the laser-induced incandescence signal with the transition occurring at a laser fluence of approximately 1.2×10^8 W/cm^2. Spectral response of the laser-induced incandescence involves a continuous spectrum in the visible wavelength range due to the blackbody nature of the emission. Simultaneous measurements of laser-induced incandescence and light-scattering yield encouraging results concerning the mean soot particle diameter and number concentration. Thus, laser-induced incandescence can be used as an instantaneous, spatially-resolved diagnostic of soot volume fraction without the need for the conventional line-of-sight laser extinction method, while potential applications in two-dimensional imaging and simultaneous measurements of laser-induced incandescence and light-scattering to generate a complete soot property characterization are significant. These results are presented in detail in Appendix D.

Recently, the laser-induced incandescence technique was used to make novel planar measurements of soot volume fraction within turbulent diffusion flames and droplet flames. The two-dimensional imaging technique was developed and assessed by systematic experiments in a coannular laminar diffusion flame, in which the soot characteristics have been well established. With a single-point calibration procedure, agreement to within 10% was found between the values of soot volume fraction measured by this technique and those determined by conventional laser scattering--extinction methods in the flame. As a demonstration of the wide range of applicability of the technique, soot volume fraction images were also obtained from both turbulent ethene diffusion flames and from a freely falling droplet flame that burns the mixture of 75% benzene and 25% methanol. For the turbulent diffusion flames, approximately an 80% reduction in soot volume fraction was found when the Reynolds number of the fuel jet increased from 4000 to 8000. In the droplet flame case, the distribution of soot field was found to be similar to that observed in coannular laminar diffusion flames. The development of the laser-induced technique, therefore, is a significant new contribution to the array of laser-based diagnostics available for combustion measurements. The results of studies involving extensions of the technique to planar measurements are given in Appendix E.

4.0 Conclusions

The major conclusions of studies undertaken as part of this contract are:

1. Soot particle surface growth terminates because of the depletion of the hydrocarbon species responsible for surface reactions which add mass to the particle. In particular, the measurements of acetylene and benzene clearly show these species decrease to trace concentration levels at the peak of the soot volume fraction location. Additional measurements using gas chromatography analysis have provided additional species concentration information and allowed an estimate of the accuracy and precision of the measurements. The availability of such an estimate was viewed as critical to meaningful comparison with soot chemistry model predictions.
2. Comparisons with results describing the aging process, which soot particles have been observed to experience under premixed flame conditions, show that this mechanism has only a small contribution to the reduction in the surface growth rate for these laminar flame conditions.
3. A current detailed model of soot formation in laminar diffusion flames was shown to be capable of reproducing the major gas phase species and soot particle fields reasonably well (i.e. to within a factor of two). Better agreement appears possible with further refinements in the model. Of particular note is that both measurement and prediction show that radical species in these soot laden diffusion flames are far from equilibrium. This observation is critical to the development of appropriate combustion models for soot laden flows.
4. A novel quantitative laser diagnostic approach has been developed and applied to the measurement of soot volume fraction in laminar diffusion flames based laser-induced incandescence. This diagnostic approach has been validated using well known soot particle measurements previously obtained in laminar diffusion flames. The technique has recently been extended to turbulent flame, droplet burning and Diesel engine experiments.

5.0. References

1. Santoro, R. J., "Fuel Structure and Pressure Effects on the Formation of Soot Particles in Diffusion Flames," AFOSR-TR-88-0664, 1989.

2. Quay, B., Lee, T-W, Ni, T., and Santoro, R. J., "Spatially-Resolved Measurements of Soot Volume Fraction Using Laser-Induced Incandescence, "*Combustion and Flame*," In press.

3. Puri, R. and Santoro, R. J., "The Role of Soot Particle Formation on the Production of Carbon Monoxide in Fires," *Fire Safety Science Proceedings of the Third International Symposium*, Elsevier Applied Science, London, pp. 595-604 (1991).

4. Santoro, R. J., Semerjian, H. G. and Dobbins, R. A., "Soot Particle Measurements in Diffusion Flames," *Combustion and Flame*, 52, pp. 204-218 (1983).

5. Santoro, R. J., Yeh, T. T., Horvath, J. J. and Semerjian, H. G., "The Transport and Growth of Soot Particles in Laminar Diffusion Flames," *Combustion Science and Technology*, 53, p. 89 (1987).

6. Santoro, R. J., "Fuel Molecular Structure Effects on Soot Particle Growth in Diffusion Flames," *Twentieth Fall Technical Meeting of the Eastern Section of The Combustion Institute*, Paper #19, Gaithersburg, MD, Nov. 2-5, 1987.

7. Richardson, T. F. and Santoro, R. J., "Soot Growth in Diffusion Flames Burning Fuel Mixtures," *Twenty-First Fall Technical Meeting of the Eastern Section of The Combustion Institute*, Paper #44, Clearwater Beach, FL, Dec. 5-7, 1988.

8. Santoro, R. J., "Optical Measurements of Soot Particles in Flames," *Mat. Res. Soc. Symp. Proc.*, 117, pp. 157-163 (1988).

9. Puri, R., Richardson, T. F., Santoro, R. J. and Dobbins, R. A., "Aerosol Dynamic Processes of Soot Aggregates in a Laminar Ethene Diffusion Flame," *Combustion and Flame*, 92, pp. 320-333 (1993).

10. Puri, R., Moser, M., Santoro, R. J. and Smyth, K. C., "Laser-Induced Fluorescence Measurements of OH Concentration in the Oxidation Region of Laminar, Hydrocarbon Diffusion Flames," *Twenty-Fourth Symposium (International) on Combustion*, The Combustion Institute, Pittsburgh, PA, pp. 1015-1022 (1992).

11. Frenklach, M. and Wang, H., "Detailed Modeling of Soot Particle Nucleation and Growth," *Twenty-Third Symposium (International) on Combustion*. The Combustion Institute, Pittsburgh, PA, pp. 1559-1566 (1990).

12. Smooke, M. D., Lin, P., Lam, J. K. and Long, M. B., "Computational and Experimental Study of a Laminar Axisymmetric Methane-Air Diffusion Flame," *Twenty-Third Symposium (International) on Combustion* , The Combustion Institute, Pittsburgh, PA, pp. 575-582 (1990).

13. Kennedy, I. M., Kollmann, W. and Chen, J-Y., "A Model for Soot Formation in Laminar Diffusion Flames," *Combustion and Flame*, 81, pp. 73-85 (1990).

14. Megaridis, C. M. and Dobbins, R. A., "Comparison of Soot Growth and Oxidation in Smoking and Non-Smoking Ethylene Diffusion Flames," *Combustion Science and Technology*, 66, pp. 1-16 (1989).

15. Smyth, K. C., Miller, J. H., Dorfman, R. C., Mallard, W. G. and Santoro, R. J., "Soot Inception in a Methane/Air Diffusion Flame as Characterized by Detailed Species Profiles," *Combustion and Flame*, 62, pp. 157-181 (1985).

16. Puri, R. and Santoro, R. J., "Sonic Probe Sampling in Particle Laden Combustion Flows," *Twenty-Third Fall Technical Meeting of the Eastern Section of The Combustion Institute*, Orlando, FL, Dec. 3-5, 1990.

17. Honnery, D. R and Kent, J. H. , "Soot Formation in Long Ethylene Diffusion Flames," *Combustion and Flame*, 82, p. 426 (1990).

18. Kent, J. H. and Honnery, D. R., "Soot Formation Rates in Diffusion Flames - A Unifying Trend," *Combustion Science and Technology*, 75, p. 169 (1991).

6.0 Publications

1. Santoro, R. J. and Richardson, T. F., "Concentration and Temperature Effects on Soot Formation in Diffusion Flames," in *Mechanisms and Models of Soot Formation*, (Bockhorn, H., ed), Springer-Verlag, 1994, pp. 221-238.

2. Puri, R., Richardson, T. F., Santoro, R. J. and Dobbins, R. A., "Aerosol Dynamic Processes of Soot Aggregates in a Laminar Ethene Diffusion Flame," *Combustion and Flame*, 92, pp. 320-333 (1993).

3. Quay, B., Lee, T-W, Ni, T. and Santoro, R. J., "Spatially-Resolved Measurements of Soot Volume Fraction Using Laser-Induced Incandescence, "*Combustion and Flame*," 97:384-392 (1994).

4. Rapp, D. C. and Santoro, R. J., "Growth Species and Soot Growth in a Laminar Diffusion Flame," Paper /CI 94-052, 1994 Spring Meeting of the Western States Section of the Combustion Institute, University of California at Davis, Davis, CA, March 21 and 22, 1994.

5. Smyth, K. C., Norton, T. S., Miller, J. H., Smooke, M. D., Puri, R., Moser, M. and Santoro, R. J., "Radical Concentration Measurements in Hydrocarbon Diffusion Flames," in *Mechanisms and Models of Soot Formation*, (Bockhorn, H., ed), Springer-Verlag, 1994, pp. 113-133.

6. Ni, T., Pinson, J. A., Gupta, S. and Santoro, R. J., "Two-dimensional imaging of soot volume fraction by the use of laser-induced incandescence," *Applied Optics*, 34, pp. 7083-7091 (1995).

7.0 Meetings and Presentations

1. Lee, W., Richardson, T. F. and Santoro, R. J., "The Effects of Operating Pressure on soot Formation in Laminar Diffusion Flames," Paper #100, 1993 Joint Technical Meeting of the Central and Eastern States Sections of the Combustion Institute, New Orleans, LA, March 15-17, 1993.

2. Rapp, D. C. and Santoro, R. J., "Measurements of Soot Growth Species Concentration in Diffusion Flames," Chemical and Physical Processes in Combustion, 1993 Technical Meeting of the Eastern States Section of the Combustion Institute, Princeton University, Princeton, NJ, October 25-27, 1993, pp. 370-373.

3. Quay B., Lee T-W., and Santoro, R. J., "Spatially-Resolved Measurements of Soot Volume Fraction Using Laser-Induced Incandescence," Chemical and Physical Processes in Combustion, 1993 Technical Meeting of the Eastern States Section of the Combustion Institute, Princeton University, Princeton, NJ, October 25-27, 1993, pp. 386-389.

4. Rapp, D. C., Seo, S. and Santoro, R. J., "Species Measurements in Laminar Diffusion Flames of Different Fuel Mixtures," Chemical and Physical Processes in Combustion, 1995 Technical Meeting of the Eastern States Section of the Combustion Institute, Worcester Polytechnic Institute, Worcester, MA, October 16-18, 1995, pp. 273-276.

5. Santoro, R. J., "Soot Formation: A view of Current Understanding," Chemical and Physical Processes in Combustion, 1995 Technical Meeting of the Eastern States Section of the Combustion Institute, Worcester Polytechnic Institute, Worcester, MA, October 16-18, 1995, pp. 37-44.

8.0 Participating Professionals

Dr. Robert J. Santoro, Professor of Mechanical Engineering
Dr. Tuqiang Ni, Research Associate (Currently employed at LAM Research Corporation)
Dr. Tae-Woo Lee, Research Associate (Currently Assistant Professor, Arizona State University)
Dr. Rahul Puri, Graduate Student and Research Associate, Department of Mechanical Engineering (Ph.D. 9/92, currently employed at Allison Gas Turbine)
Dr. Thomas Richardson, Graduate Student, Department of Mechanical Engineering (Ph.D. 5/93, currently employed at Allison Gas Turbine).
Mr. Darrell Rapp, Graduate Student (AFRAPT), Department of Mechanical Engineering (Ph.D. expected 2/96).
Mr. Bryan Quay, Graduate Student (ASSERT), Department of Mechanical Engineering (Ph.D. expected 1/97).
Mr. Daniel Boone, Technician

9.0 Interactions

A number of researchers have directly used the extensive data set developed as part of this work to compare with or extend their own research. Some of those who have been directly provided data include:

Professor R. A. Dobbins, Brown University, Providence, RI
Dr. R. Hall, United Technologies Research Center, East Hartford, CT
Dr. R. Davis, the National Institute of Standards and Technology, Gaithersburg, MD
Dr. P. Solomon, Advanced Fuel Research, Inc., East Hartford, CT
Dr. I. Kennedy, University of California, Davis, CA
Drs. C. Merkle and S. Turns, The Pennsylvania State University, University Park, PA
Dr. H. Mongia, Allison Gas Turbine Division-GM, Indianapolis, IN and General Electric, Aircraft Engines Division, Cincinnati, OH
Dr. K. Smyth, National Institute of Standard and Technology, Gaithersburg, MD
Dr. G. Mulholland, National Institute of Standards and Technology, Gaithersburg, MD
Prof. L. Pfefferle, Yale University, New Haven CT

In addition to the interactions resulting from interest in soot particle data, there have been interactions with researchers on particle diagnostic problems. In some cases this has resulted in direct visits to particular laboratories to assist in solving these problems. These interactions include:

Dr. M. Zachariah, The National Institute of Standards and Technology, Gaithersburg, MD
Dr. Valerie Lyons, NASA-Lewis Research Center, Cleveland, OH
Dr. Alan Scaroni, Penn State University, University Park, PA
Dr. Randy Van derWaal, NASA Lewis Research Center, Cleveland, OH

Several other interactions have also occurred through a general interest in the work supported by AFOSR with:

Colombian Chemical Company, Monroe, LA
Cummins Engine Company, Columbus, IN
E. I. DuPont De Nemours, Wilmington, De
Eastman Kodak, Rochester, NY
Allison Gas Turbine Division, Indianapolis, IN
General Electric, Aircraft Engine Division, Cincinnati, OH
Lubrizol, Wickliffe, OH

DuPont supported work on titanium dioxide particle formation as a direct result of the AFOSR research program. A student, Peter Strakey, spent two summers with DuPont exchanging expertise and technology developed as part of this research and is now working at the Phillips Laboratory.

Lubrizol has an ongoing grant with our laboratory to examine the surface reactivity effects of soot particles on lubricants. This work complemented an AASERT grant associated with this current AFOSR contract. Two students, Mr. Chris Chandler and Mr. Sherman Creighton, have been supported on this project and works closely with Mr. Bryan Quay, as well as with personnel at Lubrizol.

Recent work with Allison Gas Turbine Division involving the incorporation of a revised soot model in their gas turbine combustion codes also occurred as a result of the present work. Mr. Darrell Rapp, who is an AFRAPT participant, has spent two summers working at Allison on the implementation of that model. This work is an attempt to directly transfer the results of our work to industry. Additionally, two former Ph.D. students associated with the present contract are now permanent employees of Allison and work on gas turbine related problems.

We have also previously participated by invitation in two international workshops on soot formation:

"Current Problems in Soot Formation During Combustion,: sponsored by The Commission on Condensation Phenomena of the Academy of Science, held in Gottingen, Germany, March 20-30, 1989.

"Mechanisms and Models of Soot Formation--An International Workshop," sponsored by Volkswagen, Heidelberg, Germany, September 29 - October 2, 1991.

Appendix A: Soot Formation: A View of Our Current Understanding

by

R. J. Santoro

Presented at the 1995 Technical Meeting of the Eastern States Section of The Combustion Institute, Worcester Polytechnic Institute, Worcester, MA, October 16-18, 1995, pp. 37-44.

SOOT FORMATION: A VIEW OF OUR CURRENT UNDERSTANDING

R. J. Santoro
Propulsion Engineering Research Center
and
Department of Mechanical Engineering
The Pennsylvania State University
University Park, PA 16802-2320

INTRODUCTION

Over the past three decades a significant amount of research has been directed to understanding, from both a fundamental and applied viewpoint, the processes responsible for soot formation and destruction in combustion systems. Several excellent reviews have been published which describe much of this previous work [1-6]. The basic sequence of events which compose the formation and destruction processes for soot particles in combustion systems is now well established. This sequence includes: 1) a chemically kinetic controlled reaction sequence which results in the formation of the precursor species needed to form the first particles, 2) a particle inception stage which results in the formation of large numbers of small primary particles, 3) a particle growth region in which surface growth and particle coagulation processes contribute to the increase in particle size, and, finally, 4) a stage in which material is no longer added to the soot particles, and size and number concentration are controlled by agglomeration or even are reduced through oxidative attack [7]. This sequence of events describes soot formation in a wide variety of combustion systems including laboratory-scale premixed and diffusion flames as well as practical combustors such Diesel and gas turbine engines. Differences observed in various combustion environments are a result of variations in the importance of the individual steps under the actual operating conditions. Thus, an understanding of soot formation and destruction not only requires a knowledge of the individual steps involved, but also how they are coupled.

Below a review of the soot formation and destruction is presented in four sections dealing with soot particle precursor chemistry, soot particle inception, surface growth and soot oxidation. The studies reviewed emphasize simple combustion systems in which suitable conditions can be achieved which allow differentiation of the various aspects of the problem. A variety of experimental apparatus have been employed for such studies including shock tubes [9,10], laminar premixed [11-20] and diffusion [21-46] flames, and turbulent flames [47-53]. Key to these laboratory-scale studies has been the development of a variety of diagnostic capabilities, both for gas phase species and soot particle measurements. Most prominent among these techniques have been mass spectrometric sampling methods for species concentration measurements [12] and laser light scattering techniques for soot particle characterization [15]. Of particular importance has been the capability to obtain spatially resolved measurements of key species and soot particle concentrations [12, 23-25] to provide mechanistic information on the evolution of the soot precursor and particle fields.

An additional development which has had an important impact is the application of large detailed numerical models representing the entire soot formation and destruction process [54-71]. The development of these models has helped to focus research in several areas including chemical precursor mechanisms, particle nucleation, surface growth phenomena, and oxidation processes. Although differences in interpretation and understanding remain, a coherent modeling process is emerging from which to examine likely routes to soot particle formation.

SOOT PARTICLE PRECURSOR CHEMISTRY

Any understanding of the soot formation process must begin with the reactions involving the parent hydrocarbon fuel. These typically are relatively small hydrocarbon species which undergo pyrolysis and oxidative reaction steps to form intermediate radical species that react with other hydrocarbons present to form larger species. It is useful in this endeavor to concentrate on two distinct groups of hydrocarbon reactions, following the work of Frenklach and co-workers [54-59]. The first group involves reactions which lead to formation of the first and second aromatic ring species. While the second group involves the reactions which lead to subsequent multiple ring species, i.e., polycyclic aromatic hydrocarbons (PAH). The emphasis of aromatic hydrocarbons is a reflection of the established fact that soot is composed of species with an aromatic ring structure [1]. Consequently, at some point in the soot formation process these aromatic species must form. Currently, data supports the view that the gas phase precursors to soot particles are PAH species. Although the description here emphasizes a neutral species mechanism, other studies have examined an ion molecule reaction pathway to soot [5,18,72].

A key feature of any mechanism explaining soot formation must account for the thermodynamic stability of the intermediate hydrocarbon species. Since soot formation occurs under high temperature conditions, one would expect larger molecular species to dissociate unless they are thermodynamically stable. Additionally, the reactions leading to these larger hydrocarbon species should be fast, in order to account for the observed rapid formation of soot particles in combustion systems. In some sense, the conditions of rapid reaction rates and thermodynamically stable molecules pose contradictory requirements which must be resolved within the model.

Frenklach et al. [54,55] proposed a mechanism in which reactions between acetylene (C_2H_2) and key radicals, such as vinyl (C_2H_3), vinylacetylene (C_4H_4) and butadienyl (C_4H_5), lead to the formation of the first aromatic ring through the cyclization of C_6H_5. Cole et al. [20] proposed a slightly different reaction route involving C_6H_7 to form benzene (C_6H_6) which Colket [60] used to explain the temperature sensitivity observed in shock tube studies of C_2H_2 at lower temperatures than the original work of Frenklach et al. [54]. Frenklach et al. [55] later showed that the difference in sooting tendency of various fuels was due to the sensitivity of these radical species concentrations to fuel molecular structure and temperature. Other routes to the formation of the first ring have also been examined including the reaction involving the propargyl radical (C_3H_3) to form 1,5 hexadiyne which rapidly is converted to benzene [73]. Although details remain to be resolved, significant progress has been made in achieving a basic framework for understanding this important first step in the soot formation process.

The formation of the second ring, begins with the C_6H_5 radicals reacting with C_2H_2, followed by a subsequent reaction with H-atom to reform a radical species. This radical again reacts with C_2H_2 and undergoes ring closure to form the naphthalene radical [54]. Acetylene, which is present in large concentrations, thus, represents a primary building block in the growth of large hydrocarbon species. Hydrogen atom reaction steps are key to recreating the radical species, and are continually necessary in the subsequent steps to the formation of multiple ring PAH species. Since all these reactions are reversible, dissociation of the products to reactants is likely to some degree, thus both the forward and reverse reactions are important.

A point to emphasize is that fuel molecular structure is likely important in establishing the concentrations of acetylene and important C_2H_x and C_4H_y hydrocarbon radicals. Furthermore, modeling studies have shown that these reactions are very sensitive to temperature in the range around where soot is observed to rapidly form ($1300K < T < 1800K$). For aromatic fuels some support has been given for a more direct route to a two ring aromatic species through biphenyl formation [55], again emphasizing that fuel molecular structure likely impacts the early steps in the soot formation process significantly.

Once one and two ring compounds are formed growth to much larger species is required. Typically incipient soot particles are viewed to achieve molecular weights between 3000 and 10,000 amu. To achieve the continued molecular growth needed, Frenklach et al. [54,55] proposed a series of reactions where an aromatic radical undergoes sequential reactions with C_2H_2 and H-atoms to form a subsequent ring. Interspersed along the reaction path is the formation of highly stable species, such as acenaphthylene, which contain a five membered ring. The formation of these species is substantially more favorable in the forward direction which "pushes" the species growth to larger molecules. Because of their stability these species have been termed "islands of stability" and are key to providing a thermodynamically allowable path to soot. Before leaving this point it should be noted that although such species are stable, they do not represent termination points in the reaction pathway. Subsequent attack by H-atoms provides a means to again form a radical species which will react with C_2H_2 to eventually lead to another "island of stability". The above described process answers the earlier mentioned requirement for highly stable intermediate species which can also react rapidly to form larger hydrocarbons.

Although developments related to the details of individual steps involved in the mechanism continue, the breadth of application of this approach in both full and reduced reaction schemes is impressive [62-63,67,71,74]. The advances made in the last decade in the area of reaction mechanisms describing soot precursor formation may be the most impressive achievement in the field over that time period.

SOOT PARTICLE INCEPTION

Although the basis the soot particle formation is closely linked to the formation and growth of PAH species, little direct measurements exists of the rate of inception of soot particles under conditions where PAH concentration fields are known. Furthermore, light scattering techniques use to measure soot particles have difficulties yielding quantitative results due broadband background fluorescence induced by the laser itself. Consequently, in the author's opinion, soot inception is an area where further quantitative results are needed to further clarify the phenomena resulting in soot particles. However, much has been learned over the past decade in this area as well. It is now clear that the formation of soot particles is not due to a classical nucleation event, but is a result of continual growth of hydrocarbon precursors to soot. Recent work has more clearly linked the decrease in larger PAH species with the appearance of soot particles [75-77], qualitatively

demonstrating the relationship between PAH production and soot particle formation. These studies of particle inception conducted under premixed flame conditions are being complemented by laminar diffusion flame studies where soot particle inception is directly measured [78]. Previous qualitative measurements indicated that the first detected soot particles in laminar ethene flames occur in the region of maximum observed PAH fluorescence, but no quantitative inception rate data was obtained [24]. Recently based on the limited experimental measurements related to inception, simple nucleation rate expressions are being developed [68] and compared with measurements where possible [78]. These initial developments show some potential for success and should be followed closely in the future as more data become available.

Despite the lack of detailed experimentally measured inception rates, modeling efforts have met with considerable success in representing inception as a coagulation process with a critical molecular size identified with the incipient soot particles [57,58,62,66,71,74,75,79]. McKinnon and Howard have used the term "reactive coagulation" to describe their work in this area to indicate that the "sticking collisions between PAH are stabilized by the formation of a chemical bond" [75]. Recent modeling work has also considered the relative importance of C_2H_2 and PAH collision partners on the growth of soot precursors and incipient particles and identified under what conditions these species contribute to precursor formation, as well as surface growth process [57,58,62,66,71,74,75].

SURFACE GROWTH

Although particle inception is one of the key processes in the formation of soot, it actually accounts for only a small fraction of the mass addition. The major mass addition process involves the surface growth stage which follows inception. A great deal of attention has been given to this process in both premixed and diffusion flames [14,19,80,81,82]. Major contributions to the present understanding of surface growth have been made by Wagner [13] and Harris [14]. The mechanisms developed in these studies differ significantly in concept and work is continuing to further understand the surface growth process [83-86].

Most approaches to soot surface growth phenomena argue that acetylene, or a species closely associated with acetylene, provides the major surface reactant. Simple mass balance considerations provide the basis for this observation, since only acetylene appears to be present in sufficient concentration to account for the amount of mass added to the soot particles [14]. However, other workers have pointed out that under suitable conditions large PAH species may directly add to the growing soot particles [57,61,66,75].

Recently there has been increased interest in the specific phenomena controlling the surface reactivity in soot surface growth processes [57,61,66,83-86]. Each of these studies has focussed on the concept of active surface sites as reaction centers for the addition of carbon through reactions with gas phase species such as acetylene. The objectives of these studies differ, but they do raise a set of common features. First, soot particles possess highly reactive surfaces, exceeding by two orders of magnitude the reactivity of pyrolytically formed carbon particles (pyrocarbon) [85]. The regeneration of active sites appears to be related to atomic hydrogen reactions with the surface to form new reactive sites [57,61,66,79], which have a relativity constant concentration in many situations [79,85]. This approach has been used to reconcile the disparate observations in the literature regarding the sensitivity of the surface growth process to the available soot particle surface area. The results of Harris and Weiner [14,19] indicate a direct proportionality to available surface areas as indicated by:

$$\frac{dm}{dt} = k\, S[C_xH_y]$$

where m is the soot mass, k is the growth rate constant, S is the surface area, and C_xH_y represents the growth species, e.g. C_2H_2.

Results from the work of Haynes et al. [86] and Weischnowsky et al. [16] indicate that the surface growth process is independent of the available surface area. In the recent work, Harris [79], Haynes [85] and Frenklach [57,58] have replaced or augmented the surface area arguments with the addition of a surface active site concentration. Although the details of the representations are different, the basic approach involves similar concepts with regard to the importance of these surface sites. For example, Haynes [85] represents the increase in soot volume fraction with time as:

$$\frac{df_v}{dt} = \alpha \frac{c}{4} N_s A_s v_g N_g$$

where f_v is the soot volume fraction, α is the growth reaction probability on collision, N_g is the number density of gas phase growth species, v_g is the molecular volume of the growth species when incorporated in the soot particle, c is the mean free speed of the gas phase growth species $(8kT/\pi m_g)^{1/2}$, N_s is the total concentration of active sites and A_s is the active area of a single site. In this representation the difference in the experimental results is determined by the behavior of the active sites in the various flames. In the results of Harris and Weiner [14,17], the active site concentration remains nearly constant and, thus, scales with particle surface area. In contrast, for the higher temperature flame studies by Haynes et al. [86] and Weischnowsky [16], the surface site concentration is argued to decrease with time. The basis for the decay in the active surface site is not known, although the higher temperature flames can be argued to provide an environment in which more rapid annealing of the soot particles may be present. Frenklach [57] has argued in a somewhat similar manner that the state of the initial surfaces of the soot particles may differ in the two flames with the higher temperature flames having fewer active sites.

Much of the above work emphasizes detailed treatment of the chemistry and physics important in surface growth. Other workers have explored the potential to relate surface growth to more global properties of the flames which may allow more universal, simpler representations of soot formation that can be incorporated into more complicated flow field calculations, such as require for turbulent combustion conditions [63,81,82,87]. In these approaches, the surface growth process, or in some cases the actual soot volume fraction [49], are determined from measured mixture fraction and temperature conditions in diffusion flames. These results are then used as a basis for predicting surface growth over a wide range of flame conditions. A major advantage of this approach is the reduced detail which must be given to representing the chemical kinetic processes involved in the surface reaction mechanism.

The above work illustrates the detail to which present soot models and experiments can consider the fundamental mechanisms controlling individual processes. Despite the questions concerning the specifics of the surface growth mechanism, recent efforts to model soot particle growth in diffusion flames have met with some success in reproducing the general features of the soot formation process [57-68,81,82,88]. However, the model representation for the surface growth process shows a strong sensitivity to the specific surface growth rate constant [65]. In this case, small differences in the growth rate constant could be argued to be responsible for variations in the sooting propensity of various fuels. To resolve such questions further detailed measurements of surface growth rates, particularly under diffusion flame conditions are needed.

Before leaving the topic of surface growth, it is worth mentioning the importance that developments in the measurement of soot size and morphology are having in this area. The application of fractal concepts to laser light scattering measurements is providing more accurate determination of the actual soot particle surface area [7,33,34,41,89-92]. It has been well established that soot particle size is affected by coagulation and classical coagulation models have been well suited to describing the evolution of the number concentration of particles [9]. However, the specific nature of the resulting aggregate was typically argued to be spherical by necessity of the optical analysis employed. Although this approach yields reasonable relative trends with regard to particle size and surface area, it does have an inherent error since the particles are not truly spherical. The fractal approaches introduced recently are providing a better measurement capability for the determination of soot particle surface area and allowing a more detailed understanding of the structure of soot formed in flames.

SOOT PARTICLE OXIDATION

Following the termination of surface growth, oxidation of the soot particles can occur resulting in either total destruction or emission of some fraction of the soot particles. To effectively predict the oxidative destruction of soot particles, an understanding of the reaction rates as a function of temperature for various oxidizing species is required. Limited attention has been given to this area recently. An appropriate review of the present understanding of soot particle oxidation is provided by Neoh et al. [93]. Although discrepancies between various studies of soot oxidation have been described in the literature, there is a general consensus that the reactions with O_2 and OH are the dominant reaction pathways. Under lean conditions, O_2 is expected to be the dominant oxidizing species and the Nagle and Strickland-Constable expression has been traditionally used [94]. For fuel rich conditions, where the O_2 concentration is small, OH is the major oxidizing

species whose reactivity has been quantified by Neoh et al. [93].

Recent work has examined reaction rate data for O_2 and indicates that the tradition use of the Nagle and Strickland-Constable expression may lead to errors in assessing the importance of this oxidation route [95]. Studies of the importance of OH as oxidation species have also raised questions about the rate of O_2 reaction with soot particles [96a,b]. Additional work has also been reported on O and OH radicals [97]. These developments point to the need for continued examination of the oxidation stage of the soot formation and destruction process.

SUMMARY

The above discussion provides an overview of the key developments which have occured over the last decade in terms of increasing our understanding of soot formation and destruction. Not all the important work could be reviewed with the recent studies of soot formation in high pressure flames the most glaring omission. As we look into the future, we can expect to see increase attention given to turbulent flame systems and high pressure environments. More emphasis is likely to focussed on practical systems such as gas turbine and Diesel engines where soot impacts both performance and emissions issues.

ACKNOWLEDGEMENT

The author would like to acknowledge the support of the Air Force Office of Scientific Research, the National Institute of Standards and Technology, and the Office of Naval Research for their support of his research in this area.

REFERENCES

1. Palmer, H. B. and Cullis, C. F., *The Chemistry and Physics of Carbon*, (P. L. Walker, Ed.) Marcel Dekker, NY, Vol. 1 pp. 265-325 (1965).
2. Wagner, H. Gg., *Seventeenth Symposium (International) on Combustion*, The Combustion Institute, Pittsburgh, 1979, pp. 3-19.
3. Haynes, B. S. and Wagner, H. Gg., *Prog. Energy Combust. Sci.*, 7, pp. 229-273 (1981).
4. Wagner, H. Gg., "Soot Formation - An Overview," in *Particulate Carbon Formation During Combustion*, (D. C. Siegla and G. W. Smith, Eds.), Plenum Press, New York and London, 1981, pp. 1-29.
5. Calcote, H. F., *Combustion and Flame*, 42:215-242 (1981).
6. Glassman, I., *Twenty-Second Symposium (International) on Combustion*, The Combustion Institute, Pittsburgh, 1988, pp. 295-311.
7. Megaridis, C. M. and Dobbins, R. A., *Twenty-Second Symposium (International) on Combustion*, The Combustion Institute, Pittsburgh, 1988, pp. 353-362.
8. Puri, R., Richardson, T. F., Santoro, R. J. and Dobbins, R. A., *Combustion and Flame*, 92:320-333 (1993).
9. Graham, S. C., *Sixteenth Symposium (International) on Combustion*, The Combustion Institute, Pittsburgh, 1977, pp. 663-669.
10. Frenklach, M., Taki, S., Durgaprasad, M. B., and Matula, R. A., *Combustion and Flame*, 54:81-101 (1983).
11. Homann, K. H. and Wagner, H. Gg., *Eleventh Symposium (International) on Combustion*, The Combustion Institute, Pittsburgh, 1967, pp. 371-379.
12. Bittner, J. D. and Howard, J. B., *Eighteenth Symposium (International) on Combustion*, The Combustion Institute, Pittsburgh, 1981, pp. 1105-1116.
13. Böhm, H., Hesse, D., Jander, H., Luers, B., Pietsher, J., Wagner, H. Gg. and Weiss, M., *Twenty-Second Symposium (International) on Combustion*, The Combustion Institute, Pittsburgh, 1988, pp. 403-411.
14. Harris, S. J. and Weiner, A. M., *Combust. Sci. and Tech.*, 31, pp. 155-167 (1983).
15. D'Alessio, A., DiLorenzo, A., Sarofim, A. F., Beretta, F., Masi, S. and Venitozzi, C., *Fifteenth Symposium (International) on Combustion*, The Combustion Institute, Pittsburgh, 1974, pp. 1427-1438.
16. Wieschnowsky, U., Bockhorn, H. and Fetting, F., *Twenty-Second Symposium (International) on Combustion*, The Combustion Institute, Pittsburgh, 1988, pp. 343-352.
17. Bastin, E., Delfau, J.-L., Reuillon, M., Vovelle, C. and Warnatz, J., *Twenty-second Symposium (International) on Combustion*, The Combustion Institute, Pittsburgh, 1988, pp. 313-332.
18. Keil, D. G., Gill, R. J., Olson, D. B. and Calcote, H. F., *Twentieth Symposium (International) on Combustion*,

The Combustion Institute, Pittsburgh, 1984, pp. 1129-1137.
19. Harris, S. J. and Weiner, A. M., *Combust. Sci. and Tech.*, 32. pp. 267-275 (1983).
20. Cole, J. A., Bittner, J. D., Longwell, J. P. and Howard, J. B., *Combustion and Flame*, 56, p. 51, (1984).
21. Haynes, B. S. and Wagner, H. Gg., *Ber. Bunsenges. Phys. Chem.*, 84, pp. 499-506 (1980).
22. Kent, J. H., Jander, H. and Wagner, H. Gg., *Eighteenth Symposium (International) on Combustion*, The Combustion Institute, Pittsburgh, 1980, pp. 1117-1126.
23. Kent, J. H. and Wagner, H. Gg., *Combust. Flame*, 47, pp. 53-65 (1982).
24. Santoro, R. J., Semerjian, H. G. and Dobbins, R. A., *Combustion and Flame*, 52:204-218 (1982).
25. Santoro, R. J., Yeh, T. T., Horvath, J. J. and Semerjian, H. G., *Combust. Sci. and Tech.*, 53, p. 89 (1987).
26. Hura, H. S. and Glassman, I., *Twenty-second Symposium (International) on Combustion*, Pittsburgh, 1988, pp. 371-378.
27. Axelbaum, R. L., Flower, W. L. and Law, C. K., *Combust. Sci. and Tech.*, 61, pp. 51-73 (1988).
28. Axelbaum, R. L., Law, C. K. and Flower, W. L., *Twenty-second Symposium (International) on Combustion*, The Combustion Institute, Pittsburgh, 1988, pp. 379-386.
29. Vansburger, U., Kennedy, I. M. and Glassman, I., *Twentieth Symposium (International) on Combustion*, the Combustion Institute, Pittsburgh, 1984, pp. 1105-1112.
30. Schug, P., Manheimer-Timnat, Y., Yaccarino, P. and Glassman, I., *Combust. Sci. Tech.*, 22, pp. 235-250 (1980).
31. Axelbaum, R. L., and Law, C. K., *Twenty-third Symposium (International) on Combustion*, The Combustion Institute, Pittsburgh, 1990, pp. 1517-1523.
32. Honnery, D. R. and Kent, J. H., *Combustion and Flame*, 82:426-434 (1990).
33. Megaridis, C. M. and Dobbins, R. A., *Combust. Sci. and Tech.*, 71. pp. 95-109 (1990).
34. Megaridis, C. M. and Dobbins, R. A., *Combust. Sci. and Tech.*, 66, pp. 1-16 (1989).
35. Dobbins, R. A., Santoro, R. J. and Semerjian, H. G., *Progress in Astronautics and Aeronautics*, Vol 92., p. 208 (1984).
36. Glassman, I. and Yaccarino, P., *The Eighteenth Symposium (International) on Combustion*, The Combustion Institute, Pittsburgh, 1980, pp. 1175-1183.
37. Santoro, R. J. and Semerjian, H. G., *Twentieth Symposium (International) on Combustion*, The Combustion Institute, Pittsburgh, 1984, pp. 997-1006.
38. Kent, J. H. and Wagner, H. Gg., *Combust. Sci. and Tech.*, 41, pp. 245-269 (1984).
39. Kent, J. H. and Wagner, H. Gg., *Twentieth Symposium (International) on Combustion*, The Combustion Institute, Pittsburgh, 1984, pp. 1007-1015.
40. Flower, W. L. and Bowman, C. T., *Twentieth Symposium (International) on Combustion*, The Combustion Institute, Pittsburgh, 1984, pp. 1035-1044.
41. Megaridis, C. M. and Dobbins, R. A., *Twentieth Symposium (International) on Combustion*, The Combustion Institute, Pittsburgh, 1988, pp. 353-362.
42. Smyth, K. C., Miller, J. H., Dorfman, R. C., Mallard, W. G. and Santoro, R. J., *Combustion and Flame*, 62:157-181 (1985).
43. Gülder, Ö. L. and Snelling, D. R., *Twenty-third Symposium (International) on Combustion*, The Combustion Institute, Pittsburgh, 1990, pp. 1509-1515.
44. Gülder, Ö. L. and Snelling, D. R., *Combustion and Flame*, 92:115-124 (1993).
45. Gülder, Ö. L., *Combustion and Flame*, 88:74-82. (1992).
46. Shaddix, C. R., Harrington, J. E. and Smyth, K. C., *Combustion and Flame*, 99: 723-732 (1994).
47. Kent, J. H. and Bastin, S. J., *Combustion and Flame*, 56:29-42 (1984).
48. Nishida, O. and Mukohara, S., *Combustion and Flame*, 47:267-279 (1982).
49. Gore, J. P. and Faeth, G. M., *Twenty-First Symposium (International) on Combustion*, The Combustion Institute, Pittsburgh, 1986, pp. 1521-1531.
50. Sivathanu, Y. R. and Faeth, G. M., *Combustion and Flame*, 81:150-165 (1990).
51. Kent, J. H. and Honnery, D., *Combust. Sci. and Tech.*, 54, pp. 383-397 (1987).
52. Coppalle, A. and Joyeux, D., *Combust. Sci. and Tech.*, 93, pp 375-386 (1993).
53. Coppalle, A. and Joyeux, D., *Combustion and Flame*, 95:275-285 (1994).
54. Frenklach, M., Clary, D. W., Gardiner, W. C., Jr. and Stein, S., *Twentieth Symposium (International) on Combustion*, The Combustion Institute, Pittsburgh, 1984, pp. 887-901.
55. Frenklach, M., Clary, D. W., Gardiner, W. C., Jr. and Stein, S., *Twentieth-First Symposium (International) on*

Combustion, The Combustion Institute, Pittsburgh, 1986, pp. 1067-1076.
56. Frenklach, M., Yuan, T. and Ramachandra, M. K., *Energy and Fuels*, 2, pp. 462-480 (1988).
57. Frenklach, M. and Wang, H., *Twenty-Third Symposium (International) on Combustion*, The Combustion Institute, Pittsburgh, 1990, pp. 1559-1566.
58. Yoshihara, Y., Kazakov, A., Wang, H. and Frenklach, M., *Twenty-Fifth Symposium (International) on Combustion*, The Combustion Institute, Pittsburgh, 1994, pp. 941-948.
59. Kazakov, A., Wang, H. and Frenklach, M., *Combustion and Flame*, 100:111-120 (1995).
60. Colket, M. B., *Twenty-First Symposium (International) on Combustion*, The Combustion Institute, Pittsburgh, 1986, pp. 851-864.
61. Howard, J. B., *Twenty-Third Symposium (International) on Combustion*, The Combustion Institute, Pittsburgh, 1990, pp. 1107-1127.
62. Frenklach, M. and Harris, S. J., *J. of Colloid and Interface Sci.*, 118, pp. 252-261 (1987)
63. Kennedy, I. M., Kollmann, W. and Chen, H-Y., *Combustion and Flame*, 81:73-85 (1990).
64. Syed, K. J., Stewart, C. D., and Moss, J. B., *Twenty-Third Symposium (International) on Combustion*, The Combustion Institute, Pittsburgh, 1990, pp. 1533-1541.
65. Kennedy, I. M. and Markel, D. B., *Combust. Sci. and Tech.*, 94, pp. 303-314 (1994).
66. Mauss, F., Schäfer, T. and Bockhorn, H., *Combustion and Flame*, 99:697-705 (1994).
67. Markatou, P., Wang, H. and Frenklach, M., *Combustion and Flame*, 93:467-482 (1993).
68. Leung, K. M., Lindstedt, R. P. and Jones, W.P., *Combustion and Flame*, 87:289-305 (1991).
69. Lindstedt, R. P. and Skevis, G., *Combustion and Flame*, 99:551-561 (1994).
70. Norton, T. S., Smyth, K. C., Miller, J. H. and Smooke, M. D., Combust. Sci. and Tech. 90, pp. 1-34 (1993).
71. Hall, R. J., Smooke, M. D. and Colket, M. B., *Combustion Science and Technology Book Series*, in press.
72. Wang, H., Weiner, B. and Frenklach, M., *J. Phys. Chem.*, 97, pp. 10364-10371 (1993).
73. Stein, S. E., Walker, J. A., Suryan, M. M. and Fahr, A., *Twenty-Third Symposium (International) on Combustion*, The Combustion Institute, Pittsburgh, 1990, pp. 85-90.
74. Miller, J. H., Honnery, D. R., and Kent, J. H., *Twenty-Fourth Symposium (International) on Combustion*, The Combustion Institute, Pittsburgh, 1992, pp. 1031-1039.
75. McKinnon, T. J. and Howard, J. B., *Twenty-Fourth Symposium (International) on Combustion*, The Combustion Institute, Pittsburgh, 1992, pp. 961-971.
76. D'Alessio, A., D'Anna, A., D'Orsi, A., Minutolo, P., Barrella, R. and Ciajolo, A., *Twenty-Fourth Symposium (International) on Combustion*, The Combustion Institute, Pittsburgh, 1992, pp. 973-980.
77. Ciajolo, A., D'Anna, A., Barrella, R. and Tregrossi, A., *Twenty-Fifth Symposium (International) on Combustion*, The Combustion Institute, Pittsburgh, 1994, pp. 679-685.
78. Sunderland, P. B., Köylü, Ü, Ö, and Faeth, G. M., *Combustion and Flame*, 100:310:322 (1995).
79. Harris, S. J. and Weiner, A. M., *Twenty-Second Symposium (International) on Combustion*, The Combustion Institute, Pittsburgh, 1989, p. 333.
80. Roth, P. and Hospital, A., *Twenty-Fourth Symposium (International) on Combustion*, The Combustion Institute, Pittsburgh, 1992, pp. 981-989.
81. Honnery, D. R. and Kent, J. H., *Twenty-Fourth Symposium (International) on Combustion*, The Combustion Institute, Pittsburgh, 1992, pp. 1041-1047.
82. Delichatsios, M. A., *Combust. Sci. and Tech.*, 100, 283-298, 1994.
83. Dasch, C. J., *Combustion and Flame*, 61:219-225 (1985).
84. Tesner, P. A., *Combustion and Flame*, 85:279-281 (1991).
85. Woods, I. T. and Haynes, B. S., *Combustion and Flame*, 85:523-525 (1991).
86. Haynes, B. S., Jander, H. and Wagner, H. Gg., *Seventeenth Symposium (International) on Combustion*, The Combustion Institute, Pittsburgh, 1979, pp. 1365-1375.
87. Villasenor, R. and Kennedy, I. M., *Twenty-Fourth Symposium (International) on Combustion*, The Combustion Institute, Pittsburgh, 1992, pp. 1023-1030.
90. Leung, K. M. and Lindstedt, R. P., *Combustion and Flame*, 102:129-160 (1995).
89. Puri, R., Richardson, T. F., Santoro, R. J. and Dobbins, R. A., *Combustion and Flame*, 92:320-333 (1993).
90. Köylü, Ü. Ö., and Faeth, G. M., *Combustion and Flame*, 89:140-156 (1992).
91. Köylü, Ü. Ö., and Faeth, G. M., *Combustion and Flame*, 100:621-633 (1995).
92. Köylü, Ü. Ö., and Faeth, G. M., *J. Heat Transf.*, 116:152-159 (1994).

93. Neoh, K. G., Howard, J. B. and Sarofim, A. F., in *Particulate Carbon Formation During Combustion*, (D. C. Siegla and G. W. Smith, Ed.), Plenum Press, N.Y., 1981, p. 261.
94. Nagle, J. and Strickland-Constable, R. F., *Proc. of the Fifth Carbon Conf.*, Pergamon Press, London, 1963, 1, 1:154.
95. Cadman, P., Cornish, R. and Denning, R. J., *Seventeenth International Shock Tube Symposium*, 1990, pp. 751-755.
96. Puri, R. Santoro, R. J. and Smyth, K. C., (a) *Combustion and Flame*, 97:125-144 (1994); (b) *Combustion and Flame*, 102:226-228 (1995).
97. Roth, P. Brandt. O, and Gersum, S. von, *Twenty-Third Symposium (International) on Combustion*, The Combustion Institute, Pittsburgh, 1990, p. 1485.

Appendix B: Measurement and Analysis of Growth Species and Soot Surface Growth in a Laminar Diffusion Flame

by

D. C. Rapp and R. J. Santoro

To be submitted to Combustion and Flame for publication

MEASUREMENT AND ANALYSIS OF GROWTH SPECIES AND SOOT SURFACE GROWTH IN A LAMINAR DIFFUSION FLAME

Darrell C. Rapp and Robert J. Santoro
Propulsion Engineering Research Center
and
Department of Mechanical Engineering
The Pennsylvania State University
University Park, PA 16802-2320

RUNNING TITLE: Soot Growth: Species Measurements and Analysis

MEASUREMENT AND ANALYSIS OF GROWTH SPECIES AND SOOT SURFACE GROWTH IN A LAMINAR DIFFUSION FLAME

Darrell C. Rapp and Robert J. Santoro
Propulsion Engineering Research Center
and
Department of Mechanical Engineering
The Pennsylvania State University
University Park, PA 16802-2320

ABSTRACT

Newly added measurements of the spatial distribution of species concentrations in a ethene/air, coannular, laminar diffusion flame have been integrated with previous measurements of soot and flowfield (parameters, quantities) to establish the mechanism controlling the cessation of soot surface growth. In particular, the measurements of C_2H_2 and other hydrocarbons have revealed that soot surface growth ceases due to the depletion of hydrocarbons and not due to the loss of soot particle reactivity. This observation is in agreement with recent work by Honnery and Kent, who have shown that in long laminar diffusion flames, soot growth can be extended to very long residence times. Values for the specific surface growth rates in this diffusion flame are in agreement with previous measurements in both premixed and diffusion flames. Now that concentrations of many intermediate hydrocarbons, including C_2H_2 and C_6H_6 are available in a diffusion flame, the rate coefficient for surface growth by C_2H_2 can be calculated and is in agreement with values found in premixed flame studies.

INTRODUCTION

The evolution of soot particles has been the object of study in a wide variety of flame environments. Although studies conducted in practical devices, such as gas turbine combustors or Diesel engines, have yielded much useful engineering insight, fundamental understanding of soot formation and destruction has been typically gleaned from simpler flame studies. Much of the basic understanding of soot formation is a result of experimental work in shock tubes, low pressure and atmospheric pressure premixed flames, and diffusion flames [1-19]. However, knowledge of the chemical environment as it relates to soot formation has come primarily from experiments in premixed flat flames [3-11] and been supplemented by computer models [20-23]. These experimental conditions differ from many practical applications which involve non-premixed conditions. Therefore, it is important to study soot formation processes under conditions where diffusive and mixing processes control the reaction rate (high Damköhler Number). Furthermore, when focusing on fundamental soot phenomena it is important to select as simple an environment as possible while retaining the major characteristics of diffusion flames. Though all practical combustion devices can have turbulence to very high levels, it is more tractable to

study soot formation under laminar conditions where the complexities of turbulence do not obscure the primary object of study.

Among the simplest laminar diffusion flames which contains many characteristics of practical combustors is an axisymmetric system of gaseous fuel issuing from a tube with a larger flow of air surrounding it. The experimental setup is straightforward and the flames are quite stable. In the present experiment, the burner configuration and dimensions are identical to that used by previous researchers to acquire a significant set of data on flow variables (temperature and velocity) [14], and on the soot aerosol (volume fraction, number density and particle diameter) [12]. Recently, hydroxyl radical (OH) mole fractions have been determined using laser-induced fluorescence [24] and fluorescence from polycyclic aromatic hydrocarbons (PAH) have been examined [25]. Due to this extensive database, researchers involved in the numerical modeling of the soot formation and/or chemical kinetics in diffusion flames have endeavored to model this system [26, 27].

The present work expands on this set of data for a laminar diffusion flame burning C_2H_4 in air at atmospheric pressure. The information to be added to the existing measurements involve the spatial distribution of the molecular species in the flame. When combined with the velocity measurements, knowledge of the environment surrounding the soot particles on a temporal basis is gained. The following discussion will pursue a more sophisticated analysis of the data than previously possible in the surface growth region.

In order to determine the distribution of molecular species throughout the flame, a method of measuring the concentrations is necessary. Although several non-intrusive laser-based techniques exist for species measurements (e.g. LIF, absorption, CARS, Raman) many are limited in the number of species that can be quantitatively measured. Furthermore, when soot particles are present interference with the measurements can make these techniques difficult if not impossible to implement [28]. Therefore, intrusive probes, which have been used for many years, will be used to extract gas samples for on-line or later batch analysis.

EXPERIMENTAL

A laminar ethene/air diffusion flame was established on a coannular burner similar in design to that used in previous studies [12] and only a brief description will be given here. This burner consists of a 1.11 cm diameter brass fuel tube surrounded by a 10.2 cm diameter air annulus. A brass cylindrical chimney was used to shield the flame from laboratory air currents with access for sampling provided by slots machined in the chimney wall. The ethene and air flow rates were 3.85 cm^3/s and 713 cm^3/s respectively, which were measured with calibrated rotameters. Ethene with a stated purity of 99.5% was used, while filtered and dried air was supplied by an in-house compressor. These conditions replicate those of Santoro and coworkers [12-14, 24, 25, 29] so that the current and previous measurements can be brought together synergistically.

The extraction of gas samples is accomplished throughout the flame using an intrusive quartz microprobe sampling approach. Quartz microprobes have been used in many studies to perform the extraction of gas samples from premixed flames [4, 11, 30, 31] and diffusion flames [32-36]. Until

recently their use has been limited to regions where the soot volume fraction is low to avoid clogging the small probe orifice (≈100 μm). A variation of the standard quartz microprobe design, referred to as an Electro-Mechanical Sonic (EMS) probe developed by Puri [36], is shown in Figure 1 and enables sampling in flame regions where soot volume fractions are on the order of 10^{-5}.

The EMS probe utilizes a fiber that extends through the orifice and is attached to a solenoid core with springs on either side of the core. A solenoid is placed around the outside of the quartz tube and the current to the solenoid is interrupted at 20 - 30 Hz, providing for constant oscillatory motion of the fiber within the orifice, thus keeping an annular region open for gas sampling. The fiber for this study is ≈125 μm in diameter and is made from sapphire, while the orifice diameter is ≈200 μm. The annular sampling region has an area equivalent to a ≈150 μm diameter orifice.

At the soot levels encountered in this flame (volume fraction up to 10^{-5}), it is required to supplement the EMS probe with a rapid insertion procedure similar to that originally described by Kent and Wagner [19] for use with thermocouples in flames with high soot concentrations. This procedure involves alternately removing the probe tip from the sample location in the flame to a lean, high temperature region where soot will burn from the tip leaving a clean orifice before moving to the next sample location.

SPECIES ANALYSIS

Analysis of the collected gas samples was performed using a gas chromatograph (GC) and a mass spectrometer (MS). The use of these two techniques allowed an independent verification of the concentration profile measurements as well as providing specific species measurement capability as described below.

Gas Chromatograph: A Hewlett-Packard 5890 GC employed Porapak Q and Porapak S columns coupled with a molecular sieve (5Å) for species separation using a column sequence reversal technique and temperature programming. A dry ice bath was used to extract H_2O from the sample to simplify storage requirements. A Thermal Conductivity Detector (TCD) was used for detection of all non-hydrocarbons (N_2, O_2/Ar, CO, and CO_2). A Flame Ionization Detector (FID) was used for detection of hydrocarbons in small concentrations. For concentrations of hydrocarbons which were beyond the linear range of the FID, the TCD was used. A signal integrator is attached to each detector for the recording of the chromatogram.

Since the gas chromatograph requires the sample to be at atmospheric pressure for analysis and the EMS probe collects sample gas at low pressure, a method was devised to collect a sample in a cylinder and compress it with a piston for storage in a multiloop sample storage system [36]. The schematic of this compression apparatus is shown in Figure 2. Each sample is stored in a 10 cm^3 loop at a pressure of two atmospheres. After fifteen samples are collected in separate storage loops, the sample storage system is connected to the GC and each sample is analyzed sequentially. One of the GC signal integrators controls the GC and the multiposition valve connected to the sample storage system.

Calibration of the GC was primarily done using commercially available gas mixtures with accuracy of ±2%. The GC was also calibrated for fuel species concentrations much greater than that available commercially using laboratory prepared mixtures. The GC signal integrators used with the TCD and FID were able to perform multi-level calibrations for species which spanned large ranges in concentrations. The molecular species calibrated and measured directly with the GC are N_2, O_2/Ar, CO_2, CO, CH_4, C_2H_2, C_2H_4, C_2H_6, C_3H_6, C_3H_8, C_4H_6 and C_6H_6. The columns cannot separate O_2 and Ar. Therefore, a procedure which assumes the mole fractions of N_2 and Ar remains in the same ratio as in air is used to determine the mole fraction of O_2 and Ar individually.

For optimal detection of species with the TCD, helium was used as the carrier gas. Since detection depends on the difference in thermal conductivities, measurements of molecular hydrogen are problematic. In addition, the samples were dried prior to storage, thus, the H_2O concentration is obtained by a hydrogen atom balance approach developed by Puri [36] which assumes all species diffuse similarly. This method calculates the total amount of H atom present in the sample from the hydrocarbon species present, equation 1a. The total amount of carbon atom is then calculated from the carbon containing species, equation 1b. Then the total amount of H atom which should be present in the sample based on the amount of carbon present and the carbon to hydrogen ratio in the fuel, and the actual H atom present are used to calculate the amount of H_2O present in the flame at that position, equation 1c. Finally the dry measurements were normalized with the calculated H_2O concentration assuming the measured species mole fractions sum to one. This method overestimates the concentration of H_2O since it ignores molecular hydrogen, but the mole fractions are unaffected since both species contain two hydrogen atoms.

$$H = \sum y X_{C_x H_y} \tag{1a}$$

$$C = \sum x X_{C_x H_y O_z} \tag{1b}$$

$$X_{H_2O} = ({}^{H}/_{C_{fuel}} \cdot C - H)/2 \tag{1c}$$

Since not all hydrocarbons in the flame sample are quantitatively determined and the hydrogen to carbon ratio in these unsaturated hydrocarbons and soot is less than in the fuel, the amount of H_2O/H_2 is underpredicted as a result. This factor along with the higher diffusivity of H_2 could be a factor in bringing the H_2O measurement back in line with what is actually present in the flame.

Mass Spectrometer: The mass spectrometer employed an Extrel model 7-324-9 quadrupole mass filter with mass range of 1-500 u for separation of ions and an electron multiplier for detection. A computer controlled the ionizer, the mass filter and the burner position while the signal was recorded by the computer through an A/D converter.

As shown in Figure 3, a staged vacuum pumping system was employed. The EMS probe was used to continuously extract sample gas from the flame. The pressure in the small vacuum chamber was on the order of 1 Torr. The orifice of a second quartz probe was situated in the exit stream of the EMS probe and allowed a small amount of the flame sample gas to pass into the high vacuum

chamber where the pressure was on the order of 10^{-6} Torr. The secondary probe discharges the sample into the electron impact ionizer which has tungsten filaments. The resultant ions were extracted, focused and accelerated into the mass filter for separation. The mass filter was operated in single ion mode and the ionizer was operated at 20 eV or less to reduce molecular fragmentation.

The calibration method for the MS follows the procedure given by Ermolin et al. [37] as shown in equation 2 where F_i and S_i are the calibration factor and signal intensity respectively for species i. This method is mathematically similar to Bittner [31] and Crowhurst and Simmons [33]. The method relies on the signal response relative to other species remaining constant. That is, for a given mixture the ratio of the signals due to two gases will always be the same and, therefore, is independent of variations in mass flow through the orifice due to orifice clogging or variations in density. Secondly, this method assumes that the species measured constitute all of the gases present which are normalized to a mole fraction of one.

$$X_i = \frac{F_i S_i}{\sum F_j S_j} \tag{2}$$

Determination of the calibration factors were performed with a gas of known mole fraction of a given species flowing through the burner fuel tube so that any biases relating to the sampling procedure or MS characteristics are included in the calibration factor, F_i. Calibrations for N_2, O_2, and Ar used air as the standard gas. Calibration of H_2O employed a N_2 stream saturated with H_2O vapor at a known temperature. Other species used commercial calibration mixtures or calibrated flowmeters to mix pure gases in the appropriate ratios. The molecular species quantitatively measured by the MS are N_2/CO, O_2, H_2O, CO_2, H_2, CH_4, C_2H_2, C_2H_4, and Ar.

One limitation of the use of a MS in the present study is the coincidence of C_2H_4, N_2 and CO at mass 28. For C_2H_4, the fragment at mass 27 was used as an independent measurement. Calibration of C_2H_4 at both masses 27 and 28 was necessary so that the signal contribution of C_2H_4 at mass 28 could be subtracted from the mass 28 signal. C_2H_4 was similarly calibrated and subtracted at mass 26 where C_2H_2 was measured.

Furthermore, it is not possible to determine the signal of N_2 or CO independently with the MS. Therefore, the analysis is performed as though there was no CO present. Since CO, as determined by the GC measurements, can yield mole fractions of close to 0.10 at some locations in the flame, this approach will overpredict the N_2 by somewhat more than the measured CO concentration due to the greater sensitivity of the MS to CO and reduce the mole fractions of other species slightly due to the normalization procedure shown in equation 2.

To determine the centerline position, the MS data was used since these data were obtained across the entire diameter of the flame and were generally symmetrical. The primary method was to assign the two locations where fuel and oxygen disappear to the same radius. At higher axial positions where the fuel was totally consumed, either the C_2H_2 or H_2 profiles were used in a similar manner or directly to center the data. Due to sample storage limitations, samples for GC analysis

were obtained for only one-half of the flame diameter. Therefore, the radial position of the GC data was determined by setting the position where fuel and oxygen disappear to match the MS measurements.

Measurements using the above instrumentation will be combined with the temperature (fine wire thermocouples), velocity (Laser Doppler Anemometer) and soot aerosol information (laser extinction and scattering) which have been published earlier for this same flame [12-14]. The experimental details of those measurements are not discussed here.

RESULTS

Spatially resolved measurements of molecular species have been determined throughout the region of the flame where soot undergoes growth processes. Measurements at a given axial position were taken at 0.5 mm radial steps with the MS, while the GC measurements were limited to 15 samples per experiment, so samples were taken judiciously to resolve the important features in the flame. For the species measured by both instruments the results generally agreed to ±20% or better with the exception of acetylene which displayed a somewhat larger difference for the two measurement techniques. However, due to the subtraction procedure for calculating the mole fraction of C_2H_2 with the MS the measurements of acetylene agreed within the measurement errors. As an illustration of the spatial distribution of the mole fractions of C_2H_4 and C_2H_2, Figure 4 shows the radial measurements of these species for several heights in the flame for both the GC and MS. Note that the rapid consumption of the fuel results in a maximum C_2H_4 mole fraction of less than 0.01 at 30 mm above the burner outlet while the luminous flame height is approximately 88 mm.

Examination of the radial profile for the C_2H_2 mole fraction at the 7 and 10 mm heights indicates the maximum value occurs at a radial position different from the centerline. This result implies that the highest production rates for C_2H_2 occurs in an annular region approximately 4-5 mm in radius. The temperature and C_2H_4 mole fraction in this region of the flame ranges from approximately 1300 - 1700 K and 0.0345 to 0.185 respectively. The quantity of C_2H_2 at the centerline indicates some production of C_2H_2 throughout the central region of the flame where the C_2H_4 mole fractions are much greater. In fact, the increase in the maximum mole fraction, indicating net production of C_2H_2, continues through to the 20 mm axial measurement location where the temperature is 1421 K. After the 30 mm height, the peak C_2H_2 mole fraction decreases by a factor of about four by 40 mm to 0.01 and further decreases by a factor of about ten by 50 mm to 0.001 as reactions proceed. The peak in the integrated soot volume fraction in this flame occurs at the 40 mm height and the concentrations measured show only a small amount of measured hydrocarbons remaining to be oxidized. At this height, soot represents 14% of the total carbon flow rate in the flame [14]. The major gaseous species remaining to be oxidized at this height are CO, H_2, and C_2H_2 with peak mole fractions of approximately 0.07, 0.02, and 0.01 respectively.

Several other intermediate hydrocarbon species were measured quantitatively by the GC and may be considered important in soot formation in this flame. These include C_4H_6 and C_6H_6 shown as radial profiles at several axial positions in Figure 5. C_4H_6 is closely related to C_4H_5 which has

been proposed to play an important role in the formation of the first aromatic ring [6] and C_6H_6 is the first aromatic. Note that the mole fractions for these species have a spatial development which is characteristic of intermediate species in this flame, that is similar to C_2H_2. For these intermediate species, the mole fraction is low initially, sometimes with a peak concentration in the annular region or a broad region where the mole fraction is relatively constant. The concentration increases with height and the maximum moves towards the centerline, and then the concentration decreases as consumption becomes dominant. This behavior has been seen previously in similar flames burning methane [38]. The species CH_4, C_2H_6 and C_3H_6 also show similar characteristics during their development through the flame. These species have maximum mole fractions in the flame of 0.0038, 0.00027 and 0.00020 respectively.

Finally, several peaks on the GC chromatogram were present throughout much of the fuel rich region. However, only the elution times and integrated areas are available since these species are not identified. A double peak elutes very close in time to that of C_3H_6 and C_3H_8. Analysis of a flame sample on a GC with an HP-1 capillary column shows a large peak with a retention index very close to both propadiene (allene) and propyne (methyl-acetylene), both are C_3H_4 structures. Propadiene is related to the propargyl radical (C_3H_3) which has been proposed to play an important role in the formation of the first aromatic ring directly from C_3 species [23]. Estimating the calibration factor for these unidentified species as similar to that of the C_3H_6 and C_3H_8 would give these species maximum mole fractions greater than 100 ppm.

Measurements were also taken with the MS at masses 50 and 78. The molecular formula for these masses are C_4H_2 and C_6H_6 respectively. These species have no calibrations for them so only relative signal values are available. These masses could also be fragments of species at larger masses. For instance, at mass 50, the signal could be a combination of this species that is present in the flame and other species from the flame with larger masses (e.g. C_4H_4, C_4H_6) which have been fragmented in the ionizer of the MS. The measurements of these intermediate species with the MS indicate a similar development through the flame as found in the GC measurements for other intermediate species.

Most of the discussion which follows will focus on the measurements from the GC. This is due to the lack of interference between species at different masses from fragmentation during ionization in the MS. Moreover, identification and quantification of several additional species is possible with the GC.

DISCUSSION

One question which arises in both premixed and diffusion flames with respect to soot formation pertains to the cessation of growth of soot particles in the flame. In rich premixed flames, it has been found that significant quantities of C_2H_2 and other hydrocarbons are present in the post flame region [5, 8]. It is in this region that particle inception occurs and the surface growth reactions proceed. Furthermore, the rate of these surface reactions decreases with time while the smaller hydrocarbon species concentrations do not change appreciably. This experimental result has been

used to argue that the reactivity of the particles decreases with time and has been discussed by others [15, 39, 40].

In diffusion flames with significant soot levels, no experimental information has been available about the chemical environment surrounding the soot particles as they traverse the flame. The combination of the previous measurements of Santoro and coworkers [12-14] with the spatial species measurements enables analysis which can help to elucidate greater understanding about some of the soot chemistry which is occurring.

The following analysis integrates the previous measurements of flowfield and soot with the molecular species information now available. From the velocity and temperature measurements, soot particle paths have been determined and, thus, the spatial measurements can be transformed into temporal measurements along a particle path [14]. Consequently, the detailed temporal evolution of soot particle growth with respect to its thermochemical environment can be obtained. In the present case, the soot growth process will be examined in relation to the concentration field of several hydrocarbon species. In particular, the C_2H_2 mole fraction will be examined in greater detail since this species has been argued to be the primary growth species in premixed flames [8]. In examining this process, a total of seven particle paths will be considered which are numbered 1 - 7 with the centerline being particle path 1 and proceeding radially outwards through particle path 7. Three particle paths will be discussed in greater detail. One particle path is the centerline of the flame (PP 1). A second considers the particle path which passes through the maximum observed local soot volume fraction for the entire flame (PP 6). A third particle path is partway between these two and is designated the middle particle path (PP 3). For the paths away from the centerline, the appropriate data from both sides of the flame have been averaged and then the analysis performed. This is due to the symmetric nature of the flame and the arbitrary choice which would be necessary when combining the two sets of data.

Figure 6 shows the local soot volume fraction, f_v, and the C_2H_2 mole fraction as a function of time along particle paths 1, 3 and 6. The trends on these three particle paths are typical of the evolution observed along other particle paths in the flame. The important characteristic is that the soot volume fraction achieves a maximum at the same axial location where the C_2H_2 concentration falls to near or below detectability (approximately $2x10^{-5}$ for the GC). The measurements of the other hydrocarbons from both the GC and MS indicate a similar depletion at the same height or even earlier in the flame. Thus, it is argued that the depletion of hydrocarbons available for soot particle growth is the reason for particle growth ceasing. The present measurements for this ethene/air diffusion flame show a different mechanism for the cessation of soot growth is operative as compared to premixed flames.

The underlying phenomenon of this growth cessation presented above has two parts. These are best explained by looking at a general rate equation for soot formation in equation 3. It is first important to notice that when the changes in the local soot volume fraction are plotted on a time coordinate along a particle path, it is the net result of the growth and oxidation rates which is determined. So obviously, a transition from net soot formation to net soot destruction occurs when the soot concentration reaches its maximum along a given particle path.

$$\dot{\omega}_{soot} = Growth - Oxidation \tag{3}$$

When one proceeds to examine why such a transition occurs, it is necessary to consider the structure of the flame and the specifics of the soot growth process. In a coannular, laminar diffusion flame, fuel is transformed into products as one proceeds higher in the flame. The data from the present study shows that beyond the 30 mm height above the burner exit, all measured hydrocarbon concentrations decrease dramatically. This decrease in hydrocarbons available for soot growth will slow the growth reactions since this rate would generally be dependent upon the concentration of the hydrocarbon species participating in surface growth reactions.

Secondly, this decrease in hydrocarbons is followed by an increase in species (especially O_2) available to participate in the oxidative reactions. The concentrations of H_2O and CO_2 which could also participate in soot oxidation is relatively high everywhere in the flame. Coincident with this transition from hydrocarbon rich to oxygen rich is a reaction zone with an (associated) temperature rise. Therefore, the growth reactions in equation 3 decrease and the oxidation reactions increase, which yields the position of maximum local soot volume fraction along a given particle path. This corresponds to the position where the local equivalence ratio based on measured gaseous species as calculated with the method discussed by Mitchell et al. [41] has fallen below a value of one as shown in figure 7.

Additional evidence that supports a mechanism of soot growth cessation in laminar diffusion flames which differs from that dominant in premixed flames can be gleaned by examining the temperatures along these particle paths and using the analysis results from premixed flames of Dasch [39] and Woods and Haynes [40] to examine the decrease in soot particle reactivity. Equation 4 expresses the decay in the reactivity of the soot surface as taken from Dasch [39] and Woods and Haynes [40]. The term k_{SG}, which was determined from Woods and Haynes [40], is the same term as α used by Dasch [39]. Figure 8 shows the temperatures along the three particle paths with the time a particle path crosses the 3 mm axial height set to zero.

$$k_{C_2H_2} \Big/ k^o_{C_2H_2} = N_s \Big/ N^o_s = \exp(-\alpha t) \tag{4a}$$

$$\alpha = 3.5X10^7 \exp(-T_a / T) \tag{4b}$$

While it may not be good practice to apply the above formula for reactivity decay to non-isothermal flames [15, 42] there is insight to be gained by proceeding along this line of analysis. If the maximum temperature along the particle path for the soot growth region (i.e. from initial detection of soot to the maximum soot volume fraction along a given particle path) is chosen, one can calculate a conservative estimate of the decrease in the soot particle reactivity along that particle path based on the results from premixed flames. For particle paths 1, 3 and 6 the maximum temperatures and soot residence times are shown in Table 1. Data for two additional flames are also shown in Table 1. The first is an atmospheric pressure premixed flame burning C_2H_4/air and the second is the centerline of a C_2H_4/air diffusion flame discussed by Honnery and Kent [43]. The latter flame has a residence time that is about five times longer than any observed for the

TABLE 1 Data for and calculation of particle reactivity decrease along several particle paths

Particle Path	Maximum Temperature (K)	Soot Growth Residence Time (s)	Characteristic Time (s)	Fraction of Initial Reactivity
PP 1	1439	0.017	0.196	0.92
PP 3	1567	0.035	0.054	0.69
PP 6	1613	0.026	0.036	0.49
Harris and Weiner [9]	1750	0.02	0.012	0.19
Honnery and Kent [43]	≈1250	>0.2	2.11	0.91

present study. The characteristic time, $1/\alpha$, for soot particle reactivity decrease is calculated using the activation temperature and expression of Dasch [39] (see equation 3) which uses an activation temperature of 22650 K. The fraction of initial reactivity that would remain when growth ceases in this flame is also shown in Table 1. The Arrhenius nature of the expression for the reactivity decrease can be expected to differ somewhat in the temperature range observed in the present diffusion flame. However, Woods and Haynes [40] did not expect this effect to be significant.

Particle path 7 (not shown) has the highest maximum temperature (1786 K) and the fraction of initial reactivity by this conservative estimate is 0.03. However, the temperature during much of the growth along this and all the other particle paths is typically 1300 - 1600 K. So the values of the fraction of initial reactivity from Table 1 are more typical of that in the bulk of the flame. Furthermore, when the data from Honnery and Kent [43] is used along the centerline of their flame, this analysis yields a fraction of initial reactivity available at the end of growth of 0.91. These values for the surface reactivity indicate that the continued growth of soot in diffusion flames to very long residence times is not in conflict with the results obtained by others in premixed flames. The premixed flame has higher temperatures and comparable residence time to the current flame, resulting in a lower reactivity. These calculations further support the interpretation that soot surface growth in laminar diffusion flames ceases due to the depletion of gas phase reactants.

Rate Analysis: Previous analysis of soot surface growth in laminar diffusion flames has been limited to analysis of data from the soot aerosol itself [14, 25, 44] due to a lack of species measurements in flames with significant soot levels. To perform an analysis of the chemistry of the growth process requires the determination of a specific chemical mechanism. Surface growth of soot particles can result from a number of processes including heterogeneous reactions of a gaseous molecule with the surface and condensation of large hydrocarbons, generally PAH, on the surface. The mechanism which has received much attention is a reaction between the soot surface and a gas phase hydrocarbon. The work of Harris and Weiner [8] has been instrumental in

determining constraints on the potential growth species which could be important in the surface growth process in premixed flames. Their conclusion was that the rate of growth of the volume fraction of soot is a result of the heterogeneous reaction of C_2H_2 with the soot surface and can be expressed as equation 5. With the data available, the rate coefficient in this expression can be determined and compared to premixed flames.

$$\dot{\omega}_{soot} = k_{C_2H_2} S X_{C_2H_2} \tag{5}$$

This equation assumes that the oxidation rates under the fuel rich, premixed flame conditions they studied are much smaller than the growth rates, and the species terms in the equation describing general soot growth, equation 3, are small except for the term involving C_2H_2. Harris and Weiner [10] estimated that only 10-15% of the growth of soot comes from C_4H_2. It was also found that C_2H_2 explained the soot growth rate in an ethene/toluene premixed flame [10], where levels of aromatic species are expected to be much greater than in a pure C_2H_4 flame. Moreover, recent modeling work [22] has shown that C_2H_2 can explain the growth of soot in high pressure, premixed ethene flames.

In previous studies of both premixed and diffusion flames [8, 17, 25, 29, 44, 45], the formation rate of soot, $\dot{\omega}_{soot}$, along a particle path was calculated from equation 6. This expression is valid when the gas density (temperature and molecular weight) remains constant. However, because the volume fraction is tied directly to the gas density, the mass growth of soot becomes equation 7 when the soot conservation equation is solved. This expression assumes an ideal gas and a constant molecular weight. The latter assumption is well satisfied in this flame since the fuel molecular weight is 28.05 and the air has an average molecular weight of 28.96. Measurements of the average molecular weight also bear this out. As can be seen from figure 8 the rate of change of temperature is relatively low except as the particle path crosses a reaction zone. In the case of a particle path exiting the fuel rich region, this increased density correction term coincides with the soot volume fraction reaching its peak and the corresponding mass growth rate of soot being small. Therefore, measurements in this region can have large relative corrections due to changes in gas density. For this reason, locations where this correction is greater than 20% of df_v/dt, are not included in the analysis.

$$\dot{\omega} = \rho_{soot} \frac{df_v}{dt} \tag{6}$$

$$\dot{\omega} = \rho_{soot} \left(\frac{df_v}{dt} + \frac{f_v}{T} \frac{dT}{dt} \right) \tag{7}$$

As previously mentioned, the changes in the soot mass along a particle path is a reflection of the difference of the growth rate and the oxidation rate of soot, equation 3. Therefore, it could be important to account for oxidation reactions when determining the rate of reactions contributing to the growth of soot. The major species available to participate in soot oxidation are O_2, CO_2 and H_2O. Rate expressions for the reaction rates of these species with soot are given in references [46-48]. As seen in figure 9 there is generally about 0.003 mole fraction of O_2 in the fuel rich region of

the flame. This has been noted previously in coannular diffusion flames [34, 38, 41, 49] and is generally attributed to leakage of O_2 at the burner lip where reactions are quenched [41]. In addition, the mole fractions of CO_2 and H_2O in the soot growth region range from 0.06 to 0.14 and 0.14 to 0.19 respectively.

The rate expression for O_2 from Bradley, Dixon-Lewis et al. [48] is the mechanism from Nagle and Strickland-Constable [50]. This mechanism for soot oxidation has been used quite extensively in recent studies [26, 51, 52]. This expression was validated by Park and Appleton [53] in a shock tube study of soot oxidation. However, the range of temperature and O_2 concentrations in that study are above those found in this experiment. In addition, the Nagle and Strickland-Constable rate has been found to overpredict the oxidation rate of soot at lower temperatures [54, 55]. In comparison, the O_2 reaction mechanism from Libby and Blake [46, 47] indicates a reaction rate from five to ten times *faster* than the Nagle and Strickland-Constable rate [50] at the temperatures and O_2 mole fractions encountered in this flame. Additional evidence that the Nagle and Strickland-Constable [50] rate could be too fast is the calculated oxidation rate in the lean part of several C_2H_2 flames exceeding the measured rate of soot oxidation by a factor of roughly 7 [52].

Further examination of the rate for CO_2 oxidation by the Libby and Blake [46, 47] mechanism is generally within a factor of two of the rate given by the Nagle and Strickland-Constable [50] mechanism for O_2 at their respective concentrations. Therefore, these oxidation rates will not be used in further analysis. Though the evidence cited above indicates that the Nagle and Strickland-Constable [50] soot oxidation rate is not accurate under the conditions present in this flame, this is still the most popular mechanism for calculating soot oxidation rates by O_2 by those mentioned earlier. Therefore, these O_2 rates and the rates for CO_2 and H_2O from Bradley et al. [48] will be used. In the region of large net soot growth, the correction due to oxidation is on the order of 10% of $^{df_v}/_{dt}$, primarily from O_2. However, near the end of soot growth, this correction becomes a much greater fraction of the growth rate. The following analysis will exclude locations where the oxidation correction is greater than 50% of the $^{df_v}/_{dt}$.

Two procedures were performed to find $^{df_v}/_{dt}$ in this two dimensional flame. For the first procedure, the first step is to transform the volume fraction data along a given particle path into rates of growth ($^{df_v}/_{dt}$) at the measurement points. To accomplish this, a weighted polynomial curve fit (typically fifth order) was performed on the volume fraction data and the derivative taken. This approach was chosen since all of the data (f_v, species, etc.) were taken at the same axial positions. The soot volume fraction data and the particle paths coordinates for this analysis were taken from Santoro et al. [14]. Deciding the best fit to represent the soot growth when varying the polynomial order and capturing the transition from growth to oxidation was somewhat subjective.

Therefore, a second approach which used data available in our lab through the technique of 2-D Laser Induced Incandescence (LII) was performed [56]. The steps were to take the 2-D image of the soot volume fraction field and extract a smaller section with dimensions 6.02 mm axially and 1.35 mm radially (this corresponds to a section 41 by 10 pixels respectively) that was centered on the location of interest. A third order, polynomial least squares fit of this surface (ten coefficients) was performed on this smaller section of volume fraction data. The particle path locations and the

velocities were taken from [14]. The measured velocities are important for the directional derivative along the surface, equation 8.

$$\frac{df_v}{dt} = \bar{V} \cdot \nabla f_v \qquad (8)$$

The two methods of determining df_v/dt give comparable growth rates. Typically, the LII method resulted in slightly greater values. On average, the LII results were approximately 30% greater than that determined by curve fitting and most were within a factor of two. Many of the instances where the two growth rates differed by the largest amounts were at the point where soot is first detected or near the peak in soot volume fraction where the transition from growth to oxidation occurs. Both of these locations are difficult to capture accurately with the limited data available along a particle path from light scattering and extinction since data is only taken every 10 mm in the axial direction. Other factors also contribute to the systematic uncertainty in estimating the soot mass growth rate [9].

The values of the species mole fractions at a given axial position along a particle path were interpolated from the measured radial locations. This procedure was done on the same seven particle paths in order to accumulate 27 points. When locations with corrections due to density changes larger than that allowed in this were eliminated, 22 points remained. The locations that were eliminated for having large density corrections, also corresponded to the same locations that had large oxidation corrections. It is important to note that C_2H_2 and CH_4 are the only hydrocarbon species which are detected throughout the soot growth region.

Before comparing soot growth results from premixed and diffusion flames, several things should be pointed out. The soot growth region in the premixed flames listed in Table 2 can be at significantly greater temperatures than the bulk of the soot growth region in the diffusion flame of this study. The temperature range of some of the premixed flames is 1600-1700K [9]. In the laminar diffusion flame studied here, the temperatures where soot growth occurs is lower, generally 1300-1500K [14], though several points near the end of growth have temperatures above 1600 K. The higher temperatures in the premixed flames could lead to oxidation corrections that are important. However, in most previous studies, the calculation of the Specific Surface Growth Rate (SSGR), equation 9, and the rate coefficient for the premixed flames, $k_{C_2H_2}$, no correction for oxidation was made. Therefore, the SSGR and rate coefficients of this study presented in Table 2 have only been corrected for the density changes which occur along a particle path. The rate coefficients with oxidation correction included are not appreciably different than those calculated with only the density correction. In addition, no density correction is applied to the premixed flame data since the temperature in the postflame zone of the 1-D flames is relatively constant.

$$SSGR = k_{C_2H_2}[C_2H_2] = \frac{\omega_{soot}}{S} \qquad (9)$$

Table 2 Specific Surface Growth Rate (SSGR), Rate Coefficient (k) and Equivalence Ratio (Φ) from selected flames burning ethene except as noted

Source	SSGR (g-soot cm^{-2}-soot s^{-1})	Rate Coefficient, k (g-soot cm^{-2}-soot s^{-1} atm^{-1}-C_2H_2)	Equivalence Ratio, Φ
Harris and Weiner [8]	$8x10^{-6}$ to $6x10^{-5}$	NA	2.1-2.4
Harris and Weiner [9]	$7x10^{-5}$ to $1x10^{-4}$	$4x10^{-4}$ to $4x10^{-3}$	2.28-2.82
Harris and Weiner [10] *a*	$6x10^{-6}$ to $3x10^{-5}$	$7x10^{-4}$ to $3x10^{-3}$	1.78-1.92
Kent and Wagner [16]	$5x10^{-5}$ to $3x10^{-4}$	NA	*b*
Vandsburger et al. [44]	$1x10^{-5}$ to $1x10^{-4}$	NA	*c*
Puri et al. [29] *d*	$3x10^{-5}$ to $9x10^{-5}$	$1x10^{-3}$ to $3x10^{-3}$	1.12 to 1.77
Present Study	$3x10^{-5}$ to $5x10^{-4}$	$6x10^{-4}$ to $2x10^{-1}$	0.71 to 4.3
Richardson [25]	$2x10^{-5}$ to $2x10^{-4}$	NA	*e*
Sunderland et al. [52]	$2x10^{-6}$ to $2x10^{-3}$	NA	*f*

NA - Not Available

NOTES FOR TABLE:

a) A mixture of ethene and toluene was the fuel for this study.

b) The SSGR was estimated by Harris and Weiner [9] from Kent and Wagner [16] from laminar ethene diffusion flames on a Wolfhard-Parker burner.

c) This was a counterflow ethene diffusion flame.

d) Puri et al. [29] uses Fractal Aggregate Theory for the aerosol surface analysis. The rate coefficient quoted is calculated from the SSGR as published [29] and the C_2H_2 mole fraction from the experimental section of this study.

e) The flames of Richardson [25] are CH_4 and mixture flames with CH_4 and either C_4H_{10}, C_4H_8, or C_4H_6.

f) These were C_2H_2 diffusion flames below atmospheric pressure and includes density and oxidation corrections during growth.

In general, the values of SSGR from both premixed and diffusion flames overlap as noted in Table 2. The SSGR from diffusion flames are greater than those found in premixed flames. In premixed flames, it was estimated that uncertainties in the surface area, index of refraction of soot, and the differentiation procedure could lead to systematic errors of a factor of two to three in the calculated rate coefficients [9]. The rate coefficients as calculated in premixed and diffusion flames follow the same pattern as the SSGR. That is, the ranges of calculated values overlap with the maximum value from this diffusion flame exceeding the maximum value found in premixed flames.

Recent work introducing Fractal Aggregate Theory (FAT) to the measurement of the soot aerosol has enabled an improvement in the accuracy of the determination of the soot surface area [29]. The volume fraction along PP 6 that is calculated by the scattering/extinction data and analyzed by Mie theory differs by approximately 20% from that analyzed by the fractal approach. However, the surface density (soot area per unit volume) as calculated with FAT is over a factor of 3 greater than the Mie calculation as a result of the more detailed treatment of shape of the scattering particles and the additional information from the TEM measurements. In a premixed flame [8] the surface density from optical measurements gave a soot area almost twice that found with a BET analysis of that soot. If the errors in measuring the areas as described above are systematic and consistent, and the FAT and BET areas are the appropriate areas for normalizing the soot growth rate, then the net effect would be to make the SSGR and rate coefficient for premixed and diffusion flames much more similar.

Another possible explanation for the greater growth rate in diffusion flames could be a greater contribution to the growth rate due to condensation of PAH species [57-60]. The two dimensional nature of this flame could even enhance this effect. That is, PAH species that form in the center region of the flame could diffuse radially outwards and be consumed by a growth reaction with the soot surface or oxidized. Therefore, the soot along a given particle path is not limited by the carbon which is initially present on that particle path.

The range of equivalence ratios where measurements of growth rate are available is broader in this diffusion flame than in premixed flames. This is due to the nature of this diffusion flame where the inception of particles can occur at equivalence ratios higher than premixed flame experiments and the particles are swept into regions with progressively decreasing equivalence ratio. Not enough measurements are available to determine any equivalence ratio effect on the growth rate. In general, the study of soot growth in premixed flames is limited to a range of equivalence ratios which will incept particles, while not producing so many particles that the burner surface becomes contaminated from the pyrolysis products and soot particles.

SUMMARY

Measurements of the spatial distribution of species concentrations in a laminar diffusion flame with significant soot loadings have been carried out. The shape of the radial profiles of intermediate hydrocarbon species indicates the importance of temperature in their formation. C_2H_2, C_4H_6 and C_6H_6, along with CH_4, are the most prominent pyrolysis products and, except for CH_4, are considered to play important roles in the formation and growth of soot.

These spatial measurements have been integrated with previous flowfield and soot measurements to establish the mechanism controlling the cessation of soot surface growth in this laminar diffusion flame. In particular, the measurements of C_2H_2 and other hydrocarbons have revealed that soot surface growth ceases due to the depletion of hydrocarbons and not due to the loss of soot particle reactivity. This observation is in agreement with recent work by Honnery and Kent [43], who have shown that in long laminar diffusion flames, soot growth can be extended to very long residence times. In addition, C_2H_2 and CH_4 are the only hydrocarbons detected throughout the region of soot growth.

Calculation of a rate coefficient for soot surface growth from C_2H_2 can now be done for this diffusion flame. The observed rate coefficient in this diffusion flame is in agreement with values found in premixed flame studies. This result suggests that the mechanism of soot surface growth dominant in premixed flames is also dominant in this diffusion flame.

ACKNOWLEDGMENTS

This work has been supported under grant F49620-92-J-0161 from the Air Force Office of Scientific Research with Dr. Julian Tishkoff as contract monitor.

NOMENCLATURE

α	Particle Reactivity Decrease Factor (s^{-1})
F_i	Mass Spectrometer Calibration Factor for species i (V^{-1})
f_v	Soot Volume Fraction (cm^3-soot cm^{-3})
k, $k_{C_2H_2}$	Surface Growth Rate Coefficient (g-soot cm^{-2}-soot s^{-1} atm^{-1}-C_2H_2)
k_{SG}	Particle Reactivity Decrease Factor (s^{-1})
N_s	Concentration of Active Sites (sites cm^{-2})
ρ_{soot}	Soot Density (1.8 g cm^{-3})
S	Soot Surface Area per unit volume (cm^2-soot cm^{-3})
S_i	Mass Spectrometer Signal for Species i (V)
t	Time (s)
T_a	Activation Temperature (K)
X_i	Mole Fraction of species i (-)
$\dot{\omega}$	Mass growth rate of soot (g-soot cm^{-3} s^{-1})
M_{soot}	Mass of soot per unit volume (g-soot cm^{-3})

REFERENCES

1. Colket, M. B., *Twenty-First Symposium (International) on Combustion*, The Combustion Institute, Pittsburgh, PA, 1986, pp. 851.

2. Frenklach, M., Taki, S., Durgaprasad, M. B., and Matula, R. A., *Combust. and Flame* 54: 81-101 (1983).

3. Bittner, J. D. and Howard, J. B., *Eighteenth Symposium (International) on Combustion*, The Combustion Institute, Pittsburgh, PA, 1981, pp. 1105-1116.

4. Bockhorn, H., Fetting, F., and Wenz, H. W., *Ber. Bensenges. Phys. Chem.* 87: 1067-1073 (1983).

5. Bockhorn, H., Fetting, F.. Heddrich, A., and Wannemacher, G., *Twentieth Symposium (International) on Combustion*, The Combustion Institute, Pittsburgh, PA, 1984, pp. 979-988.

6. Cole, J. A., Bittner, J. D., Longwell, J. P., and Howard, J. B., *Combust. Flame* 56: 51-70 (1984).

7. Wieschnowsky, U., Bockhorn, H., and Fetting., F., *Twenty-Second Symposium (International) on Combustion*, The Combustion Institute, Pittsburgh, PA, 1988, pp. 343-352.

8. Harris, S. J. and Weiner, A. M., *Combust. Sci. Technol.* 31: 155-167 (1983).

9. Harris, S. J. and Weiner, A. M., *Combust. Sci. Technol.* 32: 267-275 (1983).

10. Harris, S. J. and Weiner, A. M., *Combust. Sci. Technol.* 38: 75-87 (1984).

11. Harris, S. J., Weiner, A. M., Blint, R. J., and Goldsmith, J. E. M., *Twenty-First Symposium (International) on Combustion*, The Combustion Institute. Pittsburgh, PA, 1986, pp. 1033-1045.

12. Santoro, R. J., Semerjian, H. G., and Dobbins, R. A., *Combust. Flame* 51: 203-218 (1983).

13. Santoro, R. J. and Semerjian, H. G., *Twentieth Symposium (International) on Combustion*, The Combustion Institute, Pittsburgh, PA, 1984, pp. 997-1006.

14. Santoro, R. J., Yeh, T. T., Horvath, J. J., and Semerjian, H. G., *Combust. Sci. Technol.* 53: 89-115 (1987).

15. Haynes, B. S. and Wagner. H. G., 133: 201-213 (1982).

16. Kent, J. H. and Wagner, H. G., *Combust. Flame* 47: 53-65 (1982).

17. Kent, J. H., Jander, H., and Wagner, H. G., *Eighteenth Symposium (International) on Combustion*, 1981, pp. 1117-1126.

18. Haynes, B. S. and Wagner. H. G., *Ber. Bensenges. Phys. Chem.* 84: 499-506 (1980).

19. Kent, J. H. and Wagner, H. G., *Combust. Sci. Technol.* 41: 245-269 (1984).

20. Frenklach, M., Clary, D. W., Gardiner, W. C., and Stein, S. E., *Twentieth Symposium (International) on Combustion*, The Combustion Institute, 1984, pp. 887-901.

21. Frenklach, M. and Wang, H., *Twenty-Third Symposium (International) on Combustion*, The Combustion Institute, Pittsburgh, PA, 1990, pp. 1559-1566.

22. Kazakov, A., Wang, H., and Frenklach, M., *Combust. Flame* 100: 111-120 (1995).

23. Miller, J. A. and Melius, C. F., *Combust. and Flame* 91: 21-39 (1992).

24. Puri, R., Moser, M. D., Santoro, R. J., and Smyth, K. C., *Twenty-Fourth Symposium (International) on Combustion*, The Combustion Institute, Pittsburgh, PA, 1992, pp. 1015-1022.

25. Richardson, T. F., Ph.D. Dissertation, Department of Mechanical Engineering,, The Pennsylvania State University, 1993.

26. Kennedy, I. M., Kollmann, W., and Chen, J. Y., *Combust. Flame* 81: 73 (1990).

27. Kennedy, I. M., Yam, C., Rapp, D. C., and Santoro, R. J., Accepted pending revisions: (1995).

28. Eckbreth, A. C., Bonczyk, P. A., and Verdieck, J. F., *Prog. Ener. Combust. Sci.* 5: 253-322 (1979).

29. Puri, R., Richardson, T. F., Santoro, R. J., and Dobbins, R. A., *Combust. Flame* 92: 320-333 (1993).

30. Fristrom, R. M., Prescott, R., and Grunfelder, C., *Combust. Flame* 1: 102-113 (1957).

31. Bittner, J. D., *A Molecular Beam Mass Spectrometer Study of Fuel-Rich and Sooting Benzene-Oxygen Flames*. 1981, Massachusetts Institute of Technology:

32. Smyth, K. C., Miller, J. H., Dorfman, R. C., Mallard, W. G., and Santoro, R. J., *Combust. Flame* 62: 157-181 (1985).

33. Crowhurst, D. and Simmons, R. F., *Combust. Flame* 59: 167-176 (1985).

34. Mitchell, R. E., Ph.D. Dissertation, Department of Chemical Engineering , Massachusetts Institute of Technology, 1975.

35. Smith, S. R. and Gordon, A. S., *J. Phys. Chem.* 60: 759-763 (1956).

36. Puri, R., Ph.D. Dissertation, Department of Mechanical Engineering, The Pennsylvania State University, 1992.

37. Ermolin, N. E., Korobeinichev, O. P., Tereshchenko, A. G., and Fomin, V. M., 18(1): 36-38 (1982).

38. Saito, K., Williams, F. A., and Gordon, A. S., *Transactions of the ASME, Heat Transfer* 108(August): 640-648 (1986).

39. Dasch, C. J., *Combust. Flame* 61: 219-225 (1985).

40. Woods, I. T. and Haynes, B. S., *Combust. Flame* 85: 523-525 (1991).

41. Mitchell, R. E., Sarofim, A. F., and Clomburg, L. A., *Combust. Flame* 37: 227-244 (1980).

42. Roth, P. and Hospital, A., *Twenty-Fourth Symposium (International) on Combustion*, The Combustion Institute, Pittsburgh, PA, 1992, pp. 981-989.

43. Honnery, D. R. and Kent, J. H., *Combust. Flame* 82: 426-434 (1990).

44. Vandsburger, U., Kennedy, I. M., and Glassman, I., *Combust. Sci. Technol.* 39: 263-285 (1984).

45. Axelbaum, R. L., Flower, W. L., and Law, C. K., *Combust. Sci. Technol.* 61: 51-73 (1988).

46. Libby, P. A. and Blake, T. R., *Combust. Flame* 36: 136-169 (1979).

47. Libby, P. A. and Blake, T. R., *Combust. Flame* 41: 123-147 (1981).

48. Bradley, D., Dixon-Lewis, G., Habik, S. E.-D., and Mushi, E. M. J., *Twentieth Symposium (International) on Combustion*, The Combustion Institute, 1984, pp. 931-940.

49. Ishizuka, S. and Sakai, Y., *Twenty-First Symposium (International) on Combustion*, The Combustion Institute, 1986, pp. 1821-1828.

50. Nagle, J. and Strickland-Constable, R. F., *Oxidation of Carbon Between 1000-2000°C,* in *Proceedings of the Fifth Carbon Conference*. 1962, Pergamon Press: Oxford. p. 154-164.

51. Puri, R., Santoro, R. J., and Smyth, K. C., *Combust. Flame* 97: 125-144 (1994).

52. Sunderland, P. B., Köylü, Ü. Ö., and Faeth, G. M., *Combust. Flame* 100: 310-322 (1995).

53. Park, C. and Appleton, J. P., *Combust. Flame* 20: 369-379 (1973).

54. Chan, M.-L., Moody, K. N., Mullins, J. R., and Williams, A., *Fuel* 66(December): 1694-1698 (1987).

55. Levendis, Y. A., Flagan, R. C., and Gavalas, G. R., *Combust. Flame* 76: 221-241 (1989).

56. Ni, T., Pinson, J. A., Gupta, S., and Santoro, R. J., 34: 7083-7091 (1995).

57. Lam, F. W., Howard, J. B., and Longwell, J. P., *Twenty-Second Symposium (International) on Combustion*, The Combustion Institute, 1988, pp. 323-332.

58. Lam, F. W., Longwell, J. P., and Howard, J. B., *Twenty-Third Symposium (International) on Combustion*, The Combustion Institute, 1990, pp. 1477-1484.

59. Marr, J. A., Giovane, L. M., Longwell, J. P., Howard, J. B., and Lafleur, A. L., *Combust. Sci. Technol.* 101: 301-309 (1994).

60. Harris, S. J. and Weiner, A. M., *Twenty-Second Symposium (International) on Combustion*, The Combustion Institute, Pittsburgh, PA, 1988, pp.

61. Léonard, S., M.S. Thesis, Department of Mechanical Engineering, The Pennsylvania State University, 1993.

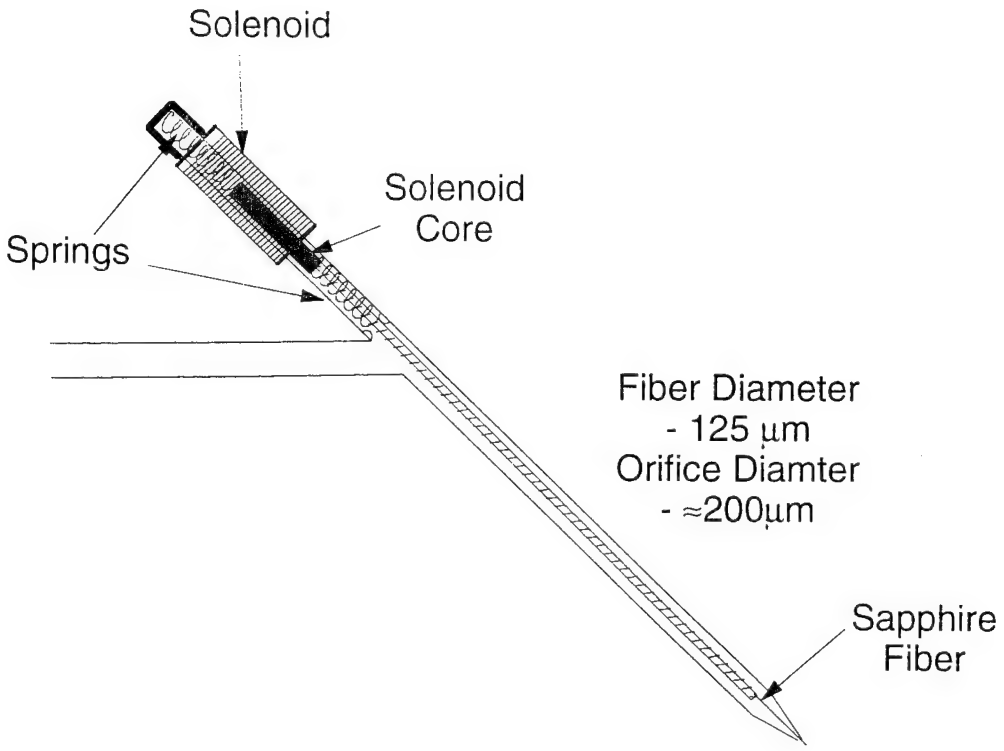

Figure 1 Electromechanical Sonic (EMS) probe Schematic

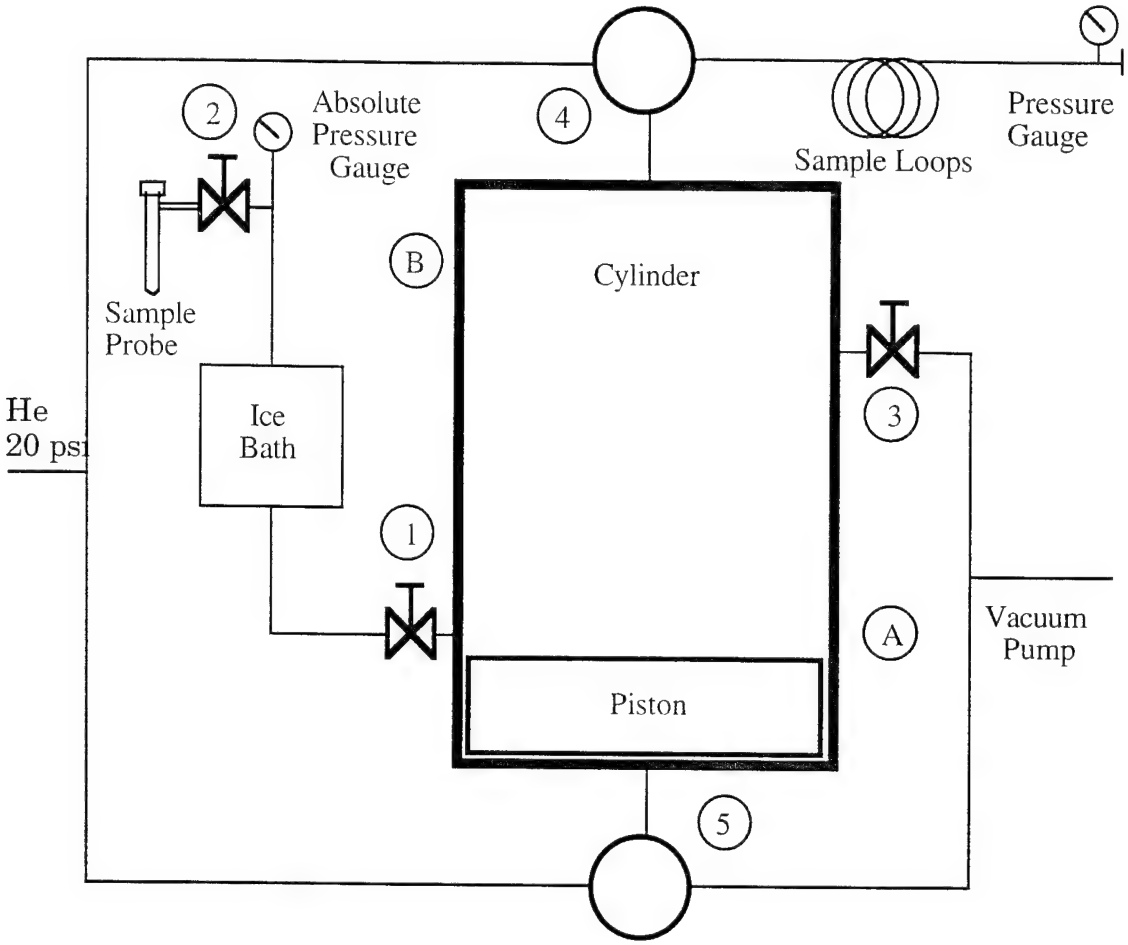

FIGURE 2 Cylinder system for compression and storage of gas sample in preparation of injection into gas chromatograph (after Léonard [61]). (1) Inlet to sample accumulation cylinder, (2) Shut-off valve to probe, (3) Exhaust valve to vacuum pump, (4) and (5) three-way valves. A and B indicate piston position prior to and following helium pressurization.

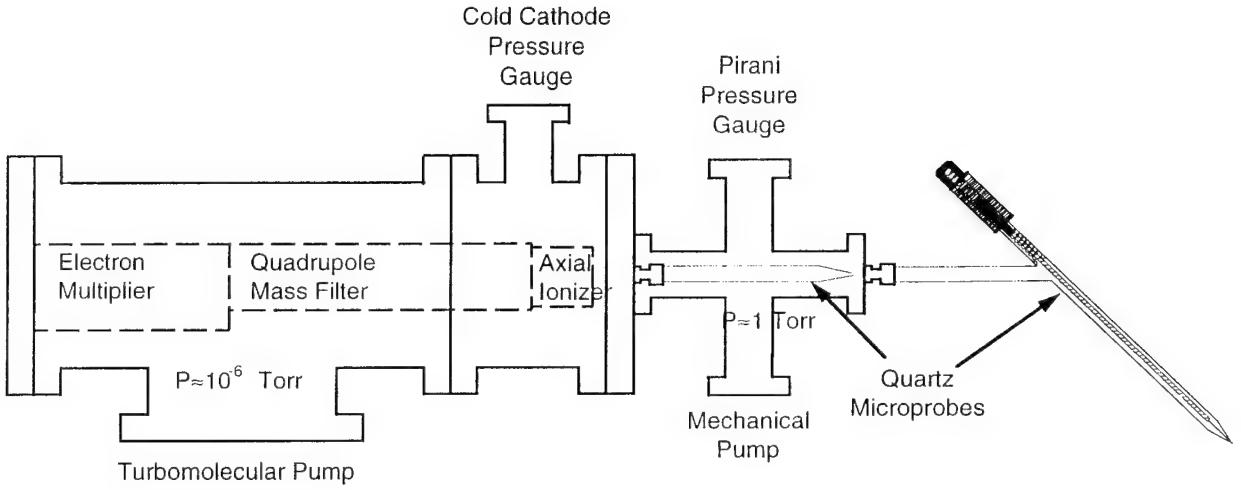

FIGURE 3 Schematic of vacuum chambers with mass spectromenter.

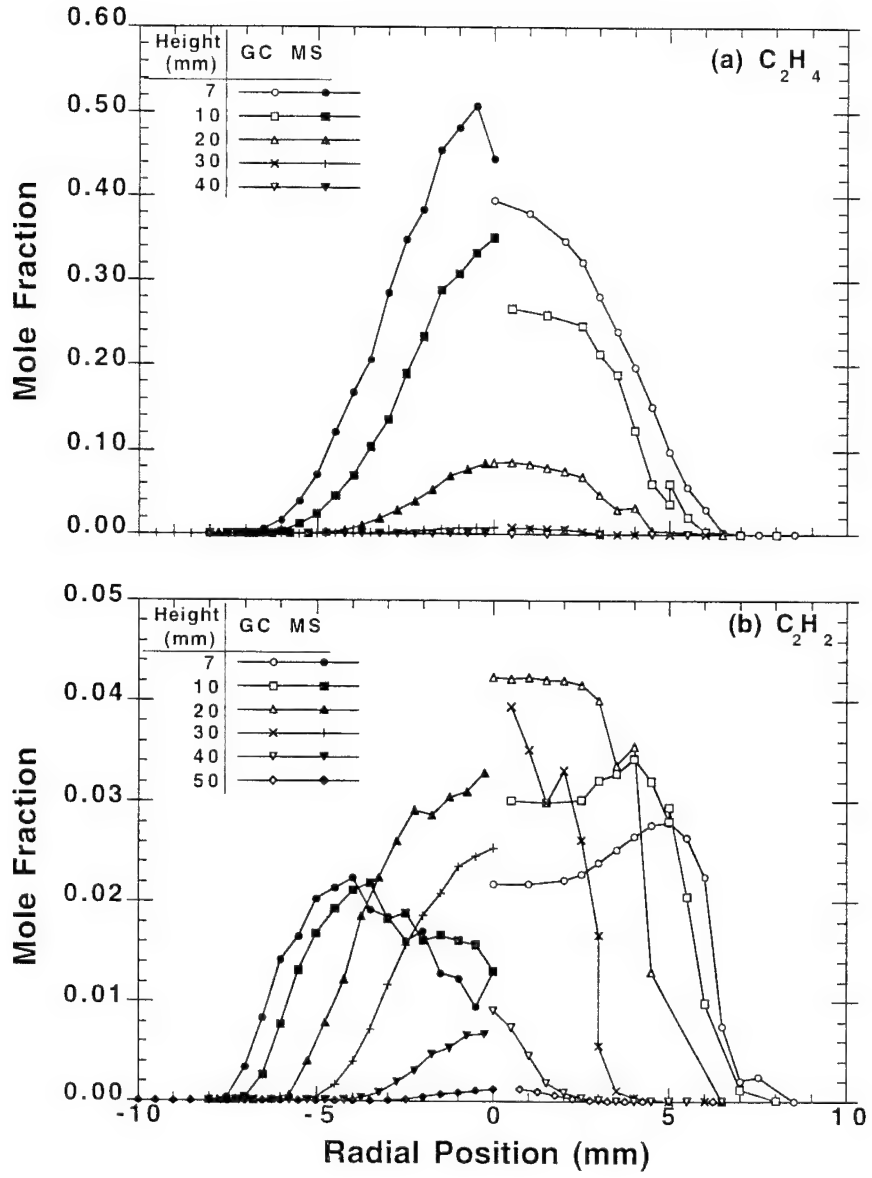

FIGURE 4 Mole fraction as a function of radial position for several heights above the burner outlet for (a) C_2H_4 and (b) C_2H_2. Comparisons can be made between data from the gas chromatograph (open symbols) and the mass spectrometer (filled symbols).

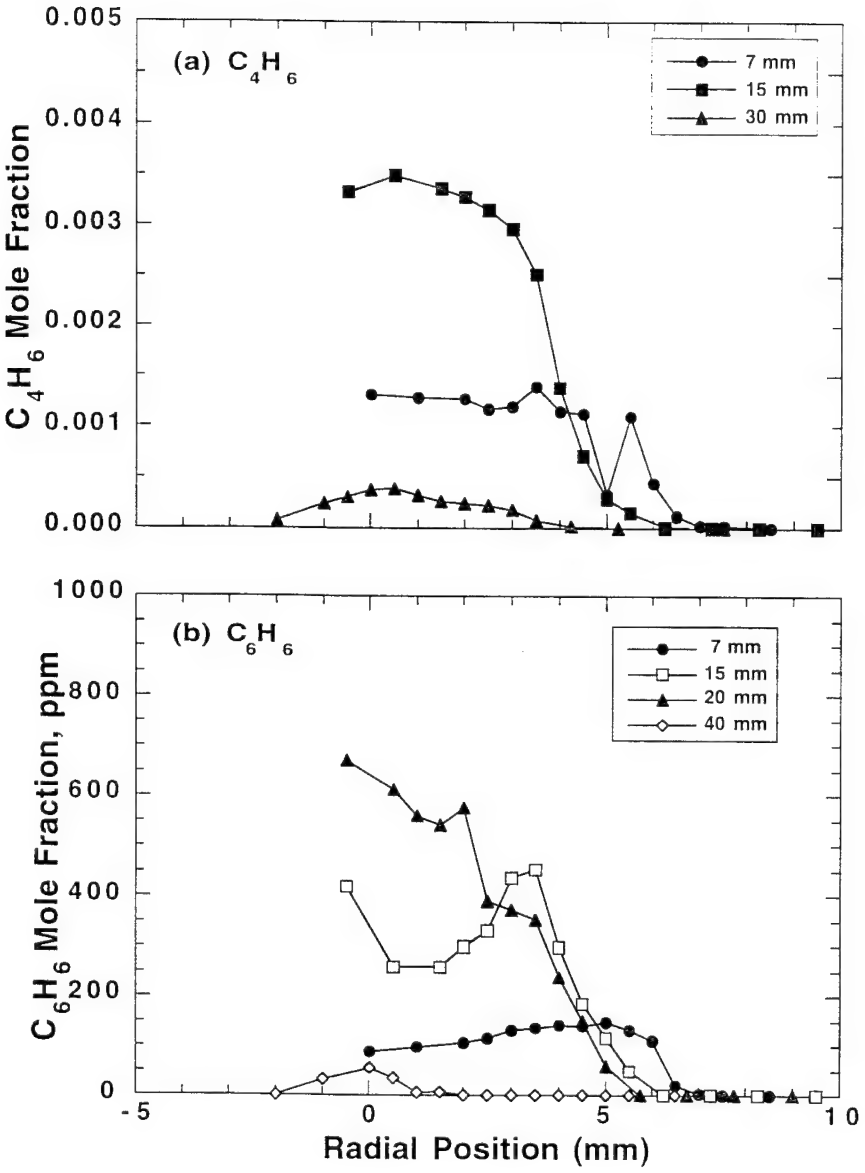

FIGURE 5 Mole fraction as measured by the gas chromatograph as a function of radial position for several heights above the burner outlet for (a) C_4H_6 and (b) C_6H_6.

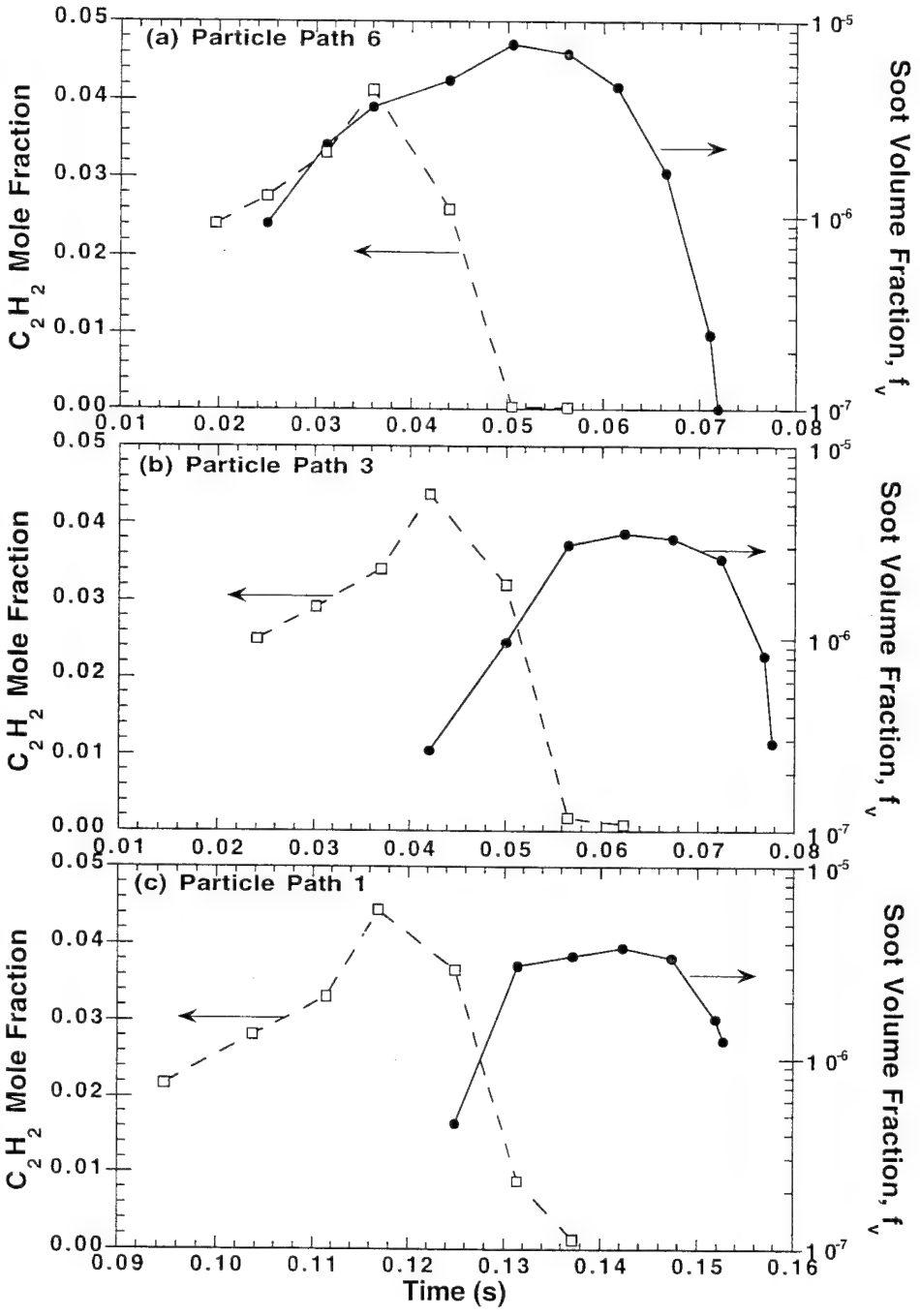

FIGURE 6 Soot volume fraction, f_v, and the mole fraction of C_2H_2 as a function of time for (a) particle path 6, (b) particle path 3 and (c) particle path 1. (see text for discussion)

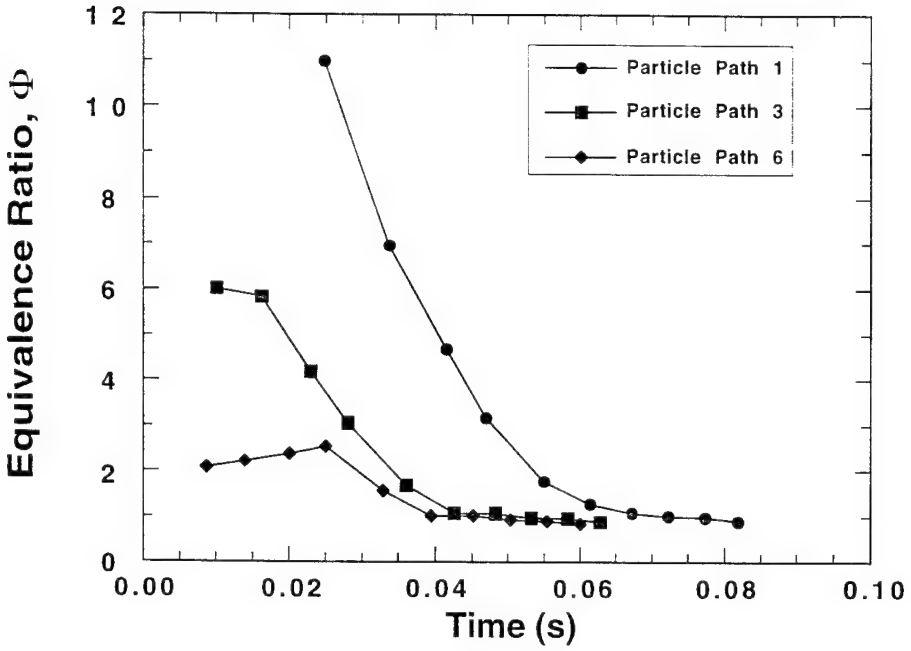

FIGURE 7 Equivalence ratio as calculated from the stable gaseous species along particle paths 1, 3 and 6.

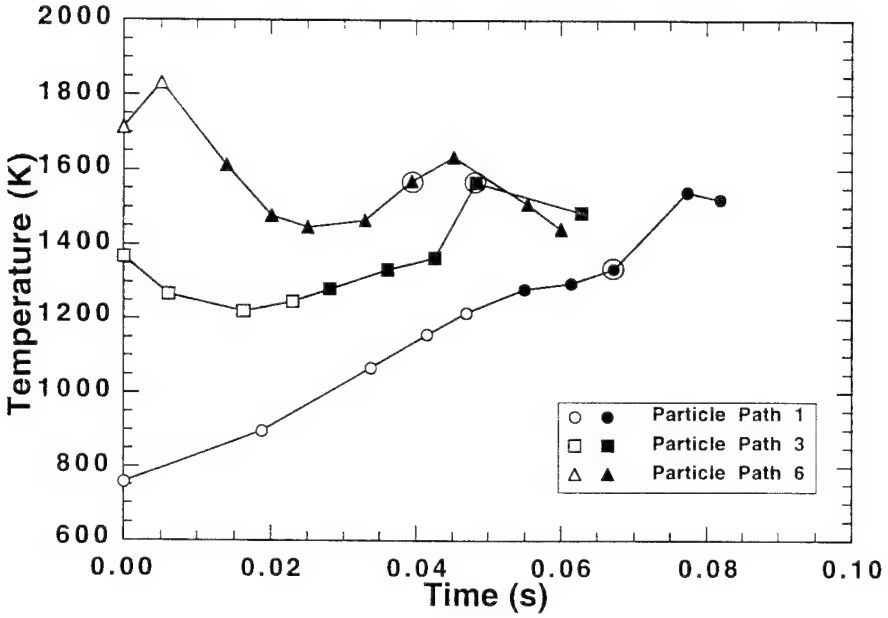

FIGURE 8 Temperatures along particle paths 1, 3 and 6. The open symbols are locations with no soot present. Locations with filled symbols indicate the presence of soot. The circled symbol on each particle path has the maximum local soot volume fraction along that particle path.

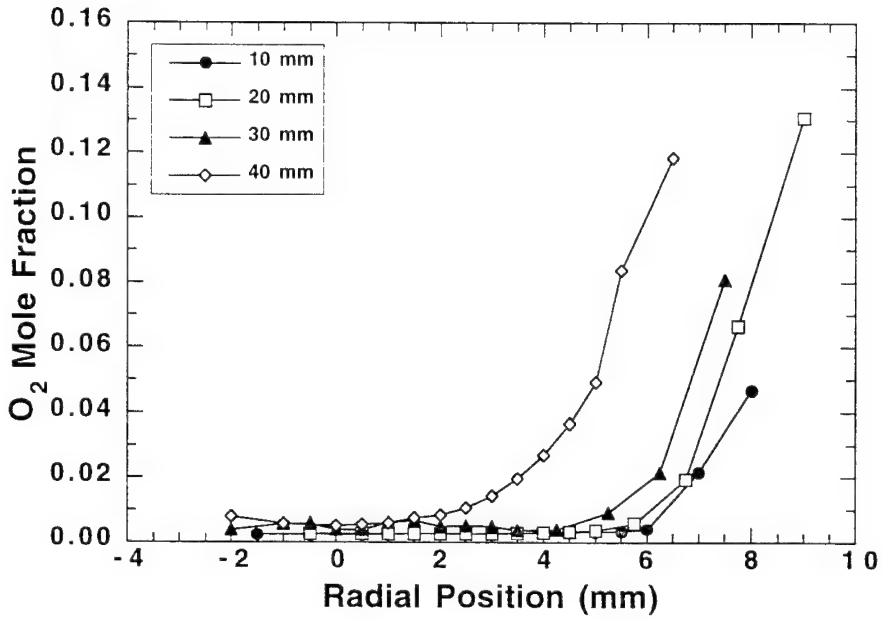

FIGURE 9 Mole fraction of O_2 as measured by the gas chromatograph as a function of radial position for selected heights above the burner outlet.

Appendix C: Modeling and Measurements of Soot and Species in a Laminar Diffusion Flame

by

I. M. Kennedy, Darrell C. Rapp, R. J. Santoro and C. Yam

Submitted for publication in Combustion and Flame

Modeling and Measurements of Soot and Species in a Laminar Diffusion Flame

Ian M. Kennedy*, Darrell C. Rapp#, Robert J. Santoro# and Clement Yam*

* Department of Mechanical and Aeronautical Engineering,
University of California,
Davis CA 95616
U.S.A.
and
Department of Mechanical Engineering,
The Pennsylvania State University,
University Park, PA 16802
U.S.A.

Spring Meeting of the Western States Section of the Combustion Institute

Paper 94-053

Abstract

A model of a laminar, ethene diffusion flame has been developed and compared with measurements. A system of elementary reactions is used to describe the gas phase C_1 and C_2 chemistry. The model incorporates a simple description of the growth of soot which performs a good job of reproducing the amount of soot in the flame and the transition from non-sooting to sooting conditions. Stable gas phase species have been measured in the flame with a combination of gas chromatography and mass spectrometry. Laser-induced fluorescence was used to measure the OH concentration. The model predicted most of the species quite well. It was found that the assumption of equilibrium concentrations for the minor radical species was grossly in error, particularly near the end of the flame where temperatures were low. Calculated radical species were found in concentrations that were orders of magnitude greater than equilibrium. Comparisons with measured OH concentrations supported this observation.

Introduction

Previous studies of a laminar ethene - air diffusion flame have suggested that the modeling of soot formation with the assumption of equilibrium chemistry may underestimate significantly the super-equilibrium concentrations of important radicals such as O and OH[1],[2]. These species are important oxidants of soot, particularly near the tip of diffusion flames where soot can escape. The original code that has been developed at U. C. Davis made use of the equilibrium assumption[2],[3] in order to determine the mole fractions of all the species in the flame. Finite rate chemistry is required in order to relax this assumption. An entirely new code was written to accommodate this modification. Detailed chemistry has been incorporated into a parabolic code that solves the boundary layer form of the conservation equations for mass, momentum and energy conservation. A much more accurate representation of radical concentrations has been achieved. Furthermore, interesting questions that are related to the interaction of soot with flame chemistry can now be investigated. The results of the modeling have been compared with the results of an experimental program at The Pennsylvania State University.

Experimental Method

A laminar ethene/air diffusion flame was established on a co-annular burner similar in design to that used in previous studies[4] and only a brief description will be given here. This burner consists of a 11.1 mm diameter brass fuel tube surrounded by a 102 mm diameter air annulus. A brass cylindrical chimney was used to shield the flame from laboratory air currents with access for sampling provided by slots machined in the chimney wall. The ethene (C_2H_4) and air flow rates were 3.85 $cm^3\ s^{-1}$ and 713 $cm^3\ s^{-1}$ respectively, which were measured with calibrated rotameters. Ethene with a stated purity of 99.5% was used; dried, filtered air was supplied by an in-house compressor.

Radial profile measurements of species concentrations have been obtained throughout the flame using an intrusive quartz microprobe sampling approach. Quartz microprobes have been used in many studies to perform the extraction of gas samples from premixed flames [5],[6] and diffusion flames[7], [8], [9], [10], [11]. Until recently their use has been limited to regions where the soot volume fraction is low to avoid clogging the probe orifice. A variation of the standard quartz microprobe design, referred to as an Electro-Mechanical Sonic (EMS) probe, was developed by Puri [11] and enabled sampling in flame regions where volume fractions were on the order of 10^{-5}. This probe has a fiber which extends through the orifice and is attached to a solenoid core with springs on either side of the core. A solenoid is placed around the outside of the quartz tube and the current to the solenoid is interrupted at about 30 Hz, providing for constant motion of the fiber in the orifice, thus keeping an annular region open for gas sampling. The fiber is ≈125 μm in diameter and is made from sapphire, while the orifice diameter is ≈190 μm. The annular sampling region has an area equivalent to a ≈130 μm diameter orifice.

A gas chromatograph and a mass spectrometer (MS) were used to analyze the samples. The use of these two techniques offered an independent verification of the concentration profile measurements as well as providing specific species measurement capability as described below. In general, the two analytical approaches yielded agreement to within ±20%. Because of difficulties in detecting H_2 with the GC, the MS measurements provide the determinations for this species. Since all of the data reported in this paper were obtained using the MS, only this instrumentation will be described in further detail.

The mass spectrometer employed an Extrel model 7-324-9 quadrupole mass filter with mass range of 1-500 amu for separation of ions and an electron multiplier for detection. Calibration of the MS employed a method used by Korobeinichev [12] which is mathematically similar to that of Bittner [13] and Crowhurst and Simmons[9]. The method relies on the signal response relative to other species remaining constant. That is, given the same mixture, the signals of two gases will always be in the same ratio and is therefore independent of mass flow through the orifice due to any possible orifice clogging or variations in density. Secondly, this method assumes that the species measured constitute all of the gases present and they are normalized to a mole fraction of one.

A limitation of the MS in this flame is the coincidence of C_2H_4, N_2 and CO at mass 28. For C_2H_4, the fragment at mass 27 was used as an independent measurement. Calibration of C_2H_4 at both masses 27 and 28 was necessary so that the signal contribution of C_2H_4 at mass 28 could be subtracted from the mass 28 signal.

Hydroxyl radical (OH•) concentration measurements were obtained in a previous study [1]. The OH• measurements were obtained using the output from a Nd:YAG pumped dye laser which was frequency doubled to produce a UV beam. The fluorescence signal was collected at 90° with an intensified cooled CCD camera. The laser wavelength was tuned to either 278.83 nm or 283.55 nm, corresponding to $S_{12}(8)$ and $Q_1(8)$ lines of the $A^2\Sigma^+ \leftarrow X^2\Pi_i$ (1,0) band of OH•, respectively. Filters attenuated elastically scattered light from soot particles and transmitted the (0,0) and (1,1) emission bands of OH•. Excitation of the $S_{12}(8)$ line of OH• was used in regions of low soot particle concentration while the stronger $Q_1(8)$ line was utilized when soot concentrations were high (see Puri et al. [1]).

Numerical Model

The most general formulation of the governing equations consists of the compressible Navier-Stokes equations, an equation to describe the conservation of energy and species transport equations that are elliptic in nature. The computer time to solve these fully elliptic equations is large [14] . A number of assumptions are introduced in the present model that permit a significant saving in computer time without a serious impact on accuracy. The boundary layer forms of the governing equations are solved with zero pressure gradient. Hence, the equations can be solved with a marching method. It is expected that the boundary layer assumption will introduce the greatest errors in the vicinity of the nozzle exit. The flame that has been investigated in this study is relatively long, of the order of 7 nozzle diameters. Therefore, it is expected that the errors will not be large in the region of most interest in relation to soot oxidation, radiation and their impact on gas phase chemistry.

The equations are solved in primitive variable form. Hence, the steady state continuity equation

$$\frac{\partial(\rho u)}{\partial x} + \frac{1}{r}\frac{\partial}{\partial r}(r\rho v) = 0 \qquad [1]$$

is solved along with the momentum equation

$$\rho u \frac{\partial u}{\partial x} + \rho v \frac{\partial u}{\partial r} = \frac{1}{r}\frac{\partial}{\partial r}\left(\mu r \frac{\partial u}{\partial r}\right) + \rho g \qquad [2]$$

The energy equation is written in terms of the temperature as

$$\rho C_P\left(u\frac{\partial T}{\partial x}+v\frac{\partial T}{\partial r}\right)=\frac{1}{r}\frac{\partial}{\partial r}\left(r\lambda\frac{\partial T}{\partial r}\right)+q^R-\frac{1}{r}\frac{\partial}{\partial r}\left(r\,\rho T\sum_{n=1}^{N}Y_n\,C_{P,n}\,V_n\right)-\sum_{n=1}^{N}M_n\,h_n\,\dot{w}_n \qquad [3]$$

in which the complete diffusion velocity of species n is V_n

$$V_n=v_n+v_n^T+V_n^{corr} \qquad [4]$$

The divergence of the radiative heat flux is represented by q^R. The normal diffusion velocity of species n is given by

$$v_n=-\frac{D_n}{Y_n}\frac{\partial Y_n}{\partial r} \qquad [5]$$

and the contribution of the thermal diffusion phenomenon to the total diffusion velocity is given by

$$v_n^T=\frac{D_n\,\kappa_n}{X_n}\frac{1}{T}\frac{\partial T}{\partial r} \qquad [6]$$

The thermal diffusion ratio, κ_n, was obtained from CHEMKIN [15]. A correction diffusion velocity, V_n^{corr}

$$V_n^{corr}=-\sum_{1}^{N}Y_n\left(v_n+v_n^T\right) \qquad [7]$$

ensures that net diffusive flux of all gaseous species is zero. An equation is solved for N-1 species mass fractions

$$\rho u\frac{\partial Y_n}{\partial x}+\rho v\frac{\partial Y_n}{\partial r}=-\frac{1}{r}\frac{\partial}{\partial r}\left\{r\,\rho\,Y_n V_n\right\}+M_n\dot{w}_n \qquad [8]$$

with the Nth species being N_2. Finally, an equation is solved for the soot mass fraction, Y_{soot}

$$\rho u\frac{\partial Y_{soot}}{\partial x}+\rho v\frac{\partial Y_{soot}}{\partial r}=-\frac{1}{r}\frac{\partial}{\partial r}\left\{r\,\rho V_T Y_{soot}\right\}+\rho\,S(Y_{soot},T,f) \qquad [9]$$

In this equation, the thermophoretic velocity is found from the appropriate expression for a free molecular aerosol [16]

$$V_T = -0.55 \frac{\upsilon}{T} \frac{\partial T}{\partial r} \qquad [10]$$

The source term in equation (9) includes the contributions of soot nucleation ($\dot{w}_{nucl}$), soot surface growth ($\dot{w}_g$) and soot oxidation ($\dot{w}_o$)

$$S(Y_{soot}, T, f) = \dot{w}_{nucl} + \dot{w}_g - \dot{w}_o \qquad [11]$$

An equation for soot particle number density is not included. Rather, an average number density is assumed. The justification for this assumption is discussed by Kennedy et al.[3] The rates of reaction for the surface growth and soot oxidation terms are identical to those used by Kennedy et al.[3].

Method of Solution

Initial Conditions

Initial conditions for all the major species as well as the temperature profiles are required in order to start the calculation. These initial conditions are obtained by first starting the calculations with an equilibrium chemistry model with the Shvab-Zeldovich approximation [17] so that the mixture fraction can be used to describe the scalar field. This is achieved by generating a table of mass fractions of all species, density and temperature as functions of mixture fractions with the chemical equilibrium code STANJAN [18]. The momentum, continuity and mixture fraction equations are then solved simultaneously. Once the mixture fraction profile is known, all the other dependent variables can be obtained by using the table. Numerical trials have established that reasonable initial conditions for the finite rate chemistry calculation can be obtained by using the mixture fraction/equilibrium calculation up to 0.15 nozzle diameters.

Chemical Mechanism

A "skeletal" mechanism has been used to describe concisely the C_1 and the C_2 reactions for ethene oxidation. The methane mechanism of Smooke et al [19] has been found to be numerically efficient and it has been implemented in the current code with the rates for all the C_1 chemistry from Reference [19]. It contains a sufficient degree of detail to describe methane oxidation for the purposes of this project. The C_2 chemistry is described by a series of reactions that convert C_2H_4 to C_2H_3 and C_2H_2. The immediate source of the rates for the C_2 reactions is the paper by Frenklach et al. [20] ; primary sources of the rate data may be found in that reference. The entire reaction mechanism is shown in Table 1 and is composed of 62 reactions involving 24 species. The important oxidation steps by O, O_2 and OH are included. The CO oxidation steps and the H_2 - O_2 steps are also included.

Table 1

Chemical Reaction Mechanism in the form $k = A T^{\beta} e^{-E/RT}$ in units of moles, cubic centimetres, seconds, Kelvin and calories/mole.

	A	β	E
1. CH2+OH → CH2O+H	3.00E+13	0 .	0
2. CH2+O2 → CO+OH+H	3.10E+13	0	0
3. C2H+H2 → C2H2+H	1.10E+13	0	2866.0
4. C2H+O2 → HCCO+O	6.02E+11	0	0
5. HCCO+H → CH2+CO	1.50E+14	0	0
6. C2H2+O → CH2+CO	7.81E+03	2.8	502.0
7. C2H2+OH → HCCOH+H	5.06E+05	2.3	13496.0
8. CH2CO+H → HCCO+H2	3.00E+13	0	8599.0
9. CH2CO+OH → HCCO+H2O	1.00E+13	0	2627.0
10. C2H3+O → CH2CO+H	3.00E+13	0	0
11. C2H3+O2 → CH2O+HCO	4.00E+12	0	-239.0
12. C2H3+M → C2H2+H+M	2.00E+38	-7.2	50567.0
13. C2H4+OH → C2H3+H2O	3.00E+13	0	2986.0
14. C2H4+M → C2H2+H2+M	2.60E+17	0	79230.0
15. C2H4+H → C2H3+H2	3.16E+11	7	8002.0
16. C2H4+O → CH3+HCO	1.60E+08	1.4	525.0
17. CH4+M → CH3+H+M	1.00E+17	0	86000.0
18. CH4+O2 → CH3+HO2	7.90E+13	0	56000.0
19. CH4+H → CH3+H2	2.20E+04	3.0	8750.0

20. CH4+O → CH3+OH	1.60E+06	2.4	7400.0
21. CH4+OH → CH3+H2O	1.60E+06	2.1	2460.0
22. CH2O+OH → HCO+H2O	7.53E+12	0	167.0
23. CH2O+H → HCO+H2	3.31E+14	0	10500.0
24. CH2O+M → HCO+H+M	3.31E+16	0	81000.0
25. CH2O+O → HCO+OH	1.81E+13	0	3082.0
26. HCO+OH → CO+H2O	5.00E+12	0	0
27. HCO+M → H+CO+M	1.60E+14	0	14700.0
28. HCO+H → CO+H2	4.00E+13	0	0
29. HCO+O → OH+CO	1.00E+13	0	0
30. HCO+O2 → HO2+CO	3.00E+12	0	0
31. CO+O+M → CO2+M	3.20E+13	0	-4200.0
32. CO+OH → CO2+H	1.51E+07	1.3	-758.0
33. CO+O2 → CO2+O	1.60E+13	0	41000.0
34. CH3+O2 → CH3O+O	7.00E+12	0	25652.0
35. CH3O+M → CH2O+H+M	2.40E+13	0	28812.0
36. CH3O+H → CH2O+H2	2.00E+13	0	0
37. CH3O+OH → CH2O+H2O	1.00E+13	0	0
38. CH3O+O → CH2O+OH	1.00E+13	0	0
39. CH3O+O2 → CH2O+HO2	6.30E+10	0	600.0
40. CH3+O2 → CH2O+OH	5.20E+13	0	34574.0
41. CH3+O → CH2O+H	6.80E+13	0	0

42. CH3+OH → CH2O+H2	7.50E+12	0	0
43. HO2+CO → CO2+OH	5.80E+13	0	22934.0
44. H2+O2 → 2OH	1.70E+13	0	47780.0
45. OH+H2 → H2O+H	1.17E+09	1.3	626.0
46. H+O2 → OH+O	2.20E+14	0	16800.0
47. O+H2 → OH+H	1.80E+10	1.0	8826.0
48. H+O2+M → HO2+M	2.10E+18	-1.0	0
49. H+O2+O2 → HO2+O2	6.70E+19	-1.4	0
50. H+O2+N2 → HO2+N2	6.70E+19	-1.4	0
51. OH+HO2 → H2O+O2	5.00E+13	0	1000.0
52. H+HO2 → 2OH	2.50E+14	0	1900.0
53. O+HO2 → O2+OH	4.80E+13	0	1000.0
54. 2OH → O+H2O	6.00E+08	1.3	0
55. H2+M → H+H+M	2.23E+12	.5	92600.0
56. O2+M → O+O+M	1.85E+11	.5	95560.0
57. H+OH+M → H2O+M	7.50E+23	-2.6	0
58. H+HO2 → H2+O2	2.50E+13	0	700.0
59. HO2+HO2 → H2O2+O2	2.00E+12	0	0
60. H2O2+M → OH+OH+M	1.30E+17	0	45500.0
61. H2O2+H → HO2+H2	1.60E+12	0	3800.0
62. H2O2+OH → H2O+HO2	1.00E+13	0	1800.0

Numerical Scheme

The governing differential equations are written in a discrete form by using a second order accurate scheme for the diffusion terms and first order accurate scheme for the convective terms with the delta formulation. The non-linear terms (convective and rate terms) are linearized by using Newton's method. The resulting Jacobian matrices are determined numerically in the manner described by Smooke [21] . The Jacobian does not need to be updated continuously since the changes from one step to the next step are small. We found that the evaluation of the Jacobian at every fifth spatial step yielded the same results as an evaluation at every step.

The resulting sets of coupled algebraic equations are solved implicitly and simultaneously by the usage of a block solver with iterations to account for the non-linear term. Typically, 8 iterations per step are required to converge the equations to a local solution. The step size (Δx) is determined by limiting the maximum changes of all the dependent variables by no more than 10 percent. If the maximum changes in any dependent variable exceed this limit, the solution is rejected and a smaller Δx is used and the calculation is redone. The equations are assumed to be solved when the residual approaches machine zero. If a local convergence cannot be reached, a smaller Δx is used and the solution is recalculated.

Grid adaptation is used in order to resolve the high gradient region in the flow field with a minimum number of grid points. This is done by adapting the grid distribution to the temperature gradient. The results shown in this report are obtained by using only 61 points in the transverse direction. All the properties of the fluid, the diffusion coefficients of all species and the chemical source term for each species were obtained by using CHEMKIN [15] .

Results

Solutions for a non-sooting and a sooting flame are presented. The predicted integrated soot volume fractions are shown in Fig. 1; they are a measure of the total amount of soot at a given axial plane. Experimental data from Santoro et al. [22] are also shown in Figure 1 . The agreement between the model predictions and the measurements of the integrated soot volume fraction is considered quite good. Burn out of soot at the end of the flame is evident. Generally, the soot model tends to underpredict the measured values of soot volume fraction. However, the spatial distribution of soot is reproduced very well including the location of the peak integrated soot volume fraction. Although it is not shown in this paper, the model manages to reproduce the transition from a non-sooting flame to a sooting flame quite well as the fuel flow rate is increased. The agreement that is shown in Fig. 1 , along with more detailed radial profiles of soot volume fractions which are not shown, provide the basis for confidence in the application of this relatively simple soot model to a calculation of detailed chemistry in an ethene flame.

In addition to a simple soot model, the code includes a radiation model, in which an optically thin model is adopted for simplicity. A comparison of the measured and predicted temperature fields offers a measure of its accuracy. Figure 2 presents radial profiles of the measured and predicted temperatures at two axial locations in the non-sooting flame. The drop in the peak temperature at the more downstream location is evidence of the heat loss due to luminosity. The agreement in the temperature field is considered good, although the radiation model leads to underprediction of the radiative heat loss, in part because gas radiation is ignored and also because the soot volume fractions are underpredicted. Similar agreement is evident in the velocity field although these results are not shown.

The fuel mole fractions in the non-sooting flame are shown in Fig. 3 at a location that is 7 mm from the fuel nozzle. A profile of C_2H_2 mole fractions at the same location is shown in Fig. 4 . There is a general tendency to overpredict the measured mole fractions of C_2H_4 and C_2H_2 in the central region of the flame while the model results show steeper gradients as the radial location increases. The finite spatial resolution of the EMS probe contributes to the observed differences in this region since species concentration gradients in the flame are steep. Further improvement in the comparisons between model and experiments will require higher spatially resolved measurements and consequently the current agreement is considered satisfactory for model validation. The loss of C_2H_2 onto soot is not accounted for at present in the balance equation for acetylene. This sink of acetylene could reduce the predicted C_2H_2 concentrations, particularly further downstream where soot mass growth rates are more intense. The hydrogen mole fraction profile at 7 mm is shown in Fig. 5 . The calculated values exhibit reasonably good agreement with the experimental data in view of the difficulty in measuring this species. At a location 20 mm from the fuel nozzle, the H_2 distribution has moved towards the centerline as the flame reaction zone approaches the centerline. The results indicate that the general structure of this luminous flame is reproduced quite well by the numerical model.

Hydroxyl mole fractions have been measured with laser induced fluorescence. The calculated hydroxyl mole fractions are compared with the measurements at 7 mm and 70 mm in Fig. 6 . The model tends to overpredict the OH mole fractions. This tendency may be due, in part, to the absence of a numerical sink for OH on soot particles. The model does not incorporate this aspect of the physics at present. A full coupling of the flame chemistry and the soot chemistry will be attempted in the future with a modified soot model that will incorporate elementary steps for soot mass growth and oxidation. It must also be born in mind that LIF measurements involve uncertainties that are related to quenching corrections and other errors. The errors were estimated to be ±50% [1].

The preceding comparison of numerical and experimental results provides grounds for some confidence in the results of the calculations. The use of a detailed kinetics model with a model for soot formation and radiation permits us to examine questions regarding the impact of the soot process on flame chemistry in a manner that experiments alone cannot attempt. For example, calculations of turbulent flames require a model for the thermochemistry. A convenient and very common approach is to use chemical equilibrium. It is instructive to examine the accuracy of this assumption when there is substantial radiative heat loss from a hydrocarbon flame. The non-equilibrium effect is greatest for the minor, radical species such as O and OH. These species are of particular interest in the formation and oxidation of pollutants such as NO and soot. The ratio of computed OH mole fractions to equilibrium mole fractions at the local computed temperature were calculated at 40 mm from the nozzle. At a radius of r/D = 0.745, $\frac{OH_{numerical}}{OH_{eq}} = 22$ while $\frac{O_{numerical}}{O_{eq}} = 478$. This location is to the air side of the reaction zone at a mixture fraction of around 0.03 (stoichiometric mixture fraction is 0.064). It is apparent that large super-equilibrium concentrations can be achieved as a result of the depressed temperatures in this radiating flame. Puri et al. [1] found that the OH super-equilibrium ratio was 9.4 at the peak OH location in this flame at a height of 70 mm. The results suggest that assumption of equilibrium chemistry is grossly inadequate for the prediction of the minor species.

Conclusions

The interaction of soot and the flame chemistry has been modeled with a relatively simple fluid and chemical scheme. A comparison of the numerical results with detailed

experimental results indicates that the flame structure is reproduced quite well. Radicals such as OH and O are predicted to be present in concentrations that are significantly greater than equilibrium. The degree of super-equilibrium is a function of the temperature and, hence, the soot loading in the flame. Future work requires the addition of sink terms in the species equations for OH and C_2H_2. It should be possible to treat other fuels by including a small number of additional reactions for the pyrolysis of the parent fuel to C_2 species.

Acknowledgments

The group at Davis acknowledge gratefully the support of the National Institute of Standards and Technology through Grant 60NANBOD1055, NSF through Grant CTS-8857477 and the National Institute of Environmental Health Sciences Superfund Basic Research Program 2 P42 ES04699.

The research at The Pennsylvania State University was supported under grant F49620-92-J-0161 from the Air Force Office of Scientific Research (AFOSR) and grant 60NANBOD1035 from the National Institute of Standards and Technology. One of the authors (DCR) would like to thank the support of the Air Force Research in Aero Propulsion Technology Program sponsored by the AFOSR during his tenure.

Nomenclature

A	pre-exponential factor in rate coefficient
C_P	specific heat at constant pressure
D	nozzle diameter
D_n	effective diffusivity of species n in the mixture
E	activation energy
f	mixture fraction
g	gravitational acceleration
h_n	specific enthalpy of species n
k	rate coefficient
M_n	molecular weight of species n
N	number of species
q^R	divergence of the radiative heat flux vector
R	gas constant
r	radial distance
S	source or sink term for soot equation
T	temperature
u	velocity in the axial direction
v	velocity in the radial direction
v_n	normal diffusion velocity of species n
v_n^T	thermal diffusion velocity of species n
V_n^{corr}	correction to diffusion velocities
V_T	thermophoretic velocity of soot particles
$\dot{w}_n$	reaction rate of species n
X_n	mole fraction of species n

x	distance along the axis
Y_n	mass fraction of species *n*
β	exponent on temperature in rate coefficient
κ_n	thermal diffusion ratio
λ	thermal conductivity
μ	absolute viscosity
ν	kinematic viscosity
ρ	density

Subscripts

eq	equilibrium
g	soot mass growth
n	soot nucleation
numerical	calculated with computer code
o	soot oxidation

References

[1] PURI, R., MOSER, M., SANTORO, R. J. and SMYTH, K. C., *Twenty-Fourth Symposium (International) on Combustion*,, The Combustion Institute, Pittsburgh,1992, pp. 1015-1022.

[2] VILLASENOR, R. and KENNEDY, I. M., *Twenty-Fourth Symposium (International) on Combustion*, The Combustion Institute, Pittsburgh, 1992., pp. 1023 - 1030.

[3] KENNEDY, I. M., KOLLMANN, W. and CHEN, J.-Y., *Combust. Flame* 81: 73 - 85 (1990).

[4] SANTORO, R. J., SEMERJIAN, H. G. and DOBBINS, R. A., *Combust. Flame* 51: 203-218 (1983).

[5] FRISTROM, R. M.,PRESCOTT, R., GRUNFELDER, C., *Combust. Flame* 1: 102-113 (1957).

[6] BOCKHORN, H., FETTING, F., WENZ, H. W., *Berichte der Bunsen-Gesellschaft für Physikalische Chemie* 87: 1067-1073 (1983).

[7] SMITH, S. R. and GORDON, A. S., *J. Phys. Chem.* 60: 759-763 (1956).

[8] MITCHELL, R. E., *Nitrogen oxide formation in laminar methane-air diffusion flames*, Ph. D. Thesis, Massachusetts Institute of Technology (1975).

[9] CROWHURST, D. and SIMMONS, R. F., *Combust. Flame* 59: 167-176 (1985).

[10] SMYTH, K. C., MILLER, J. H., DORFMAN, R. C., MALLARD, W. G., SANTORO, R. J., *Combust. Flame* 62, 157-181 (1985).

[11] PURI, R., *The Interaction of Soot Particles with Carbon Monoxide in Laminar Diffusion Flames*, Ph. D. Thesis, The Pennsylvania State University (1992).

[12] KOROBINECHEV, Combus. Expl. Shock Waves 23(5): 565-576 (1987).

[13] BITTNER, J. D., *A Molecular Beam Mass Spectrometer Study of Fuel-Rich and Sooting Benzene-Oxygen Flames*, Ph. D. Thesis, Massachusetts Institute of Technology (1981).

[14] SMOOKE, M. D., XU, Y., ZURN, R. M., LIN, P., FRANK, J. H. and LONG, M. B., *Twenty-Fourth Symposium (International) on Combustion*, The Combustion Institute, Pittsburgh, 1992,pp. 813 - 821.

[15] KEE, R. J., RUPLEY, F. M. and MILLER, J. A., *The Chemkin Thermodynamic Data Base*, Sandia National Laboratories, Livermore (1992).

[16] TALBOT, L., CHENG, R. K., SCHEFER, R. W. and WILLIS, D. R., *J. Fluid Mech.* 101: 737 - 758 (1980).

[17] WILLIAMS, F. A., *Combustion Theory*, The Benjamin/Cummings Publishing Co. 1985.

[18] REYNOLDS, W. C., *STANJAN*, Department of Mechanical Engineering, Stanford University, Stanford CA, 1986.

[19] SMOOKE, M. D., PURI, I. K. and SESHADRI, K., *Twenty-First Symposium (International) on Combustion*,, The Combustion Institute, Pittsburgh, 1986, pp. 1783 - 1792.

[20] FRENKLACH, M., WANG, H. and RABINOWITZ, M. J., *Prog. Energy Combust. Sci.* 18: 47 - 73 (1992).

[21] SMOOKE, M. D. and GIOVANGIGLI, V., *Impact of Computing in Science and Engineering* 4: 46 - 79 (1992).

[22] SANTORO, R. J., YEH, T. T., HORVATH, J. J. and SEMERJIAN, H. G., *Combust. Sci. Tech.* 53: 89-115 (1987).

Figure Captions

Fig. 1 Measured and predicted soot volume fractions integrated across a non-sooting flame

-------- calculations

■ experiments

Fig. 2 Measured and predicted temperature profiles

-------- calculations

■ experiments at 7 mm from nozzle exit

▲ experiments at 70 mm from nozzle exit

Fig 3 Measured and predicted C_2H_4 mole fractions at 7 mm from the nozzle

-------- calculations

■ experiments

Fig. 4 Measured and predicted C_2H_2 mole fractions at 7 mm from the nozzle

-------- calculations

■ experiments

Fig. 5 Measured and predicted H_2 mole fractions at 7 mm from the nozzle

-------- calculations

■ experiments

Fig. 6 Measured and predicted OH mole fractions

-------- calculations

■ experiments at 7 mm from nozzle exit

▲ experiments at 70 mm from nozzle exit

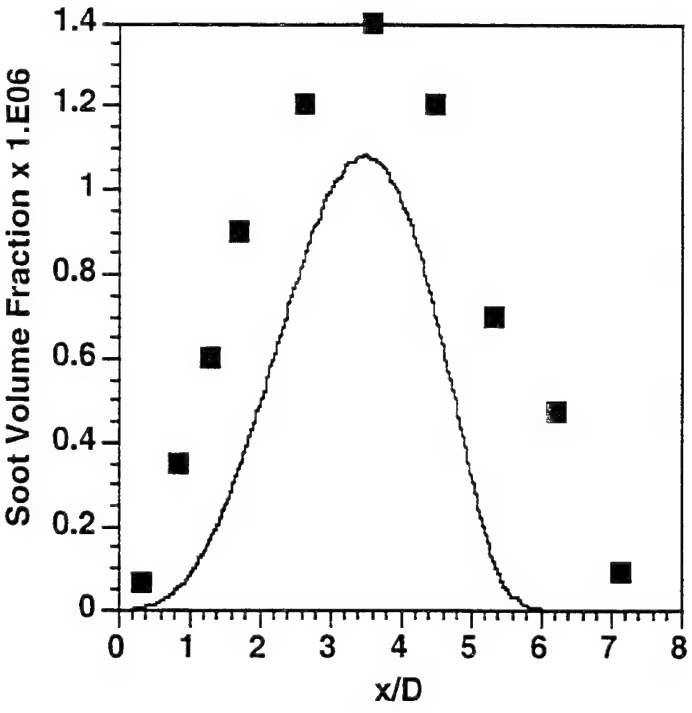

Fig 1

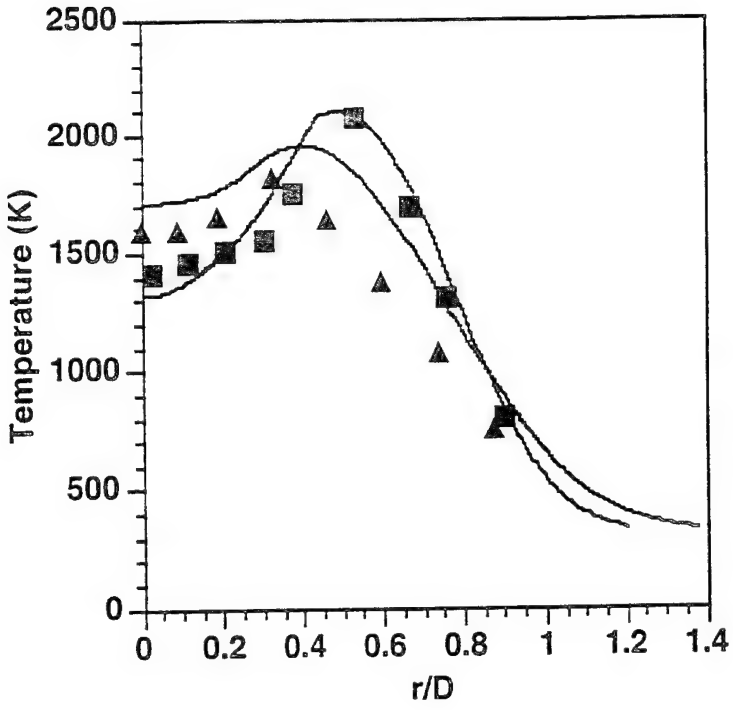

Fig 2

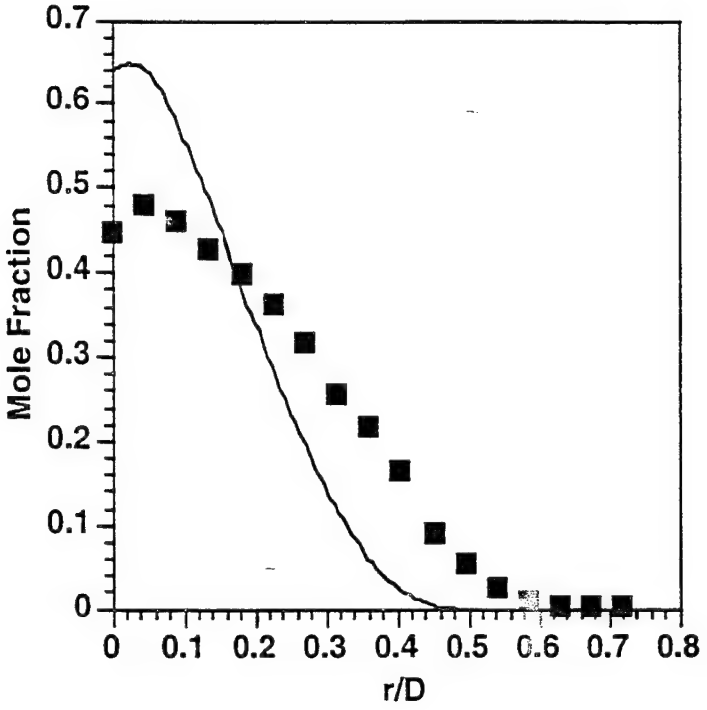

Fig 3

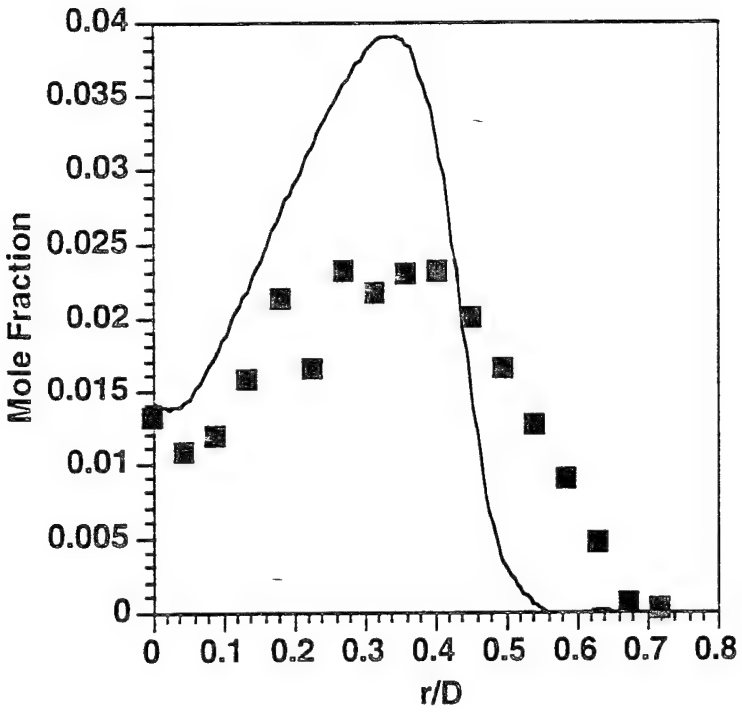
0.04
0.035
0.03
0.025
0.02
0.015
0.01
0.005
0
Mole Fraction
0
0.1
0.2
0.3
0.4
0.5
0.6
0.7
0.8
r/D

Fig 4

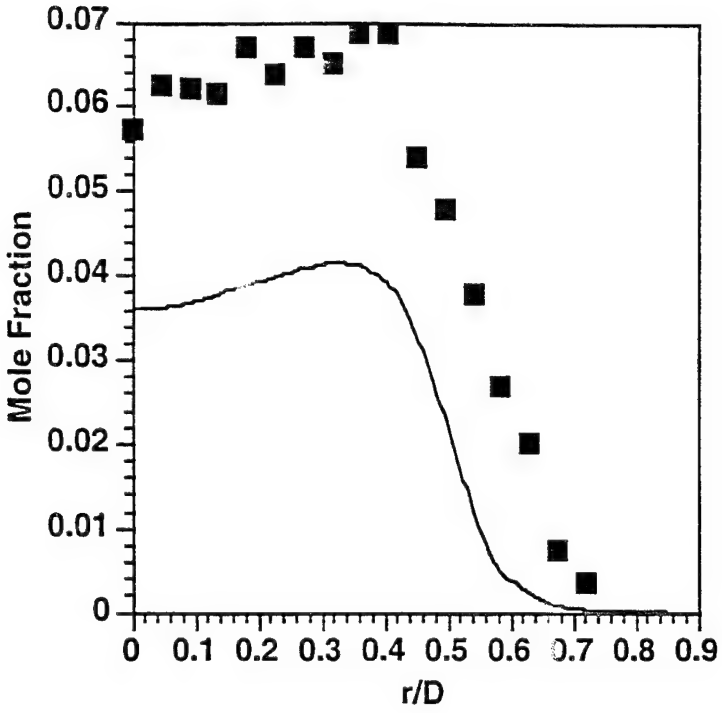
0.07
0.06
0.05
0.04
0.03
0.02
0.01
0
Mole Fraction
0
0.1
0.2
0.3
0.4
0.5
0.6
0.7
0.8
0.9
r/D

Fig 5

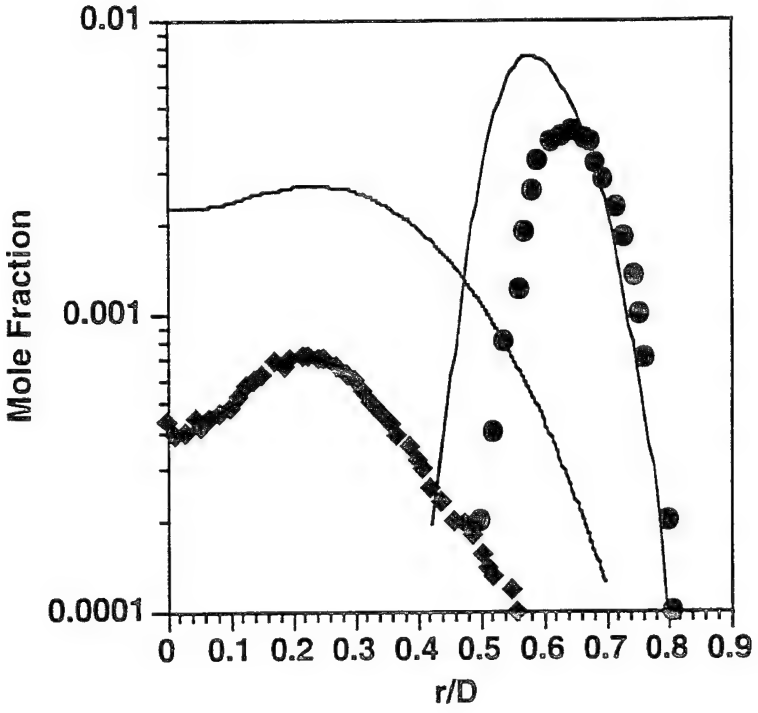

Fig 6

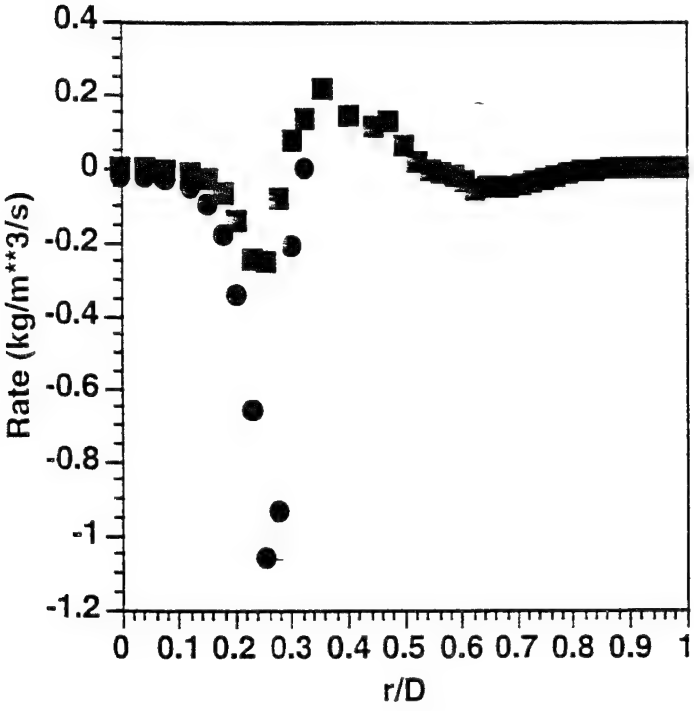

Fig 7

Appendix D: Spatially-Resolved Measurements of Soot Volume Fraction Using Laser-Induced Incandescence

by

B. Quay, T-W Lee, T. Ni and R. J. Santoro

Combustion and Flame 97:384-392 (1994)

Spatially Resolved Measurements of Soot Volume Fraction Using Laser-Induced Incandescence

B. QUAY, T.-W. LEE, T. NI, and R. J. SANTORO*
Department of Mechanical Engineering, The Pennsylvania State University, University Park, PA 16802

Laser-induced incandescence is used to obtain spatially resolved measurements of soot volume fraction in a laminar diffusion flame, in which comparisons with laser scattering/extinction data yield excellent agreement. In addition, the laser-induced incandescence signal is observed to involve a rapid rise in intensity followed by a relatively long (ca. 600 ns) decay period subsequent to the laser pulse, while the effect of laser fluence is manifest in nonlinear and near-saturated response of the laser-induced incandescence signal with the transition occurring at a laser fluence of approximately 1.2×10^8 W/cm^2. Spectral response of the laser-induced incandescence involves a continuous spectrum in the visible wavelength range due to the blackbody nature of the emission. Simultaneous measurements of laser-induced incandescence and light scattering yield encouraging results concerning the mean soot particle diameter and number concentration. Thus, laser-induced incandescence can be used as an instantaneous, spatially resolved diagnostic of soot volume fraction without the need for the conventional line-of-sight laser extinction method, while potential applications in two-dimensional imaging and simultaneous measurements of laser-induced incandescence and light-scattering to generate a complete soot property characterization are significant.

INTRODUCTION

Formation, growth, and oxidation of soot particles in diffusion flames involve a complex interaction between chemistry and fluid mechanics. The understanding of these chemical and physical processes is important not only from a fundamental scientific standpoint, but also due to their applications in practical combustion devices. For example, soot emission from automotive and gas turbine engines constitutes one of the major pollutants that needs to be minimized, while excessive soot formation and radiation in propulsion devices have adverse effects on combustor and flow components. In this regard, sooting characteristics of both turbulent and laminar flames have been investigated by numerous researchers, while in this laboratory attention has been focused on axisymmetric laminar diffusion flames. The soot property measurements made in this flame, thus far, involve the laser scattering/extinction method. This technique yields measurements of soot volume fraction, mean soot particle diameter, and number density after tomographic inversion of the laser extinction data due to the line-of-sight nature of these measurements.

However, recent studies of a process involving laser-induced incandescence (LII), in which the soot particles are heated up by the laser energy and emit blackbody radiation or incandescence at elevated temperatures, have shown that LII can be used as a nonintrusive spatially resolved soot diagnostic [1–6]. In particular, it has been pointed out by Melton [1] that the LII signal is nearly proportional to the local soot volume fraction for sufficiently large laser fluence; thus, a pointwise measurement of soot volume fraction can be made without the need for the line-of-sight laser extinction and time-consuming tomographic inversion method. While other applications of LII in soot diagnostics, for measurements of soot particle size distribution for example, have been suggested [1], the most direct and significant application of LII may be in obtaining point measurements of soot volume fraction since the line-integral nature of laser extinction and subsequent tomographic inversion technique have deficiencies in some laminar flame and most

*Corresponding author.

0010-2180/94/$7.00

turbulent flame configurations. For example, instantaneous measurements of local soot volume fraction can be made in turbulent diffusion flames using LII without being limited to time-averaged data or an axisymmetric burner geometry. Furthermore, applications of LII in investigations of soot properties include two-dimensional imaging of soot volume fraction distributions and simultaneous LII and light-scattering measurements to construct a complete soot property characterization. Recently, qualitative information on soot formation under Diesel engine conditions have been reported in which simultaneous two-dimensional LII and light-scattering images were obtained [5, 6].

In spite of these potentially significant applications of LII in soot diagnostics, no experimental verification of the LII technique for determining the local soot volume fraction has been reported to date. The objectives of this investigation, therefore, were to experimentally determine the applicability of the LII method to obtain spatially resolved measurements of soot volume fraction, to study the feasibility of making simultaneous LII and light-scattering measurements to obtain a complete soot property characterization, as well as to investigate the detailed characteristics of LII in laminar diffusion flames.

LASER-INDUCED INCANDESCENCE

Laser-induced incandescence involves the heating of soot particles to temperatures above the surrounding gas temperature due to the absorption of laser energy, and subsequent detection of the blackbody radiation corresponding to the elevated soot particle temperature. The temperature of the soot particle is determined by the rate of laser energy absorption, conductive heat transfer to the surrounding gas, soot vaporization, and radiative heat loss through blackbody radiation [1, 2]. For example, a Nd:YAG pulsed laser beam of ca. 7 ns duration used in the present LII measurements represents an energy source in the energy balance equation, and the soot particle temperature rapidly rises during the duration of the laser pulse as the soot particles absorb the laser energy. The heat sink terms in this phase are the conductive and radiative heat losses to the surrounding gas, which are much smaller than the laser energy absorption rate for laser fluence levels relevant to LII. Near a soot particle temperature of ca. 4000 K, which is close to the soot vaporization point, the temperature rise is severely curtailed by the energy expended in the vaporization of soot particles [1], although soot surface temperatures as high as 5000 K have been observed for sufficiently large laser fluence [7]. Subsequent to the laser pulse, the temperature of the soot particles gradually decreases due to conductive and radiative heat losses.

The intensity of the LII, or the blackbody radiation due to laser heating, for a single soot particle has a dependence on the soot particle temperature, detection wavelength, and the laser fluence. The total incandescence emitted from the soot particle surface has a fourth-order dependence on the soot particle temperature. The spectral shape of the incandescence is determined by Planck's law with the maximum in the blackbody radiation occurring at a wavelength inversely proportional to the soot particle temperature according to Wien's displacement law. Thus, the temporal variation in the LII signal at a given detection wavelength qualitatively follows the soot particle temperature in time, with the exact functional relationship determined by the processes described above.

Computations of the LII in response to an idealized laser pulse based on the above blackbody radiation laws and the soot particle energy balance have been performed by Melton [1] and Tait and Greenhalgh [4]. In particular, in the limit of high laser power and maximum soot particle temperature near its vaporization point, Melton [1] has shown that the intensity of the LII signal for a group of soot particles has a dependence on mean soot particle diameter raised to the power of $(3 + 0.154\lambda_{det}^{-1})$, where λ_{det} is the detection wavelength expressed in microns. For λ_{det} between 0.7 and 0.4 μm, for example, the LII signal is proportional to the mean soot diameter raised to the power of 3.22 to 3.38, or approximately to the soot volume fraction. This forms the basis for the current approach of using LII for pointwise measurement of soot volume fraction.

EXPERIMENTAL METHODS

The experimental apparatus involved a coannular laminar diffusion flame burner that was identical to the burner employed in this laboratory in previous studies of soot properties [8–10]; thus, only a brief description will be given here. The overventilated laminar flame burner consisted of two concentric brass tubes with fuel and air flowing through the inner (11.1 mm i.d.) and outer (101.6 mm i.d.) tubes, respectively, where the fuel tube extended 4 mm beyond the exit plane of the air tube. Flow conditioning for the air was achieved via a layer of 3.0-mm glass beads, a series of wire screens and ceramic honeycomb section, while the fuel passage contained a layer of 3.0-mm glass beads and a single wire screen. A 405-mm long brass cylinder that fit over the outer tube was used as a chimney to shield the flame from laboratory air disturbances; and optical access was obtained through machined slots on the brass cylinder which traversed with the burner assembly. In addition, screens and a flow restrictor were placed at the chimney exit to achieve a highly stable flame similar to previous studies [8–10]. The traverse system involved a stepper motor and controller (Daedal PC-410-288) that provided positioning capability with a resolution of 0.0127 mm.

The optical setup for the LII included an Nd:YAG pulse laser (Continuum Model NY61-10), the output beam of which was ca. 7 ns in duration and was focused to approximately 0.38 mm in diameter using a bi-convex lens of 400 mm focal length. The probe volume location was displaced ~ 25 mm from the focal point of the lens in order to achieve this 0.38 mm diameter. A schematic of the optical arrangement is shown in Fig. 1. Both the 1064-nm and frequency-doubled 532-nm beams from the Nd:YAG laser were used, the diameter of which prior to the focusing lens was approximately 9 mm with a nearly Gaussian profile. In order to observe the effect of varying the laser fluence for the 532 nm wavelength, a combination of a half-wave plate, mounted in a rotation stage, in series with a polarizing beam splitter was used to attenuate the laser energy by a varying amount. A neutral density filter (0.7 N.D.) preceded the half-wave plate to reduce the laser power to an acceptable value. By rotating the half-wave plate to vary the ratio of vertically polarized to horizontally polarized light, in conjunction with aligning the beamsplitter to transmit only the vertically polarized portion of the beam, laser energies ranging from 0.2 to 3.3 mJ were obtained corresponding to laser fluences between 2.5×10^7 and 4.2×10^8 W/cm^2. The laser energy was monitored during the experiment using a pyrometer (Molectron J1000), and was maintained during the actual measurements of the soot volume fraction at 2.4 mJ for a laser fluence of 3.0×10^8 W/cm^2 in order to minimize the effect of laser beam attenuation across the flame (see discussion below). The LII signal was collected at a 90° angle using a focusing lens with an f-number of 3 at unit magnification. Except for the spectral scans, an interference filter (400 ± 10 nm) was placed in front of the monochromator to minimize interference from light scattering. For the spectral scans, the interference filter was removed from in front of the monochromator and the 1064-nm wavelength laser probe beam was used to produce the LII signals. For these measurements, a series of neutral density filters were used to vary the laser fluence rather than the half-wave plate/beam splitter arrangement used with the 532-nm wavelength laser probe beam.

Since the LII signal had a continuous spectrum in the visible wavelength range, while

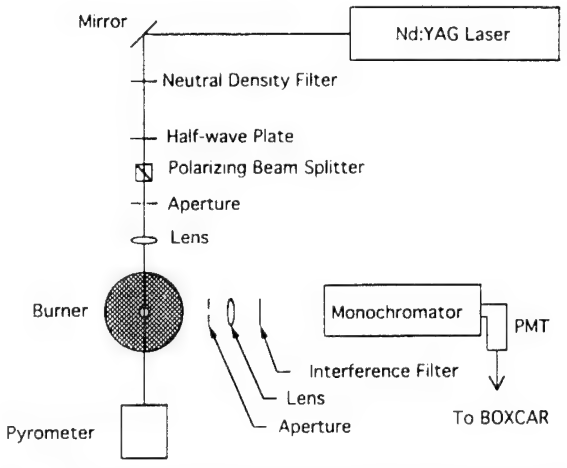

Fig. 1. Optical arrangement for laser-induced incandescence measurements.

interference from light-scattering and PAH fluorescence was expected near wavelengths of 532 nm and above [10, 11], the detection of the LII signal was made at a wavelength of 400 nm for both 532- and 1064-nm wavelength probe laser beams. Measurements made at 500- and 700-nm detection wavelengths for the 1064 nm wavelength probe laser yielded identical results due to the continuous nature of the LII spectrum in the visible wavelength range. The detection wavelength was set by using a 0.25-m monochromator (Instruments SA H20) with a grating blazed at 330 nm with 1 mm × 1 mm slits, which also defined the length on the probe volume. The bandpass of the monochromator was estimated to be 4 nm FWHM, while the spectral response of the monochromator was calibrated using an incandescent lamp (Eppley T24). A photomultiplier tube (Hammamatsu R928) was connected to the exit slit of the monochromator, the signal from which was conditioned using a boxcar integrator with a gate width of 10 ns and averaged over 100 laser shots.

Temporal variations of the LII signal were observable by moving the boxcar gate in 2–10-ns increments. LII profiles across the flame and spectral characteristics of the LII signal were observed by using the burner traverse system described above and by the scanning of the detection wavelength via the monochromator, respectively. The measurements were made in nonsmoking ethylene/air diffusion flames where the ethylene and air flow rates were 3.85 cm^3/s and 1060 cm^3/s, respectively.

RESULTS AND DISCUSSION

Figure 2 shows a typical temporal variation of the LII and vertically polarized light-scattering signals taken at a height of 40 mm above the fuel tube exit for an ethylene laminar diffusion flame at the radial location where the peak soot volume fraction is observed (r = 2.5 mm). The variation of the LII signal in time has been obtained by increasing the boxcar gate delay in 2–10-ns increments with respect to the laser pulse while averaging over 100 laser shots, as described above. It can be observed in Fig. 2 that the initial phase of the signal involves a

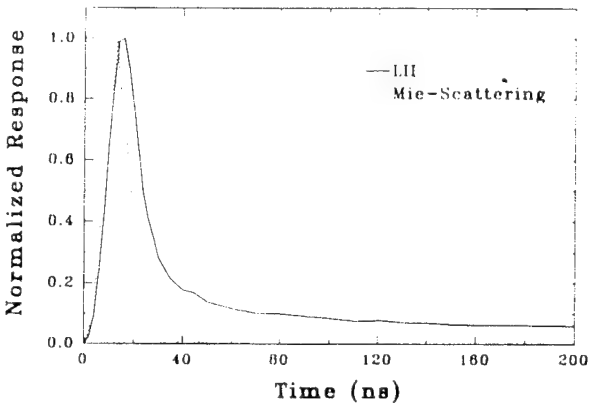

Fig. 2. Temporal response of the laser-induced incandescence.

rapid rise in the LII signal intensity due to the increase in the soot particle temperature during the laser pulse of ca. 7 ns in duration. Subsequent to the peak in the LII signal, the soot particles undergo conductive and radiative heat loss to the ambient gas and the LII signal gradually decreases, although a sensible LII signal is still observed at approximately 600 ns after the laser pulse. The temporal variation of the LII signal shown in Fig. 2 is qualitatively very similar to the LII response function for an idealized laser pulse computed by Melton [1]. A characteristic time constant for the LII process for soot particles has been shown to be linearly proportional to the soot particle diameter [3], and is estimated to be approximately 700 ns for a diameter of 100 nm. The decay time observed in Fig. 2 is approximately 600 ns for the signal to decrease to 5% of the peak value, while the mean soot particle diameter (D_{63}) at this location is approximately 135 nm (see Fig. 7b). Thus, in contrast to the light-scattering signal, which is observable in principle only during the duration of the laser pulse due to its elastic scattering nature, the LII signal exhibits a much longer temporal characteristic, as shown in Fig. 2. Melton [1] has discussed the potential for obtaining particle size distribution parameters from the temporal behavior of the LII signal. Such information is better obtained using a shorter probe laser wavelength than that used in the present study and may also suffer from interference from laser-influenced fluorescence from PAH species [1].

A comparison between the soot volume fraction measured by LII and the laser scattering/extinction technique is shown in Figs. 3a–3c, where the soot volume fraction is plotted as a function of radial location at selected heights ranging from 10 to 70 mm above the fuel tube exit. The open and dark symbols represents laser scattering/extinction and LII data, respectively. The laser scattering/extinction data for soot volume fraction in this flame has been taken from Santoro et al. [8, 9], and involves the well-known method of measuring the line-of-sight extinction of the laser beam followed by a tomographic inversion in order to reconstruct the local soot volume fraction. Further details of this technique and the data can be found in Santoro et al. [8, 9]. In order to calibrate the observed LII signal, the LII signal at a single spatial point corresponding to the radial location where the peak soot volume fraction occurs ($r = 2.5$ mm) at the 40 mm height has been equated with the known value of soot volume fraction at this location from the laser scattering/extinction measurements. All other LII data can then be converted to absolute soot volume fraction based on this single-point calibration procedure.

The radial profiles of soot volume fraction obtained in this manner, as shown in Figs. 3a–3c, exhibit the familiar physics of soot growth and oxidization in this flame. At low heights, soot particles are observed in the annular region on the fuel-rich side of the flame. Soot formed in this region undergoes net growth with increasing height up to $H = 40$ mm where the peak soot volume fraction is observed at a radial location of 2.5 mm from the centerline, while soot is observable at the centerline at a height of 30 mm in Fig. 3a. Subsequent development involves a net destruction of soot particles through soot oxidation with soot volume fraction in the annular region diminishing more rapidly than in the central region.

Figures 3a–3c show an excellent agreement between the LII and laser extinction/scattering data for the soot volume fraction with data being within 5%–10% of one another at most of the heights where measurements have been obtained. However, there is a tendency for the LII data to underestimate the soot volume

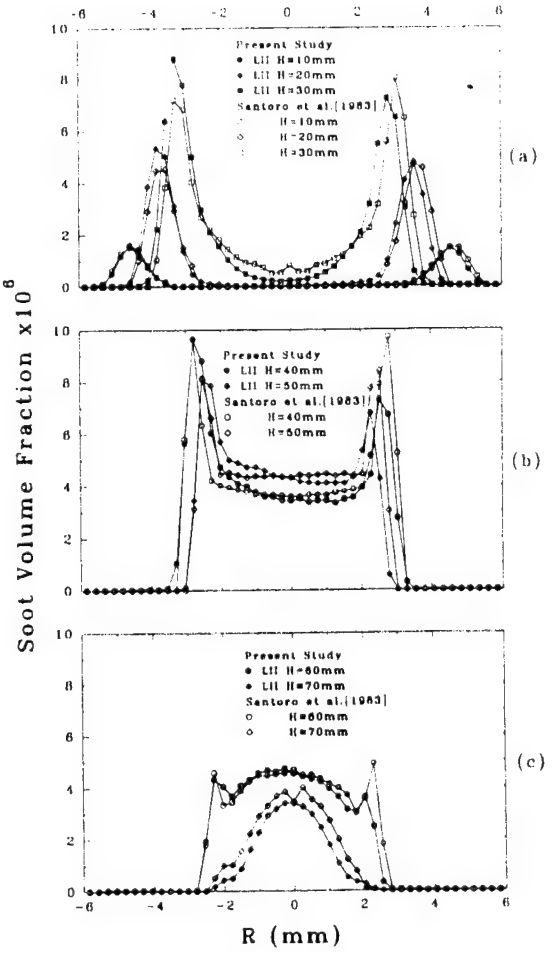

Fig. 3. Radial profiles of the soot volume fraction obtained via laser-induced incandescence and laser scattering/extinction at several heights (H) above the fuel tube exit of the burner (a) H = 10, 20, and 30 mm; (b) H = 40 and 50 mm; and (c) H = 60 and 70 mm.

fraction on one side of the flame, resulting in slightly asymmetric soot volume fraction profiles in Fig. 3b. This effect is more pronounced at the height of 40 mm than elsewhere and is attributable largely to the fact that the LII signal from the far soot peak traverses the flame in order to arrive at the signal detection site and, thus, is subject to increased path length and correspondingly increased absorption of the signal by the soot and PAH species in the flame. This effect may be correctable by estimating and integrating the local extinction of the signal across the flame. Figure 4 similarly shows the integrated soot volume fraction as a function of height. The comparison between the LII and laser extinction/scattering data [8, 9] yields reasonably good agreement

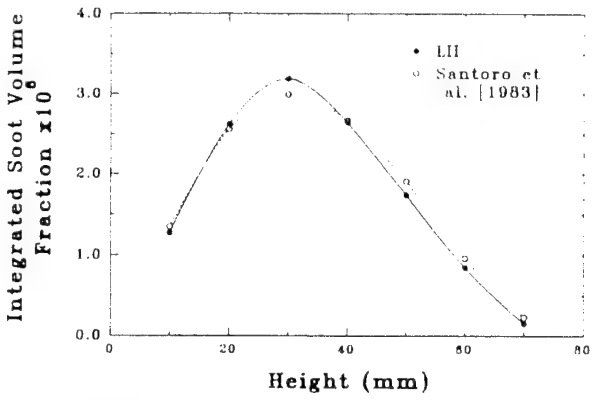

Fig. 4. Integrated soot volume fraction plotted as a function of height above the fuel tube exit of the burner.

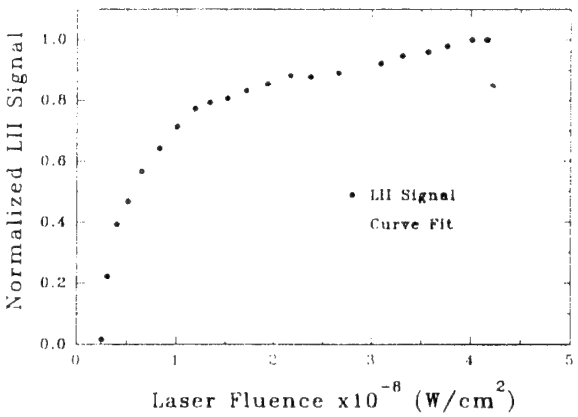

Fig. 5. Effect of laser fluence on the laser-induced incandescence signal.

with the maximum discrepancy being approximately 10% at a height of 30 mm.

The effect of laser fluence on the LII signal is shown in Fig. 5. The laser fluence has been varied from 2.5×10^7 to 4.2×10^8 W/cm^2 using the combination of the half-wave plate and beamsplitter, as described earlier. For a laser fluence from 2.5×10^7 to 1.2×10^8 W/cm^2, it can be seen in Fig. 5 that the LII signal increases rapidly as the laser fluence increases. This effect is due to the fact that the soot particle temperature increases as a function of the laser fluence, which causes a corresponding increase in the LII signal. In contrast, the LII signal for laser fluence beyond ca. 1.2×10^8 W/cm^2 exhibits a small increase with respect to an increase in the laser fluence. The influx of laser energy on the soot particles can cause vaporization of small carbon fragments, such as C_2 and C_3, from the soot particle surface. For sufficiently large laser fluence this vaporization mechanism and corresponding mass loss can become the dominant effect which limits the increase in soot particle temperature and, thus, causes a leveling of the LII signal as shown in Fig. 5. However, the LII signal intensity in this "saturation" regime increases as a weak function of the laser fluence in Fig. 5 similar to the results of Eckbreth [7] in which soot surface temperatures as high as 5000 K were observed with increasing laser fluence. From the data shown in Fig. 5, it is estimated that the "saturation" regime for the LII signal occurs for laser fluences above 1.2×10^8 W/cm^2 in the present studies. During the actual measurements of soot volume fraction, large laser fluence levels in the "saturation" regime, as were used in the present study, have the advantage of being least affected by the effects of the laser beam attenuation across the flame, since the LII signal is a weak function of the laser fluence in this regime. For the results reported here, the LII response varied by less than 5% for the range of laser fluence attenuations ($\sim 30\%$ maximum attenuation) encountered in the present study. The observed response of the LII signal to the laser fluence is sensitive to the laser beam intensity profile, the specific focusing arrangement employed for the incident beam and the timing of the boxcar gate pulse with respect to the laser pulse. Other researchers have observed more significant effects of the laser fluence on the LII signal [12] and further research is needed in this area. However, for the conditions described in the present work, reproducible results were always obtained as long as care was taken in the alignment of the optics and achievement of a near-gaussian beam intensity profile.

The spectral response of the LII signal is shown in Fig. 6, where the LII signal is plotted as a function of the detection wavelength. The spectral scan of the LII signal has been obtained by rotating the grating in the monochromator so that the detection wavelength is varied in 10-nm increments. Measurements have been taken at the radial location where the peak soot volume fraction occurs at the 40 mm height for a probe laser beam at the 1064-nm wavelength with a beam diameter of 0.5 mm

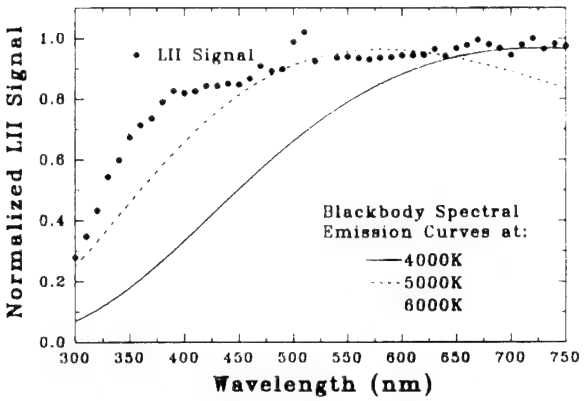

Fig. 6. Spectral response of the laser-induced incandescence where incident laser light at a wavelength of 1064 nm was used to obtain the spectrum shown.

and an energy of 1.5 mJ/pulse or laser fluence of 9.5×10^7 W/cm^2. For the 1064-nm wavelength laser probe beam, interference from light-scattering and PAH fluorescence is minimal in the visible wavelength range, although a fortuitous peak at 532 nm is seen due to the leakage of the 532-nm beam from the laser and corresponding light-scattering at this wavelength. It can be observed that as expected the LII signal exhibits a continuous spectra in the visible wavelength range with the signals decreasing to small levels below 300 nm. The LII spectrum also shows no distinct peaks and continues up to 750 nm at a nearly constant level. Comparison with computed blackbody radiation curves, as shown in Fig. 6, indicates that the LII spectrum in the 300–450-nm range corresponds to a soot temperature between 5000 and 6000 K, which is higher than the estimated soot vaporization temperature of ca. 4000 K. That the LII spectrum continues at a nearly constant level up to 750 nm and beyond, while the computed radiation curves begin to decline, is attributed to the fact that a large soot number density, and corresponding multiplicity of soot particle size, is present in the probe volume with different soot surface temperatures induced by the laser fluence. Hence, a more continuous and level spectral response is expected, as shown in Fig. 6 for a group of soot particles in comparison to a radiation curve computed for a single soot particle surface temperature. From Fig. 6, it can also be observed that by using 1064-nm wavelength probe laser, LII measurements can be taken at nearly any wavelength in the visible range, except near 532 nm for our optical arrangement, due to the absence of interference from PAH fluorescence and light-scattering as noted above, and measurements taken at detection wavelengths of 400 and 700 nm have yielded identical soot volume fraction results.

The heating of the soot particles to such high temperatures may lead one to be concerned about altering the properties of the soot particles. In the present experiments we assume that the soot properties are not seriously affected by the large laser fluence before the LII measurements are made. Furthermore, since the LII signals are calibrated against independently measured soot volume fraction values, any changes introduced, as long as they are the same throughout the soot field, are compensated for in the calibration procedure. These assumptions will need to be verified in future studies, but are not anticipated to introduce errors any more significant than the present knowledge of soot properties necessarily include.

Figure 7a shows the soot volume fraction measured by LII and the vertically polarized component of the light-scattering signal (Q_{vv}), while Fig. 7b contains the data for the mean soot particle diameter and the soot number density obtained from these measurements. To obtain the results shown in Fig. 7b, the Q_{vv} and soot volume fraction measurements were analyzed in a manner similar to that described by Santoro et al. [8]. The vertically polarized light-scattering signal has been obtained for the 532-nm wavelength laser probe beam, and

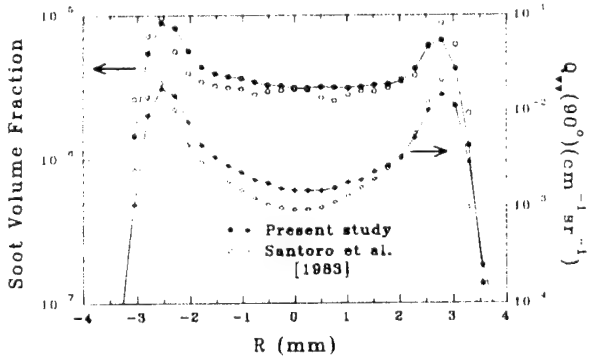

Fig. 7. (a) Radial profiles of the soot volume fraction and vertically polarized light-scattering signal, Q_{vv}, at a height, H, of 40 mm above the fuel tube exit of the burner.

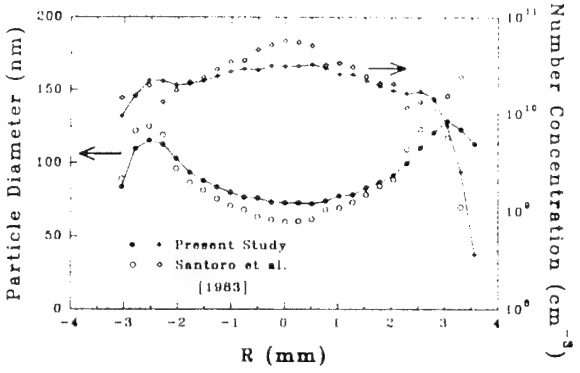

Fig. 7. (b) Radial profiles of the mean soot particle diameter, D_{63}, and soot number concentration, N, at a height, H, of 40 mm above the fuel tube exit of the burner.

the calibration for the absolute value of Q_{LII} has been obtained by matching with the known value of this signal at a single radial position using measurements by Santoro et al. [8] similar to the calibration procedure for the soot volume fraction. From the soot volume fraction and light-scattering data, which is proportional to the sixth moment of the soot particle diameter distribution, the mean soot particle diameter (D_{63}) and the soot number density (N) can be obtained as follows [8]:

$$D_{63} = \lambda^{4/3}\left(\frac{2Q_{LII}}{3\pi^3 F(\tilde{m}) f_v}\right)^{1/3}, \tag{1}$$

where

$$F(\tilde{m}) = \left|\frac{\tilde{m}^2 - 1}{\tilde{m}^2 + 2}\right|^2, \tag{2}$$

$$N = \frac{12 f_v}{\pi D_{63}^3}. \tag{3}$$

Here, f_v denotes the soot volume fraction while the complex index of refraction, $\tilde{m}$, is taken as $(1.57 - 0.56i)$ following Dalzell and Sarofim [13]. Similar to light scattering/extinction, the LII/light scattering technique yields the ratio of the sixth to third moment (D_{63}) of the particle diameter. The resultant mean soot particle diameter and the soot number density are again compared with the previous data obtained for this flame using the laser scattering/extinction method [8]. Figure 7b shows that the mean soot particle diameters are in very good agreement, with the discrepancy being mostly limited to the central region where due to the relatively low signal levels there is the largest uncertainty in both the LII and light-scattering data. The mean soot particle diameter from LII data in the present study ranges from 75 to 130 nm, while diameters of 60–135 nm have been observed by Santoro et al. [8].

It should be noted that the particle diameters reported, in some cases, exceed the size normally considered to be appropriate for a Rayleigh theory analysis. In fact, the soot particles in this flame are aggregates composed of primary particles that do satisfy the Rayleigh theory limit [14]. Thus, strictly, D and N refer to the volume equivalent diameter and number density, respectively, of these aggregates. Particle morphology effects are not included explicitly in the current study, which would require multiple-angle light scattering measurements. However, such measurements are feasible, in principle, and represent another area where the LII technique can contribute to research related to soot particle property determination.

The soot number density profiles are similarly in reasonably good agreement with the discrepancy again occurring near the centerline. Since the number density is inversely proportional to the cube of the mean soot particle diameter, the factor of 2 difference in the soot number density near the centerline is caused by the corresponding difference in the mean soot particle diameter shown in Fig. 7b. Thus, Fig. 7b shows that the single-point or two-dimensional measurements of the LII and light scattering, which can be set up with relative ease, a complete characterization of soot particle properties may be directly obtained.

CONCLUSIONS

From the discussion above, the following conclusions concerning the LII diagnostic of soot volume fraction are made:

1. Laser-induced incandescence has been used to obtain spatially resolved measurements of soot volume fraction in laminar diffusion flames, in which comparisons with laser scattering/extinction data yield excellent

agreement for both radial profiles and integrated volume fraction. Thus, LII can be used as an instantaneous, spatially resolved diagnostic of soot volume fraction without the need for the conventional line-of-sight laser extinction method.

2. The temporal characteristics of the LII signal are observed to involve a rapid rise in intensity followed by a relatively long (ca. 600 ns) decay period subsequent to the laser pulse, while the effect of laser fluence is manifest in nonlinear and saturated response of the LII signal with the transition occurring at a laser fluence of approximately 1.2×10^8 W/cm^2 for a laser pulse of ca. 7 ns in duration.
3. Spectral response of the LII involves a continuous spectrum in the visible wavelength range due to the blackbody nature of the emission, where the spectral response for 300–450-nm wavelength range indicates a soot surface temperature of ca. 5000 K with the spectrum continuing at a nearly level intensity up to 750-nm wavelength due to the multiplicity of the soot particle sizes in the probe volume.
4. Simultaneous measurements of LII and the vertically polarized light-scattering yield encouraging results concerning the mean soot particle diameter and number concentration; thus, significant applications exist in two-dimensional imaging and simultaneous measurements of LII and light scattering to generate a complete soot property characterization.

This material is based upon work supported by the Air Force Office of Scientific Research under Award No. F49620-92-J-0314 with Dr. Julian Tishkoff as contract manager and their support is gratefully acknowledged. The authors would also like to thank J. A. Pinson and S. Gupta of Penn State for many useful discussions and J. E. Harrington, C. R. Shaddix, and K. C. Smyth of the National Institute of Standards and Technology for providing us with their results on the effects of laser fluence on LII signals. We would also like to acknowledge the reviewers for their suggestions regarding the light scattering analysis and the effects of aggregates on the interpretation of the results of this work.

REFERENCES

1. Melton, L. A., *Appl. Opt.* 23:2201–2208 (1984).
2. Dasch, C. J., *Appl. Opt.* 23:2209–2215 (1984).
3. Eckbreth, A. C., Bonczyk, P. A., and Verdieck, J. F., *Prog. Ener. Combust. Sci.* 5:253–322.
4. Tait, N. P., and Greenhalgh, D. A., *Proceedings of the Optical Methods and Data Processing in Heat Transfer and Fluid Flow Conference*, London, April 1992.
5. Dec, J. E., zur Loye, A. O., and Siebers, D. L., *SAE Technical Papers Series* SAE-910224, Society of Automotive Engineers, PA, 1991.
6. Dec J., *SAE Technical Papers Series* SAE-920115, Society of Automotive Engineers, PA, 1992.
7. Eckbreth, A. C., *J. Appl. Phys.* 48:4473–4479 (1977).
8. Santoro, R. J., Semerjian, H. G., and Dobbins, R. A., *Combust. Flame* 51:203–218 (1983).
9. Santoro, R. J., Yeh, T. T., Horvath, J. J., and Semerjian, H. G., *Combust. Sci. Technol.* 53:89–115 (1987).
10. Puri, R., Moser, M., Santoro, R. J., and Smyth, K. C., *Twenty-Fourth Symposium (International) on Combustion*, The Combustion Institute, Pittsburgh, 1992, pp. 1015–1022.
11. Miller, J. H., Mallard, W. G., and Smyth, K. C., *Combust. Flame* 47:205–214 (1982).
12. Shaddix, C. R., Harrington, J. E., and Smith, K. C., personal communication.
13. Dalzell, W. H., and Sarofim, A. F., *Trans. ASME J. Heat Transf.* 91:100–104 (1969).
14. Puri, R., Richardson, T. F., Santoro, R. J., and Dobbins, R. A., *Combust. Flame* 92:320–333 (1993).

Received 15 July 1993; revised 19 January 1994

Appendix E: Two-Dimensional Imaging of Soot Volume Fraction by the Use of Laser-Induced Incandescence

by

T. Ni, J. A. Pinson, S. Gupta, and R. J. Santoro

*Applied Optics, Vol. 34, No. 30, pp. 7083-7091 (1995)**

Two-dimensional imaging of soot volume fraction by the use of laser-induced incandescence

T. Ni, J. A. Pinson, S. Gupta, and R. J. Santoro

A recently developed laser-induced incandescence technique is used to make novel planar measurements of soot volume fraction within turbulent diffusion flames and droplet flames. The two-dimensional imaging technique is developed and assessed by systematic experiments in a coannular laminar diffusion flame, in which the soot characteristics have been well established. With a single point calibration procedure, agreement to within 10% was found between the values of soot volume fraction measured by this technique and those determined by conventional laser scattering–extinction methods in the flame. As a demonstration of the wide range of applicability of the technique, soot volume fraction images are also obtained from both turbulent ethene diffusion flames and from a freely falling droplet flame that burns the mixture of 75% benzene and 25% methanol. For the turbulent diffusion flames, approximately an 80% reduction in soot volume fraction was found when the Reynolds number of the fuel jet increased from 4000 to 8000. In the droplet flame case, the distribution of soot field was found to be similar to that observed in coannular laminar diffusion flames.

Key words: Laser-induced incandescence, soot, flames.

1. Introduction

Recently the effectiveness of laser-induced incandescence (LII) for the quantitative determination of local soot volume fraction in laminar diffusion flames[1,2] was demonstrated. Because this diagnostic technique provides a direct measure of soot volume fraction without the need for a tomographic inversion process, as is used in conventional line-of-sight laser extinction methods, it was suggested that LII could be applied for instantaneous planar measurements of soot volume fraction in combustion systems, including nonsymmetric or unsteady flames. The applications of LII in qualitative two-dimensional (2-D) soot field imaging of diffusion flame and diesel engine combustion have been previously reported.[3–5] With the use of a calibration scheme described in the earlier work for point measurements,[1] it is possible to obtain quantitative 2-D imaging of soot volume fraction.

LII arises from near-blackbody emissions that originate from laser-heated soot particles. Theoretical analysis has shown that when the laser pulse is sufficiently intense, LII emission in the visible wavelength range is approximately proportional to local soot volume fraction.[6] This prediction has been verified experimentally in the previous work involving point measurements in an ethene–air laminar diffusion flame.[1] Recent work that address premixed flat flames have observed similar results and have examined the effects of interfering radiation such as background flame luminosity and fluorescence from polycyclic aromatic hydrocarbons[7] (PAH's). Studies in which LII is used to measure soot volume fraction in flickering ethene–air diffusion flames have also been reported.[8]

In this paper, we address key issues associated with quantitative measurements made by using 2-D LII imaging and describe the novel application of 2-D LII in the measurement of soot volume fraction in laminar diffusion, turbulent diffusion, and free-falling droplet flames. To gain better understanding of the behavior of the LII technique and to provide information for the design of experiments by the use of 2-D

The authors are with the Department of Mechanical Engineering and the Propulsion Engineering Research Center, The Pennsylvania State University, University Park, Pennsylvania 16802-2320.

Received 29 August 1994; revised manuscript received 11 May 1995.

0003-6935/95/307083-09$06.00/0.

LII imaging, we also made a number of point measurements.

2. Experimental Approach

A. Experimental Apparatus For Point Measurements

The optical setup for the point measurements utilizes a frequency-doubled Nd:YAG pulsed laser (Surelite II, Continuum) operating at 10 Hz with a pulse width of 7 ns FWHM. For studying the effects of the laser beam intensity profile on the LII signal, two types of intensity profiles were used. These are referred to as the near-Gaussian profile and the rectangular profile hereafter, and they indicate the shape of the intensity profile across the laser beam. The rectangular-profile beam, i.e., one in which the laser intensity is uniform across the beam, was produced when a 1-mm-diameter pinhole was placed in front of the flame, which allowed only the center portion of a 6-mm-diameter near-Gaussian laser beam to heat the soot particles. Because the 1-mm-diameter pinhole is only 6 cm away from the flame, the diffraction effects from the pinhole are negligible. The intensity of the laser beam was varied by the use of a combination of a half-wave plate and a polarization beam splitter. The LII signal at a 90° angle was focused onto the entrance slit of a 0.25-m monochrometer (Instruments SA H20) and was detected by a photomultiplier tube (PMT) (Hammamatsu R928) wired for fast response. The combination of a 0.25-mm entrance slit width for the monochrometer and the 1-mm beam diameter of the laser defined the probe volume for the point measurements. A narrow-band interference filter (10 nm FWHM, transmittance peaks at 400 nm) was placed in the front of the monochrometer in order to reject scattered laser light. The output from the PMT was input to a 100-MHz digital oscilloscope (Tektronix TSA 2440) and then transferred to a lab computer by a general-purpose interface bus. A coannular laminar diffusion flame that burns ethene in air was used in this study. The burner that was identical to the one used in previous soot studies[9,10] consists of a 1.1-cm-diameter fuel tube surrounded by a 10.2-cm-diameter air tube. The flow rates of ethene and air were 3.85 cm^3/s and 1060 cm^3/s, respectively. At this flow condition, the distribution of soot volume fraction and soot particle size have been measured by a light scattering–extinction method.[9]

B. Experimental Apparatus For Two-Dimensional Laser-Induced Incandescence Imaging

The experimental setup for 2-D LII imaging is shown in Fig. 1. A 285-mJ/pulse, 532-nm laser beam (Gaussian profile at far field) from the YAG laser was shaped into a 350-μm-thick (FWHM) laser sheet by a combination of a diverging cylindrical lens [focal length (fl) = 6 cm] and a spherical focusing lens (fl = 2 m). The thickness of the laser sheet was measured by translation of a razor blade across the laser sheet and measuring the transmitted energy. For quantitative 2-D LII measurements, the uniformity of the laser sheet is particularly important. A good laser sheet was obtained when the diverging cylindrical lens was placed close the laser exit, as the laser beam profile at near field is nearly flat. Although the laser sheet at the focal point was ~32 cm in height, only the central 10 cm were used for 2-D LII imaging to ensure the uniformity of the laser sheet. The uniformity of the center 10 cm of the laser sheet was better than 90% as determined when a 2-mm-wide slit was moved vertically along the laser sheet and the transmitted laser power was measured. The use of a very long fl lens (fl = 2 m) has the advantage of minimizing the variation of the thickness of the laser sheet across a flame, which is especially important when large-diameter flames are being studied. For an imaging area as wide as 5 cm, the variation of the thickness is estimated to be less than 5%. Furthermore, the sensitivity of LII imaging is higher when a longer fl lens is used, as the LII signal is directly proportional to the thickness of the laser sheet, which is larger for a longer fl lens. For large-diameter flames, the use of a thicker sheet is particularly important, as it helps in rejecting background luminosity, which is nearly proportional to the diameter of the flame.

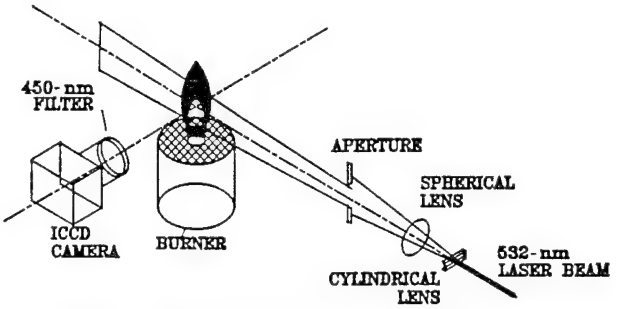

Fig. 1. Experimental setup for 2-D LII imaging.

The LII images were taken at a 90° angle to the laser sheet by a gateable intensified CCD camera (Princeton Instruments, Model ICCD-576S/RB) equipped with a 105-mm fl UV camera lens (Nikkon, $f/4.5$). The spatial resolution for these 2-D imaging studies is determined by the number of camera pixels (578 × 384) available and the field of view imaged in the experiments. The resolutions for each of the studies described here are included in the appropriate sections below. A broadband interference filter (450 ± 25 nm) was placed in front of the camera to minimize the interference from scattered light. A small amount of scattered light was found to pass through the filter. The influence of the scattered light was completely eliminated when the intensifier was gated on after the laser pulse. Although a stronger signal could be obtained if a long gate time were employed, the gate time for the intensifier in this experiment was set at 18 ns, which is much shorter than LII decay time, to minimize the effect of particle size, which is discussed below.

The interference from fluorescence of PAH's has been examined. For ethene coflow diffusion flames,

PAH's are mostly present at lower flame heights and at radial locations that are closer to the center line compared with soot particles.[2] In these PAH formation regions where soot particles are absent, no significant signal was observed in the LII imaging experiments, indicating that fluorescence from PAH does not interfere with the LII signal. This may be due to the observation that PAH species emit predominantly at wavelengths longer than the excitation wavelength (532 nm), whereas the LII signal was captured at a shorter wavelength (450 nm). To prevent flame luminosity from leaking through the intensifier when the gate is off, a mechanical shutter that opens for 5 ms during image acquisition was placed in front of the camera lens. With a modest intensifier gain, the single-shot signal from 10 parts in 10^6 (ppm) soot in an ethene diffusion flame is ~3000 counts/pixel for a probe volume of 170 μm × 170 μm × 350 μm. The sensitivity can be enhanced by increasing the bandwidth of the interference filter. In the present imaging experiment, the camera was gated on immediately after the laser pulse. When the slightly delayed LII signal was measured, the intensity of the acquired images was found to remain nearly constant for an average laser fluence beyond 0.17 J/cm^2. Measurements were taken at a laser fluence of 0.32 J/cm^2 or an intensity density of 4.6×10^7 W/cm^2. This laser fluence is approximately a factor of 8 lower than that used in our previous work for point measurements.[1] The use of low laser fluence has the advantage of minimizing intrusion of the LII process on the flame that is due to laser vaporization of soot particles and thus has potential for applications in systems in which successive images are needed.

After dark noise was subtracted, the LII images were corrected for the combined spatial variations in CCD pixel response and intensifier gain when the ratio of the LII image to a correction image was taken. The correction image was obtained by the uniform illumination of the camera by a lamp located behind a diffusor. The corrected LII images were then translated into soot volume fraction images after the imaging system was calibrated against a sooting source whose soot volume fraction is known. In this experiment, an ethene diffusion flame served as the calibration standard.[1] The LII images were not corrected for the absorption of LII signal by soot particles located between the laser sheet and the camera. Although using longer detection wavelengths could reduce the extinction of the signal, the background luminosity becomes more difficult to reject.

3. Laser-Induced Incandescence Signal Characteristics

A. Laser Fluence Effects

The intensity of a LII signal depends on the temperature of the laser-heated soot particles, which is determined by the rate of laser energy absorption and heat loss through conduction, radiation, and soot vaporization. It has been observed[1] that initially the LII signal increases rapidly as laser fluence increases. Once laser fluence reaches a saturation threshold the LII signal shows a small or no increase with respect to an increase in laser fluence. At high laser fluence it is believed that soot vaporization is the dominant effect that limits the increase in soot particle temperature. Using a laser fluence in the saturation regime is desirable when one is measuring soot volume fraction, as the LII signal is then least affected by laser beam attenuation across the flame. However, there is a significant uncertainty in measuring the local laser fluence in an ordinary laser beam, which is not uniform. It is therefore difficult to determine the saturation intensity accurately under many conditions. In order to study the effect of laser fluence on the LII signal, a rectangular-profile laser beam was used to heat the soot particles. Theoretical models[11,12] for particle heating and vaporization have been reported previously as a function of laser fluence. The use of the rectangular-profile beam allows the laser fluence to be easily determined, thereby allowing direct comparison with theory.

Figure 2 illustrates the effect of laser fluence on the intensity of the LII signal detected immediately after the rectangular-profile laser pulse. These results were obtained in an ethene laminar diffusion flame at a height 40 mm above the fuel tube exit and at a radial location where peak soot volume fraction is observed for this height. Below a laser fluence threshold of 0.06 J/cm^2, no observable LII signal was detected. Just above the laser fluence threshold, the LII signal exhibits a rapid increase with increased laser fluence. After the LII signal reaches a peak at a laser fluence of 0.27 J/cm^2, further increase of laser fluence actually reduces the LII signal intensity. Similar results have been observed recently by Vander Wal and Weiland[13], who used a Gaussian-profile laser beam. A profile that exhibits a rapid increase in the

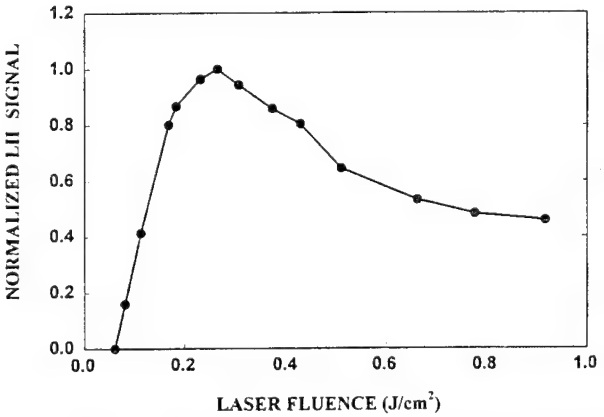

Fig. 2. Effect of laser fluence on LII for a rectangular laser intensity profile (rectangular profile). These measurements correspond to an ethene–air laminar diffusion flame at an axial position 40 mm above the fuel tube exit and a radial location exhibiting the peak soot volume fraction for that height.

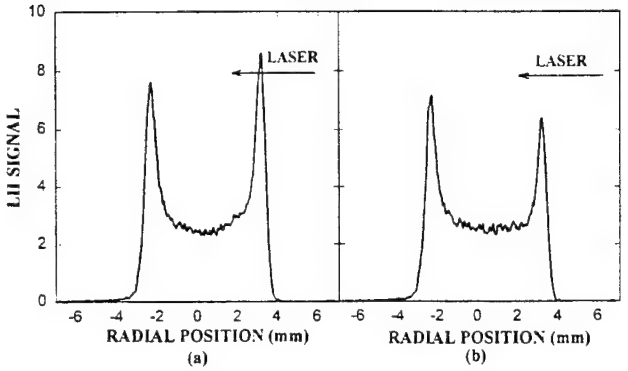

Fig. 3. Effect of laser fluence on the spatially resolved LII signal profile at a height 40 mm above the fuel exit of an ethene–air laminar diffusion flame: (a) laser fluence 0.15 J/cm^2, (b) laser fluence 0.41 J/cm^2.

LII signal followed by a slow decrease as a function of laser fluence has been predicted by Tait and Greenhalgh[3] from numerical calculations. They predicted that a decrease in particle mean volume that is due to vaporization at high laser fluence reduces the LII signal intensity. The spatially resolved LII signal profiles across an axisymmetric ethene diffusion flame at the 40-mm height are shown in Fig. 3. Because of the extinction of the laser beam by soot particles, which results in a 20%–25% reduction in the laser intensity across the flame, the LII profiles are asymmetric. For a laser fluence below saturation, the LII signal from the peak that is closer to the laser source is stronger [shown in Fig. 3(a)], as the effect of laser attenuation dominates over soot vaporization. In contrast, for a laser fluence beyond the saturation fluence, the signal from the far peak is stronger [shown in Fig. 3(b)], as soot vaporization is now the dominant perturbation that affects the LII signal.

A temporal profile of the vertically polarized light-scattering signal and the influence of laser intensity on the temporal profile of the LII signal are shown in Fig. 4. For a laser intensity slightly above the threshold, the LII signal rises slowly and reaches its maximum just after the laser pulse, which indicates that the temperature of the soot particles is constantly increasing during the laser pulse. As laser fluence increases, the rise time and the decay time of the LII signal decrease, while the maximum in the LII signal is observed to increase at lower laser fluence (<0.27 J/cm^2) and decrease at higher laser fluence (>0.27 J/cm^2). The initial increase in the maximum of the LII signal and the decrease of the LII signal rise time with increased laser fluence are consistent with the observation that soot particles are heated to a higher temperature and that the temperature rises faster at a higher laser intensity.[11] The dramatic decrease of the LII decay time with increased laser fluence, as shown in Fig. 5, is not fully understood. One explanation is that the vaporization of soot particles under intense laser heating reduces their size, and the smaller particles consequently cool faster. Dasch[12] showed that vaporization reduces the diameter of soot particles, D, exponentially with laser fluence, F, as

$$D = D_0 \exp[-(F - F^*)/F_0], \quad (1)$$

where D_0 is the initial particle diameter and F^* and F_0 are empirical parameters that can be determined experimentally. For a 7-ns laser pulse, the threshold fluence F^* and decay fluence F_0 have been reported to be 0.23 J/cm^2 and 1.9 J/cm^2, respectively.[12]

For a laser fluence of 0.54 J/cm^2, the calculated reduction in soot particle size from Eq. (1) is 15%. Under the same laser fluence, the LII decay time is approximately a factor of 10 times shorter than the decay time under a laser fluence of 0.11 J/cm^2. Such a significant decrease in the decay time cannot be explained by the vaporization mechanism alone. It is likely that, in addition to the vaporization mechanism, other physical or chemical properties of the soot particles change under the intense laser fluences involved in the particle-heating process. Dasch[12] measured light scattering and absorption of a

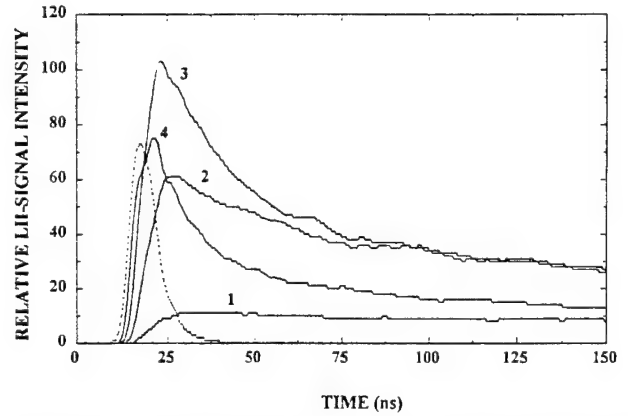

Fig. 4. Effect of laser fluence on the temporal profile of the LII signal: dashed curve, laser scattering signal; trace 1, laser fluence 0.072 J/cm^2; trace 2, laser fluence 0.14 J/cm^2; trace 3, laser fluence 0.27 J/cm^2; trace 4, laser fluence 0.72 J/cm^2.

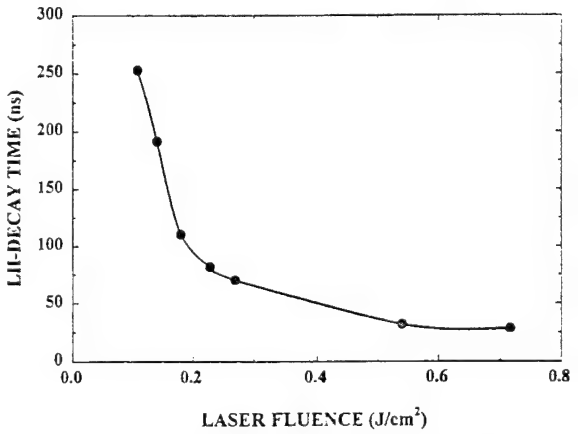

Fig. 5. Effect of laser fluence on the LII signal decay time (the time for the signal to decay to $1/e$ of peak intensity).

cw probe laser along a high-energy pulsed laser beam and concluded that soot particles vaporize rather than fragment. However, by a careful examination of the time-resolved light-scattering signal obtained by Dasch,[12] it can be found that there is a transient, but significant, reduction in light scattering during or immediately after the laser pulse, which Dasch attributed to scattered light from the laser pulse or induced incandescence. This transient signal could also be interpreted as indicating that soot aggregates undergo a rapid change in shape, resulting in an increased surface area and a faster heat loss.

From these results, it is clear that at the laser fluences required for LII measurements, significant effects on the LII signal decay time can be observed as the laser fluence is varied. Thus the observed response of LII signal intensity to the laser fluence is sensitive to the delay time for detector gate pulse with respect to the laser pulse. The LII signal during the initial laser-heating period is particularly sensitive to the laser fluence. For quantitative soot volume fraction measurements, the detector gate should be delayed by few nanoseconds with respect to the laser pulse.

B. Particle-Size Effects

Figure 6 shows the temporal profiles of a LII signal obtained in the ethene–air laminar diffusion flame at heights of 10 and 30 mm above the fuel tube exit and at the radial locations corresponding to peak soot volume fraction for these heights. These observations were made with the rectangular-profile laser beam with a laser fluence of 0.27 J/cm^2. Spatially resolved particle-size measurements on this flame have been performed by Santoro *et al.*[9] The mean particle diameter (D_{63}) of soot particles at the 30-mm height is 160 nm, which is significantly larger than that observed at the 10-mm height, where the mean size is 64 nm. As can be seen in Fig. 6, the leading edges of LII temporal profiles at the two locations in the flame closely match, which is consistent with the theoretical prediction,[3] indicating that in the Rayleigh regime all particles, regardless of size, increase in temperature at the same rate. In contrast, the LII signal at the 10-mm flame height undergoes a faster decay than that observed at the 30-mm height. This behavior is due to the difference of the soot particle size, as smaller particles have a larger surface area per unit mass and are expected to cool faster.

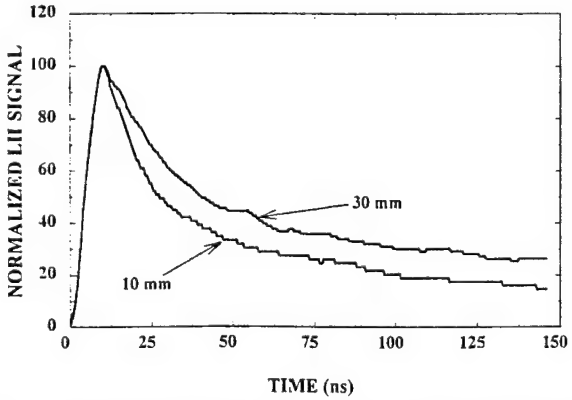

Fig. 6. Temporal profile of a LII signal obtained in the ethene–air laminar diffusion flame at heights of 10 and 30 mm above the fuel tube exit and at the radial locations corresponding to peak soot volume fraction for these heights.

To demonstrate this particle-size effect and estimate the error associated with the detection delay time, a one-dimensional (1-D) LII imaging experiment was performed. The LII signal generated by the rectangular-profile laser beam was imaged onto the gated intensified CCD camera. A narrow-band interference filter with transmittance centered at 400 nm was placed in the front of the camera to reject scattered laser light and PAH fluorescence. The camera was gated on for 5 ns. Figure 7(a) shows the normalized 1-D LII signal profiles from the ethene–air laminar diffusion flame at the 40 mm height, obtained by the varying of the delay time of the intensifier gate with respect to the laser pulse. Figure 7(a) contrasts the results obtained when the gate is placed immediately after the laser pulse compared with the case in which the gate is delayed 180 ns. It can be seen that the LII signal ratio of center line to the peaks decreases as the intensifier

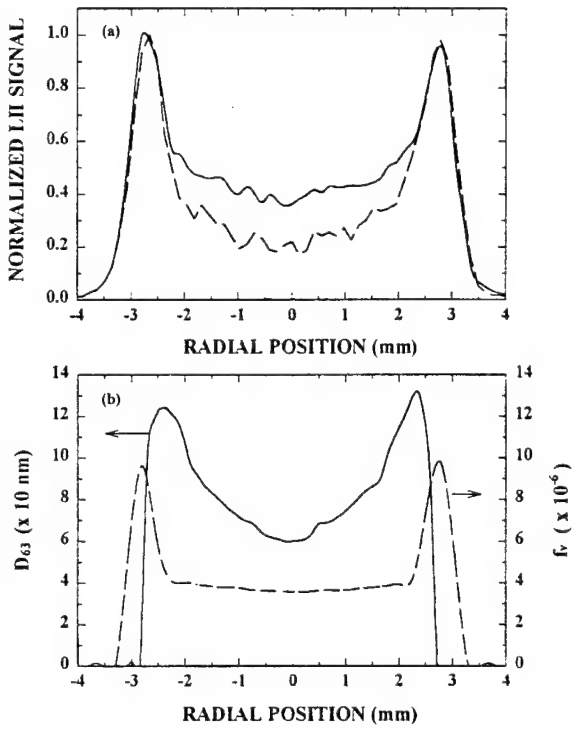

Fig. 7. Effect of the delay time of the detector gate on the spatial profile of the LII signal at the 40-mm height in the ethene–air laminar diffusion flame: (a) solid curve, LII signal observed immediately after laser pulse; dashed curve, LII signal observed 180 ns after the laser pulse; (b) laser scattering–extinction data,[9] where the solid curve is the soot mean particle diameter, and the dashed curve is the soot volume fraction.

gate pulse was delayed for 180 ns with respect to the laser pulse. This observation is consistent with the particle-size measurements at that height, which are shown in Fig. 7(b). Compared with soot volume fraction data at the same flame height [shown in Fig. 7(b)] measured by the laser scattering–extinction method,[9] the LII profile taken immediately after the laser pulse matches closely with the laser scattering–extinction data. Similar results were also observed for the Gaussian-profile laser beam. Because of this size dependence, the delay time between laser pulse and detector gate for an imaging experiment should be made as short as possible to minimize this particle-size effect. Even though the LII signal can last as long as 600 ns, a short detector gate width should be used so that the contribution from the size-sensitive portion of LII signal is minimized. For a gate width of 50 ns, the error that is due to the size effect could be as large as 10%, as estimated by the integration of the LII signals, shown in Fig. 6, over the time period of the gate width.

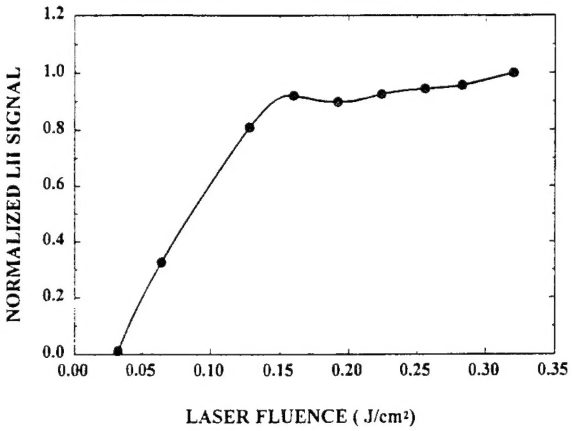

Fig. 8. Effect of average laser fluence on LII for a Gaussian-shaped laser beam. These measurements correspond to an ethene–air laminar diffusion flame at an axial position 40 mm above the fuel tube exit and a radial location that exhibits the peak soot volume fraction for that height.

C. Laser Beam Shape Effects

The results describe above were obtained with the use of a laser pulse whose spatial profile is rectangular compared with a Gaussian beam. However, typically lasers do not generate a rectangular-profile beam. Although the use of a pinhole can reshape the Gaussian beam into a rectangular-profile beam, the spatial resolution is relatively low because of the diffraction effect from the pinhole. The use of a pinhole also reduces the efficiency of laser power utilization. Thus it is not feasible to use a rectangular-profile beam in a 2-D LII imaging measurement that requires very high laser energies to form a laser sheet intense enough to saturate the LII signal.

For a near-Gaussian-profile beam, the laser intensity is not uniformly distributed. Increasing laser energy will result in an increase in the effective LII probe volume, in which the local laser fluence exceeds the threshold for the LII signal to be observed. Figure 8 shows a plot of the LII signal taken immediately after the laser pulse as a function of average laser fluence of the laser sheet. The LII signal was obtained in the ethene–air laminar diffusion flame at a height of 40 mm above the fuel tube exit and at the radial location that corresponds to peak soot volume fraction for this height. The intensified CCD detector was gated on for 18 ns. The laser intensity across the laser sheet has a near-Gaussian profile. The thickness of the laser sheet is ~350 μm (FWHM). The LII signal intensity shown in Fig. 8 is seen to be nearly constant for a laser fluence beyond 0.17 J/cm². This behavior is different from that observed for the rectangular-profile beam, in which the LII signal intensity decreases after saturation.

Previous point measurements[1] in which a near-Gaussian-profile beam was used have shown that for a sufficiently intense laser fluence the LII signal exhibits a small increase with an increase in laser fluence. A similar result was found by Tait and Greenhalgh,[3] who used a laser sheet. It was suggested that, as laser energy increases, the decrease in the LII signal that is due to vaporization of the soot particles was compensated for by an increase in the effective probe volume, resulting in a near-constant LII signal intensity. We have tried to generate LII signals by using a doughnut-shaped beam. However, the LII signal intensity observed continued to increase with higher laser fluence, suggesting that the response of the LII signal to average laser fluence is sensitive to the laser beam intensity profile. This result is likely due to differences in the expansion of the probe volume with respect to the degree of soot particle vaporization.

The interactions between laser beam and soot particles may also have significant effects on the beam profile. For a Gaussian beam, more soot content is vaporized in the center of the beam than in the outer portion, because the laser intensity in the center of near-Gaussian-profile beam is larger. The vaporization effect decreases the absorption of laser energy by soot particles, particularly in the center of the laser beam. Consequently, as the laser beam propagates through the soot field, the beam diameter becomes smaller, because the wings are preferentially absorbed. The vaporization of soot particles also affects the temporal profile of the laser pulse as the laser beam propagates through the soot field. This effect is due to the fact that the soot volume fraction in the laser beam decreases gradually during the laser pulse, the less energy in the later part of the laser pulse is absorbed. The change in the temporal profile of the laser pulse may affect the response of the LII signal to laser fluence. To minimize the experimental error caused by these effects, the laser fluence should be kept as low as possible. For these reasons, it is not recommended that the technique be used in large-diameter and heavily sooting flames unless care has

been exercised to examine the interaction between the laser beam and the soot particle field.

4. Imaging Results and Discussion

In order to examine and demonstrate various aspects of 2-D LII imaging for soot volume fraction measurements, a series of experiments were conducted that involved an ethene–air laminar diffusion flame, a turbulent ethene diffusion flame and a benzene–methanol droplet flame. These experiments were selected to demonstrate

(1) the comparative accuracy of the 2-D LII technique compared with previous laser scattering–extinction measurements in laminar diffusion flames;
(2) the capabilities of the 2-D LII technique in gaseous, unsteady turbulent diffusion flames;
(3) that 2-D LII imaging can be implemented in the presence of a liquid fuel droplet that introduces additional light-scattering interferences.

A. Laminar Diffusion Flame Measurements

The soot volume fraction image for an ethene–air laminar diffusion flame measured with the 2-D LII imaging technique is shown in Fig. 9. Because soot particle size and concentration information throughout the ethene diffusion flame has been determined,[9,10] it is possible to use this flame for the examination of the accuracy of the 2-D imaging technique.

To provide access for the laser sheet, the brass chimney for the burner used in previous work[9,10] was replaced with a glass chimney. Part of the glass chimney was painted black to minimize the reflection of LII from the chimney wall onto the detector. The flow conditions for the burner were duplicated from previous work.[9] The laser sheet was directed to pass through the center line of the flame. The flame has a visible flame height of 88 mm and does not emit smoke from the flame tip. Thus the 10-cm-wide laser sheet is large enough to cover the entire soot field in the flame. The spatial resolution for the LII images is 170 μm × 170 μm × 350 μm.

To obtain the soot volume fraction image, the observed LII image was scaled so that the LII signal from a pixel corresponding to the radial location where the peak soot volume fraction occurs at the 40-mm height is equal to the soot volume fraction at this location from laser scattering–extinction measurements. A comparison between the soot volume fraction measured by LII imaging and the laser scattering–extinction method for three heights in the flame is shown in Fig. 10. It can be seen that the data measured by the LII technique agrees very well with that obtained by the laser extinction–scattering method.[9] The small different (~5%–10%) between LII data and laser scattering–extinction data is probably due to the effect of particle size. As can be seen, the deviation usually occurs at lower heights or along the flame center line where soot particles are smaller. Numerical analysis performed by Melton[6] shows that the intensity of LII signal at the maximum temperature is proportional to the mean particle diameter raised to the power of $(3 + 0.154\lambda_{det}^{-1})$, where λ_{det} is the detection wavelength in micrometers. For λ_{det} = 450 nm, the exponent is 3.34. The deviation of the exponent from 3 could result in an underestimation of the soot volume fraction for smaller particles if the detection system is calibrated against larger particles. The mean soot particle diameter (D_{63}) in the ethene flame has been measured by Santoro *et al.*[9] to range from 15 to 160 nm. However, the difference between the LII data and the laser scattering–extinction data is significantly smaller than the theoretical prediction.

B. Turbulent Diffusion Flame Measurements

The turbulent diffusion flames were established by the injection of ethene into still air through a 1-mm-diameter 250-mm-long stainless steel tube mounted on a traversing stage. The flow rate of ethene was metered by a rotameter. The 2-D LII measurements were made for two different burner Reynolds numbers (4000 and 8000). The visible flame heights for Re = 4000 and Re = 8000 flames are ~300 mm.

The quantitative single-shot images for soot volume fraction distribution were taken when the 10-cm-wide laser sheet was passed through the center line of the turbulent flames, resulting in a spatial resolution identical to the laminar flame case discussed above.

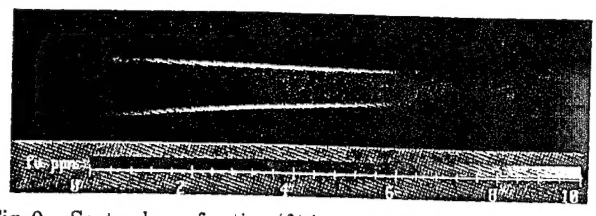

Fig. 9. Soot volume fraction (f_v) image of an ethene–air laminar diffusion flame. The maximum soot volume fraction in the image is 9.8×10^{-6}.

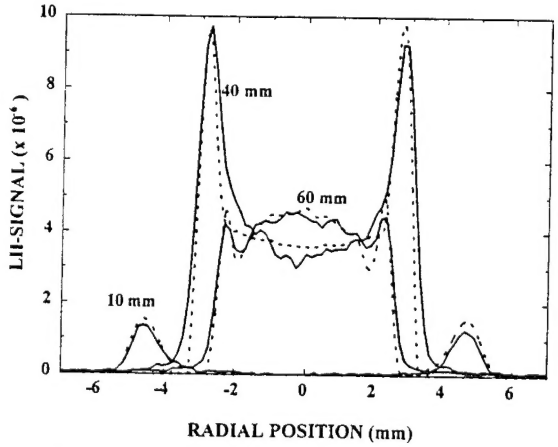

Fig. 10. Comparison of the soot volume fraction profiles obtained by LII and laser scattering–extinction.[9] Solid curve, LII data; dashed curve, laser scattering–extinction data.

The error involving the contribution from background luminosity to the signal intensity in the flames was found to be less than 2%. However, it must noted that the extinction of the LII signal by soot particles located between the laser sheet and the detector may reduce the signal intensity by as much as 10%. Typical soot volume fraction images, extending over the region from 10 to 20 cm above the fuel tube exit, are shown in Fig. 11. The LII images, which show soot particles being confined in turbulent eddies, reveal that the soot distribution is highly intermittent. This soot field structure is similar to the observations made by light-scattering studies for turbulent acetylene[14,15] and natural gas[16] flames. Figure 11 also shows that the soot volume fractions in the Re = 8000 flame are generally lower than those in the Re = 4000 flame by at least a factor of 5. It is believed that the higher Reynolds number associated with higher flow velocity enhances the fuel–air mixing, thereby reducing the time for soot growth. A similar fuel velocity effect on soot formation was reported in the study of turbulent acetylene flames by Kent and Bastin.[17]

C. Free-Falling Droplet Flame Measurements

Single benzene–methanol droplets generated from an aerodynamic droplet generator were injected downward into the postcombustion gas of a flat premixed flame burning methane. The temperature of the postcombustion gas, which contains 21% oxygen, is ~670 °C. To increase spatial resolution for LII imaging in the droplet flame, the 2-m spherical lens was replaced with a 1-m lens to shape the laser beam into a 200-μm-thick sheet. A close-up bellows was placed between the intensified CCD camera and the 105-mm camera lens to increase the magnification of the LII images. For these conditions, the spatial resolution is 30 μm × 30 μm × 200 μm.

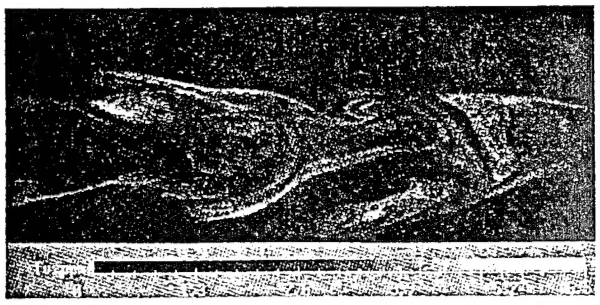

(a)

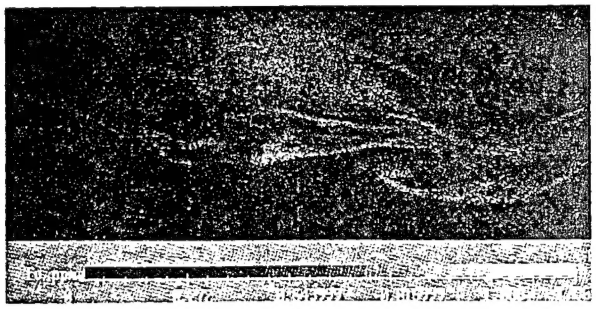

(b)

Fig. 11. Soot volume fraction (f_v) images of turbulent ethene diffusion flames: (a) Reynolds number 4000, (b) Reynolds number 8000.

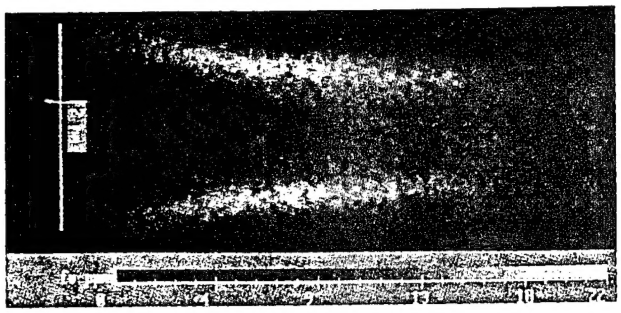

Fig. 12. Soot volume fraction (f_v) image of a freely falling droplet flame.

Figure 12 shows the distribution of soot formed from a 680-μm-diameter burning droplet that contains 75 volume % benzene and 25 volume % methanol. The image was taken 50 ms after the droplet was injected into the postflame gas. Similar to the structure of coannular laminar diffusion flames, the maximum soot volume fractions in this droplet flame are found in an annular region, not along the center line. Because benzene (bp 80 °C) and methanol (bp 65 °C) are highly volatile, the gaseous fuel vaporized from the droplet is concentrated in the wake region behind the droplet, forming a diffusion flame similar to the coannular gaseous flame geometry. The higher soot volume fractions observed in the droplet flame compared with the ethene–air laminar diffusion flame is consistent with the higher sooting tendency of benzene. The soot volume fraction observed in the droplet flame is sensitive to droplet size and methanol concentration. Significant reductions in soot volume fraction were observed by a decrease in the droplet size or an increase in the concentration of methanol.

5. Conclusions

The present investigation extends our previous work on measurements of soot volume fraction by the use of LII. The results of this investigation indicate the following:

(1) The application of LII for instantaneous, quantitative 2-D measurement of soot volume fraction was confirmed by this investigation. There is good agreement between the LII results and laser scattering–extinction data, although the soot volume fractions measured by LII are a little lower in the regions where the mean soot particle diameter is small.

(2) Time-resolved measurements show that the decay time of the LII signal is as long as several hundred nanoseconds and is sensitive to laser fluence. This significant effect of laser fluence on the LII decay time may be related to fragmentation or shape changes of the soot particles under intense laser heating.

(3) The LII signal was found to decay faster in regions where the mean soot particle diameter is smaller. To avoid the interference of elastic scattering and minimize particle-size effects, detection should be implemented immediately after the laser pulse, and the sampling (gate) time should be short (less than 50 ns).

(4) The technique has been used to obtain 2-D images of the soot volume fraction field in turbulent diffusion flames and a free-falling droplet flame, demonstrating that this technique can provide quantitative, instantaneous, and high spatially resolved measurements of soot volume fraction.

This material is based on work supported by the U.S. Office of Naval Research under grant N00014-93-0185, with Gabriel D. Roy as contract monitor, and the U.S. Air Force Office of Scientific Research under grant F49620-92-J-0161, with Julian Tishkoff as contract monitor, and is gratefully acknowledged. The authors also express their gratitude to B. Quay and M. Moser of Penn State for many useful discussions and technical assistance.

References

1. B. Quay, T.-W. Lee, T. Ni, and R. J. Santoro, "Spatially-resolved measurements of soot volume fraction using laser-induced incandescence," Combust. Flame **97,** 384–392 (1994).
2. T. Ni, S. B. Gupta, and R. J. Santoro, "Suppression of soot formation in ethene laminar diffusion flames by chemical additives," in *Twenty-Fifth Symposium (International) on Combustion* (The Combustion Institute, Pittsburgh, Pa., 1994), pp. 585–592.
3. N. P. Tait and D. A. Greenhalgh, "2D soot field measurements by laser induced incandescence," in the *Proceedings of the Optical Methods and Data Processing In Heat Transfer and Fluid Flow Conference* (Institution of Mechanical Engineers, London, 1992), pp. 185–193.
4. J. E. Dec, A. O. zur Loye and D. L. Siebers, "Soot distribution in a D.I. diesel engine using 2-D laser-induced incandescence imaging," Vol. SAE-910224 of the SAE Technical Papers Series (Society of Automotive Engineers, Warrendale, Pa., 1991).
5. J. E. Dec, "Soot distribution in a D. I. diesel engine using 2-D imaging of laser-induced incandescence, elastic scattering, and flame luminosity," Vol. SAE-920115 of the SAE Technical Papers Series (Society of Automotive Engineers, Warrendale, Pa., 1992).
6. L. A. Melton, "Soot diagnostics based on laser heating," Appl. Opt. **23,** 2201–2208 (1984).
7. P.-E. Bengtsson and M. Aldén, "Soot visualization strategies using laser techniques: laser-induced fluorescence in C_2 from laser-vaporized soot, and laser-induced soot incandescence," Appl. Phys. B **60,** 51–59 (1995).
8. C. R. Shaddix, J. E. Harrington, and K. C. Smyth, "Quantitative measurements of enhanced soot production in a flickering methane/air diffusion flame," Combust. Flame **99,** 723–732 (1994).
9. R. J. Santoro, H. G. Semerjian, and R. A. Dobbins, "Soot particle measurements in diffusion flames," Combust. Flame **51,** 203–218 (1983).
10. R. J. Santoro, T. T. Yeh, J. J. Horvath, and H. G. Semerjian, "The transport and growth of soot particles in laminar diffusion flames," Combust. Sci. Technol. **53,** 89–115 (1987).
11. A. C. Eckbreth, "Effects of laser-modulated particulate incandescence on Raman scattering diagnostics," J. Appl. Phys. **48,** 4473–4479 (1977).
12. C. J. Dasch, "Continuous-wave probe laser vaporization of small soot particles in a flame," Appl. Opt. **23,** 2209–2215 (1984).
13. R. L. Vander Wal and K. J. Weiland, "Laser-induced incandescence: development and characterization towards a measurement of soot volume fraction," Appl. Phys. B **59,** 445–452 (1994).
14. B. F. Magnussen, "An investigation into the behavior of soot in a turbulent free jet C_2H_2-flame," in the *Proceedings of the Fifteenth Symposium (International) on Combustion* (The Combustion Institute, Pittsburgh, Pa., 1975), pp. 1415–1425.
15. J. P. Gore and G. M. Faeth, "Structure and spectral radiation properties of turbulent acetylene/air diffusion flames," J. Heat Transfer **110,** 173–181 (1988).
16. R. C. Miake-Lye and S. J. Toner, "Laser soot-scattering imaging of a large buoyant diffusion flame," Combust. Flame **67,** 9–26 (1987).
17. J. H. Kent and S. J. Bastin, "Parametric effects on sooting in turbulent acetylene diffusion flames," Combust. Flame **56,** 29–42 (1984).